INVESTIGATIONS ON CHARACTERISTICS AND PERFORMANCE OF HARD THIN FILMS DEVELOPED BY CATHODIC ARC EVAPORATION

Thesis

Submitted in partial fulfillment of the requirements for the degree of

DOCTOR OF PHILOSOPHY

by

PRADEEP V. BADIGER

DEPARTMENT OF MECHANICAL ENGINEERING

NATIONAL INSTITUTE OF TECHNOLOGY KARNATAKA

SURATHKAL, MANGALORE - 575025

MAY 2019

DECLARATION

I hereby ***declare*** that the Research Thesis entitled **Investigations on Characteristics and Performance of Hard Thin Films Developed by Cathodic Arc Evaporation** which is being submitted to the ***National Institute of Technology Karnataka, Surathkal*** in partial fulfillment of the requirements for the award of the Degree of ***Doctor of Philosophy*** is a ***bonafide report of the research work carried out by me***. The material contained in this Thesis has not been submitted to any University or Institution for the award of any degree.

Register Number: 155130ME15F10

Name of the Research Scholar: **PRADEEP V. BADIGER**

Signature of the Research Scholar:

Department of Mechanical Engineering
Place: NITK - Surathkal
Date:

CERTIFICATE

This is to *certify* that the Research Thesis entitled **Investigations on Characteristics and Performance of Hard Thin Films Developed by Cathodic Arc Evaporation**, submitted by **Pradeep V Badiger** (Register Number: 155130ME15F10) as the record of the research work carried out by him, is *accepted* as the *Research Thesis submission* in partial fulfillment of the requirements for the award of degree of ***Doctor of Philosophy***.

Prof. Vijay H Desai
Research Guide

Dr. M.R. Ramesh
Research Co-Guide

Chairman - DRPC
(Signature with Date and Seal)

Dedicated to my parents and all teachers

ACKNOWLEDGMENTS

I thank Lord Shiva for giving me the confidence and presence of mind throughout this endeavor and completing this work without any problem. With respectful pranamas, my sincere gratitude towards his holiness **Dr.Sri Sri Sri Shivakumara Swamigalu**, for his blessings on the students through many years.

It is my great pleasure to express my heartfelt gratitude to my research supervisors **Prof. Vijay Desai**, Professor and **Dr. M. R. Ramesh**, Associate Professor, Department of Mechanical Engineering, National Institute of Technology Karnataka, Surathkal, Mangalore, for their exemplary guidance and encouragement throughout my research work. Their encouragement and the valuable suggestions have increased my knowledge level which led to the completion of my research work and are demonstrated through this thesis.

I sincerely thanks to the RPAC members, **Dr. M. R. Doddamani**, Department of Mechanical Engineering and **Prof. Subhash C. Yaragal**, Professor, Department of Civil Engineering for providing valuable suggestion and support extended to me on all occasion.

I wish to express my sincere thanks to **Prof. Shrikantha S. Rao**, Head of the Department, Department of Mechanical Engineering, National Institute of Technology Karnataka, Surathkal, Mangalore for their kind help in providing the facilities.

I sincerely thanks **Prof. Ramesh Singh** Department of Mechanical Engineering, Indian Institute of Technology, Bombay., **Mr. Dharmesh Gala**, **Mr. Hemanth Gourkar** and **Mr. Kapil Joshi**, Anton Paar India Pvt. Staff team of CeNSE-laboratory, Indian Institute of Science Bangalore, Bangalore Plasmatek, Bangalore NMTC-CMTI Bangalore and DST-PURSE lab Mangalore University for all the testing facilities.

Timely industrial support and lab facilities had helped to finish number of hurdles during the journey, i would like to thank Mr.Vasu B. Sr. Marketing Executive, LPS Industrial Supplies Pvt. Ltd., Mr. Girish, Srinivasa Indutries, Mr.Raveendra K. Quality Engineer, Oerlickon Blazers Pvt. Ltd., Mr. Prathiksha, Associate Project Engineer, DEP India Pvt. Ltd., and Ms. Prajwala, Tata Consultancy Services, for their selfless advice, assistance and contribution in this work.

The unfailing support of my colleagues had provided brilliant ideas, everlasting optimism and assistance. I am forever thankful to my friends Vinyas M., Vasu M., Ashrith H. S., Mithun B. R., Sapthagiri Prasad N., Arunkumar, Arun M. N., Nithin H. S., Gajanan Anne, Veeresh Nayak C., Mahantayya Matapati, Praveen T. R., Madhu Biradar, Nuthan Prasad, Deepak K., Shankar Kodate, Kiran R., Kiran Kumar D and Raghavendra P for their selfless advice, assistance and contribution in this work.

To my life-coach, my late grandfather Mr. K. E. Badiger because I owe it all to him. I would like to immensely thank my parents Mr. V. K. Badiger and Mrs. C. P. Varalaxmidevi. my sister Dr. Sushmitha V. Badiger their undying love, encouragement and moral support throughout my life and education. Without them and their blessings, achieving this goal would not have been possible.

(Pradeep V. Badiger)

ABSTRACT

The fretting and adhesive wear behavior of Ti, Al and Fe based thin solid films deposited on MDN121 steel substrate are studied. Plasma-assisted cathodic arc evaporation technique is used to develop TiC-C, Ti/TiN/TiCN/TiN/TiCN, AlCN/AlC and FeCrN coatings. FESEM-EDS, nanoindentation and Raman spectroscopy are used to characterize the coatings. The fretting and adhesive wear tracks are investigated using an optical profiler, confocal microscopy and electron microscopy. The diamond-like carbon (DLC) is observed in both the coatings. Developed coatings exhibit better mechanical properties with increase in hardness by 24.5 % in TiC-C and 29.4 % in Ti/TiN/TiCN/TiN/TiCN, 8.70 % in AlCN/AlC and 50.79 % in FeCrN coatings compared to the uncoated SNMG120408 WC substrate. During fretting wear analysis, TiC-C coating is exhibited lower coefficient of friction (COF) compared to Ti-multilayer coating. Similarly, FeCrN coating exhibited lower coefficient of friction (COF) compared to AlCN/AlC coating. The volumetric wear loss of TiC-C monolayer coating is better than the multilayer coating. The volumetric wear loss of FeCrN coating is better than AlCN/AlC coating. The wear surface morphology revealed abrasive form of fretting wear mechanism in all coatings whereas galling failure in the substrate. During adhesive wear analysis, TiC-C coating exhibited lower coefficient of friction (COF) compared to Ti-multilayer coating. Similarly, FeCrN coating exhibited lower coefficient of friction (COF) compared to AlCN/AlC coating. TiC-C, Ti/TiN/TiCN/TiN/TiCN, AlCN/AlC and FeCrN coatings exhibited low friction and high wear resistance.

Tungsten carbide cutting tool inserts are coated with customized composition of Ti/TiCN/TiN/TiCN/TiN (multilayer), TiC-C AlCN/AlC and FeCrN (monolayer) thin films using cathodic arc evaporation technique. Quality characteristics of coatings are evaluated using calo and VDI3198 tests. Thickness of the coatings are found to be in the range of 1.1-1.8 μm and adhesion quality of HF1 is attained. Machinability of highly alloyed steel MDN431 is studied using the coatings developed on SNMG120408 inserts. The

performance of coated tool inserts are evaluated using cutting speed (59-118 m/min), feed rate (0.062-0.125 mm/rev) and depth of cut (0.2-0.4 mm) as process parameters in turning MDN431 steel. Experiments are conducted based on full factorial design and regression analysis is used to analyze the cutting forces and surface roughness. Optimization of the process parameters has been done with the combination of desirability approach and PSO technique. Optimum machining condition for least cutting force and least surface roughness are obtained at the condition of Vc=118 m/min, f=0.063 mm/rev and ap=0.2 mm for Ti-multilayer coatings, Vc=59 m/min, f=0.063 mm/rev and ap=0.2 mm for TiC-C coatings, Vc=75 m/min, f=0.063 mm/rev and ap=0.3 mm for AlCN/AlC coatings and Vc=118 m/min, f=0.063 mm/rev and ap=0.2 mm for FeCrN coatings. ANN modeling has been adopted in order to improve the coefficients of determination (COD) and capability of predictive regression models. ANN trained model and mathematical regression models predict the responses, which follows the experimental data with minimum absolute error. The predicted results are validated with minimum error and developed models are adequate for further their usage. Tool wear was reduced by 3 times in Ti-multilayer, 3 times in TiC-C, 3.62 times in AlCN/AlC and 1.63times in FeCrN coated tools compared with commercially available uncoated WC-Co inserts (SNMG120408).

Keywords: Ti-based thin films; monolayer and multi-layer; Fretting wear; Adhesive wear; Diamond-like carbon; cathodic arc evaporation; Al-coating; Fe-coating; Superalloy machining; PVD; Full factorial-optimization; ANN modeling; PSO-optimization.

Contents

List of Figures

List of Tables

NOMENCLATURE

GAXRD	Glancing Angle X-ray Diffraction
SEM	Scanning Electron Microscope
EDS	Energy Dispersive Spectroscopy
FFD	Full Factorial Design
OA	Orthogonal Array
DOE	Design of Experiments
RSM	Response Surface Methodology
ANOVA	Analysis of Variance
GA	Genetic Algorithm
PSO	Particle Swarm Optimization
ANN	Artificial Neural Networks
PVD	Physical Vapour Deposition
CVD	Chemical Vapour deposition
DLC	Diamond-Like-Carbon
CAE	Cathodic Arc Evaporation

Symbols

F_x	Axial force	N
F_y	Radial force	N
F_z	Tangential force	N
V_b	Tool wear	μm
V_c	Cutting speed	m/min
a_p	Depth of cut	mm
f	Feed rate	mm/rev
R_a	Surface roughness	μm
SS	Sequential sum of squares	
$Adj.SS$	Adjusted sum of Squares	
MS	Mean square	
F	F-ratio Value	
P	Probability	
R^2	Coefficient of determination	

Chapter 1

INTRODUCTION

Nature is the blend of natural and artificial objects. Each object is expected to meet several specifications like Iron should be strong, but should also not corrode. Sometimes the specifications may be conflicting with each other. Typical examples to quote include; Gold ornaments should not be soft, but should be glittering. An ornament should have the look of gold but not too expensive. Since prehistoric times man has developed different techniques to achieve the required material properties. Surface engineering provides solutions to degradation, oxidation, corrosion and wear of materials which occur as a consequence of surface conditions or properties. Surface engineering provides an answer to the problems related to surface degradation and failures.

1.1 Surface engineering

ASM Handbook defines surface engineering as *"Treatment of the surface and near surface regions of a material to allow the surface to perform functions that are distinct from those functions demanded from the bulk of the material"*.

The desired characteristics of surface engineered components include:

- Improved corrosion resistance through a barrier or sacrificial protection.
- Improved oxidation and/or sulfidation resistance.
- Improved wear resistance.

- Reduced frictional energy losses.
- Improved mechanical properties.
- Improved oxidation and/or sulfidation resistance.
- Improved electronic or electrical properties.
- Improved thermal insulation.
- Improved aesthetic appearance.

These properties can be enhanced metallurgically, chemically or by adding a thin or thick film coating as listed in Table 1.1.

Hard surface development on the material is of the important factor to increase the life of parental surface which is the inspiration for the development of the hard surface. Modification of the surface properties of a solid by appropriate coatings has been practiced by man since prehistoric days. Hard surface is used by mankind in the manufacturing of various cutting tools since 1960. The term hard coatings refers to the property of high hardness in the mechanical sense along with good tribological properties. The development of modern technology can be seen in the areas of optical, optoelectronic, optical, manufacturing and defense applications.

The definition of the term hard coatings is *"The coatings which operate satisfactorily in a given environment can be said to be hard with respect to that environment"*.

Different hard coatings are listed in Table 1.2.. Introduction of innovative technologies like electroplating and physical vapour deposition in vacuum over the past hundred years has resulted in unparalleled growth in the entire field of science and technology. During the past two decades, non-equilibrium plasmas have revolutionized the surface coating technologies opening a variety of applications which are otherwise impossible. The thin - film coating is one of the oldest arts and one of the newest sciences.

1.2 Vapor deposition technique

Vapor deposition technique is to vaporize and deposit metal or alloys which are hard and wear resistant coatings on the substrates (example: steel, tungsten carbide, aluminium). Vacuum environment is one of such environments which protects the processes against

Table 1.1: List of surface engineering methods (Bhat, 1999)

Sl. No	Surface Treatment	Methods	Property benefits
1	Changing the surface metallurgy	Surface hardening Laser melting	Wear resistance
		Shot peening	Fatigue strength and stress relieve
2	Changing the surface chemistry	Carburizing	Wear and fatigue resistance
		Nitriding	Wear, fatigue and corrosion resistance
		Boriding	Oxidation and surface fatigue
		Laser alloying	Wear resistance
		Ion implantation	Friction and wear resistance
3	Adding a surface layer or coating	Organic coatings (paints)	Aesthetic appearance and linings
		Ceramic coatings	Corrosion resistance and porcelain enamels
		Electroless-plating	Corrosion resistance and electrical properties
		Physical vapour deposition	Improved wear (tools and dies), erosion and corrosion resistance
		Chemical deposition	Improved wear (tools and dies), Improved optical and electronic properties and decorative applications

Table 1.2: Classifications of hard materials (Bhat, 1999)

Tribological hard	**Wear resistant and low friction.**
Optically hard	Laser, and photonically inert.
Radiation hard	High threshold energies for energetic particles such as gamma rays, neutrons, and beta particles.
Electrically hard	High band gap and large electron velocities.

attack from atmospheric gases. Large mean free paths and low boiling points of target in a vacuum are helpful in depositing thin films. Vapor deposition techniques are classified as mentioned in Table 1.4.

Types of Vapor deposition technique:-

- Physical vapor deposition (PVD)
- Chemical vapor deposition (CVD)

1.2.1 Physical vapor deposition

Physical vapor deposition (PVD) processes (often called thin film processes) are atomistic deposition processes in which material is vaporized from a solid or liquid source in the form of atoms or molecules, transported in the form of a vapor through a vacuum or low-pressure gas (or plasma) environment to the substrate where it condenses. Typically, PVD processes are used to deposit films with thicknesses in the range of a few nanometers to thousands of nanometers. However, they can also be used to form multilayer coatings, graded composition deposits, very thick deposits and freestanding structures (Mattox, 2010). Material to be deposited is heated and vaporized in a vacuum. The vapors condense on the substrates which are kept at specified distance from the vapor sources. Very often the substrates are cleaned in-situ using glow discharge plasma. This improves the adhesion of the film. Increasing the substrate temperature improves the adhesion further and helps in getting denser films with fewer voids. Resistive heating, high energy electron beam heating and induction heating are some of the options available for vaporizing the source material.

Using several sources and several reactive gases, it is possible to deposit multi-layer films. Its applications include metallization for packing, decorative coatings, electronic industries, machining tools like inserts, drill bits etc., and coating on wear resistant surfaces.

1.2.2 Chemical vapor deposition

Chemical vapor deposition (CVD) is defined as the deposition of solid material from the vapor phase onto the heated substrate due to chemical reactions (reduction or decomposition). Reduction is normally accomplished by hydrogen at high temperature. Decomposition is accomplished by thermal activation. Table. 1.3 shows the characteristics of PVD and CVD processes.

Table 1.3: Characteristics of PVD and CVD processes (Mattox, 2010; Mattox and Mattox, 2003)

Description	**Physical Vapor Deposition**		**Chemical Vapor Deposition**
	Evaporation	**Sputtering**	
Method of production of vapors from targets	Thermal energy	Momentum transfer	Chemical reaction
Deposition rate	Very high (up to 750,000 Å/min)	Low except for pure metals (Cu-10,000 Å/min)	Moderate (200–2,500 Å/min)
Depositing species	Atoms and ions	Atoms and ions	Atoms
Metal deposition	Yes	Yes	Yes
Alloy deposition	Yes	Yes	Yes
Refractory compound deposition	Yes	Yes	Yes
Energy of deposited species	Low (0.1–0.5 eV)	Can be high (1–100 eV)	Can be high with plasma-aided CVD

Table 1.4: Classifications of PVD and CVD process (Mattox and Mattox, 2003)

Physical Vapor Deposition processes	
Metal	**Compounds**
Basic PVD Processes	Basic PAPVD Processes
Evaporation Deposition	Activated Reactive Evaporation (ARE)
Sputter Deposition	Reactive Sputtering (RS)
"Ion Plating"	"Reactive Ion Plating"
Chemical Vapor Deposition processes	
Basic CVD Process	Basic PACVD Processes
	RF Excitation
Thermal CVD	Microwave Excitation
	Photon Excitation

Among the PVD and CVD techniques, Vacuum arc deposition is generally more often accepted deposition technique. Plasma process is reported as versatile technology and it has been adopted in many industries due to its flexibility, cost-effectiveness and superior quality of the coating produced. Arc deposition techniques can produce thin coating films in the range of 500 nm to 4 μm. In this process, there won't be any degradation of mechanical properties of the substrate. In order to get a good adhesion between the coating and the substrate, it must be ground, polished and lapped to the surface roughness of less than 0.1 μmm (Harlin *et al.*, 2006).

1.3 Applications of thin film coatings

Thin films have significance for large industrial applications. Depending upon their area of interest, coatings are decided. Which include manufacturing engineering and processing, optical, chemical, optoelectronics, thermal power plants and biomedicines is briefed in Table 1.5.

Table 1.5: Applications of thin film coatings (Bhat, 1999)

Field	Applications
Manufacturing Engineering and processing	1. Tribological Applications: Protective coatings to reduce wear, corrosion and erosion, low friction coatings
	2. Hard coatings for cutting tools
	3. Surface passivation
	4. Protection against high temperature corrosion
	5. Self-supporting coatings of refractory metals for rocket nozzles, crucibles, pipes
	6. Decorative coatings
	7. Catalysing coatings
Optical	1. Anti-reflex coatings (”Multicoated Optics”)
	2. Highly reflecting coatings (laser mirrors)
	3. Interference filters
	4. Beam splitter and thin film polarizers
	5. Integrated optics
Chemistry	1. Diffusion barriers.
	2. Protection against corrosion & oxidation.
	3. Sensors for liquid & gaseous chemicals.
Optoelectronics	1. Photo detectors
	2. Image transmission
	3. Optical memories(CD/DVD/BRDVD)
	4. LCD/TFT
Thermal power plants	1. Solar collectors and solar cells
	2. Thermal insulation (metal coated foils)
Bio medicines	1. Biocompatible implant coatings
	2. Neurological sensors
	3. Claddings for depot pharmacy

1.4 Coatings on cutting tools

Cutting tools are the materials used to remove the material from the workpiece by shear deformation. Shearing may happen by a single point or multipoint cutting tools. Single

point cutting tools are used for turning, shaping, planning and similar operations. Multi point cutting tools are used for milling, grinding and drilling operations. Cutting tools are made of a material harder than the material to be cut. Over the time solid HSS tools were replaced by tungsten carbide inserts Figure (1.1).

Figure 1.1: Commercial coatings developed by Oerlickon Balzers on cutting tools [Photo courtesy: Oerlickon Balzers Pvt. Ltd. India]

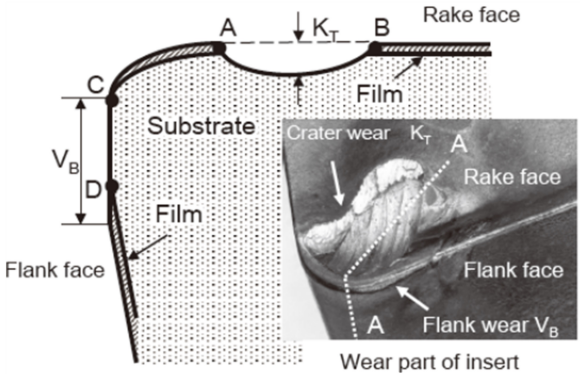

Figure 1.2: Cross section A-A at the wear part of insert (FUKUI, 2016)

Tool wear of the WC-insert is indicated in Figure 1.1 (FUKUI, 2016). Performance of carbide inserts is less percentage compared to conventional tools. To improve the tool performance and tool life, in 1969 coating of cutting inserts with a thin ceramic film was begun by the West German company Krupp. Krupp used thermal CVD to deposit carbide cutting inserts with titanium carbide (TiC) film. Thereafter, carbide cutting insert manufacturers in Japan and abroad competed fiercely to develop coated cutting inserts.

In 1976, Sumitomo Electric developed a cemented carbide substrate provided with the Company's proprietary tough surface layer, surpassing the earlier technology of other manufacturers. Subsequently, the use of CVD-coated inserts grew remarkably.

Figure 1.3 shows features of tool inserts that indicate the reduction in tool wear and hence improvement in the tool life due to coating (FUKUI, 2016). It is evident from the above discussion that thin solid films are developed on the tool surfaces to hold a great potential for research, specifically, their performance in machining of steels are noteworthy. When the tool wear resistance at elevated temperature is required, the application of Ti-based coatings has received widespread use. Al-based and Fe-based coatings are the new types of coatings where research is minimal. There are several challenges faced by the manufacturers for the coating development based on its application (material to be machined) which gives the present research investigation a goal to establish firm grounds on betterment in this regard. The present investigation aims to study the microstructure, mechanical properties and performance of hard thin film coatings.

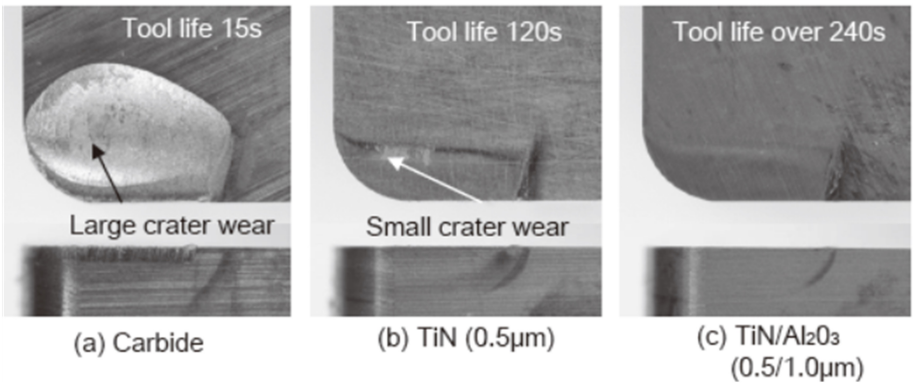

Figure 1.3: Comparison of tool wear after alloy steel turning (FUKUI, 2016)

1.5 Outline of the thesis

The thesis has been presented in 5 chapters:

Chapter 1 introduces surface engineering, vapor deposition techniques, application of thin film coatings, coatings on cutting tools.

Chapter 2 gives a detailed review of the published literature relevant to the present study. The literature review presented mainly include earlier research work carried out on development of alloys for turbine applications, surface coatings, physical vapour depositions, characterization of thin films, wear behavior of thin films and machinability studies using coated inserts. The broad objectives of the present research work are drawn based on the gaps observed in available literature.

Chapter 3 provides description of equipment and the various characterization techniques used for analysis of microstructural features, mechanical properties, fretting wear, adhesive wear and machinability characteristics using coated inserts.

In chapter 4 the results and discussion of experimental investigations have been included. The results of coating development, microstructure, mechanical, physical properties, coating quality characteristics, fretting wear behavior, adhesive wear behavior, wear track deformation studies and machinability characteristics are discussed.

Chapter 5 presents the conclusions drawn based on the results obtained in this research work and future scope of work is also enlisted.

Chapter 2

LITERATURE SURVEY

A detailed review of the published literature relevant to the present study is presented in this chapter. Literature review is discussed with reference to the development of alloys for turbine applications, surface coatings, physical vapor depositions, characterization of thin films, the study of wear on thin films and machinability studies using coated inserts.

The present work has been motivated by the excellent wear resistant properties exhibited by the PVD thin film coatings. The life of the tool is an essential factor in the industries. PVD coatings on the drill bits, tool inserts and milling inserts not only increase their lives but also produce the best performance compared to conventional tools. Thin film coating on the alloys for turbine application is to improve its performance, surface properties and to improve its wear resistant properties. PVD is the most accepted method for the development of thin film coating on the surfaces due to versatility on the process parameters. The literature survey is based upon the development of alloys for turbine applications, thin film surface coatings, characterization of coatings, tribological properties and machinability studies using coated materials.

2.1 Development of alloys for turbine application

In the turbine industries, the operating temperatures are between 900-1600°C. In modern industrial turbines, the inlet temperature exceeds 900°C and in addition, the life

requirement demand for the highly loaded high-temperature components are of the order of 25,000-50,000 hours (Benea *et al.*, 2015). Further the efficiency requirements limit the amount of compressed air available for cooling of turbine parts (Bunshah and Weissmantel, 2001) . During operating conditions, blades and vanes of the gas turbine are subjected to high-temperature stresses, thermal fatigue and these turbine components also undergo chemical attack like oxidation and corrosion due to molten alkali sulphates. It is almost impossible for a single material to have properties to withstand the above requirements (Sidhu *et al.*, 2005). So, alloying of materials with different elements is necessary so that the components can work under highly critical environment and reach the demand (Budinski, 2007; Bunshah and Weissmantel, 2001; Eriksson, 2013; Eriksson and Olsson, 2011; Jegadeeswaran *et al.*, 2014; Kong *et al.*, 2015, 2018; Sidhu *et al.*, 2005; Whitehouse, 2010).

Figure 2.1 shows drastic reduction in chromium content (from 15 to 3 weight %) in the Ni-based super alloy composition since 1960 while still retaining better oxidation and corrosion resistance. The Al content has increased to about 5 weight %. The interesting fact is that over the 30 years period between 1965 and 1995 the refractory element contents, such as additions of tantalum, rhenium, tungsten and molybdenum have increased from 8 to 20 weight percent, which resulted in increase of high-temperature strength on account of solid solution strengthening (Pomeroy, 2005; Rajendran, 2012). The reasons for these changes in composition are twofold; one is for promoting strengthening mechanisms involved in developing Ni-based alloys and the other for optimum creep resistance at temperatures up to 1100°C (Kumar *et al.*, 2018).

Co-based superalloy has cobalt as primary element along with many alloying elements like Cr, W, C and Ni. Chromium provides protection against hot corrosion and oxidation with a small percentage of Al, Zr and Ce, whereas W, Mo, Ta, Cb strengthen the metals due to solid solution strengthening. Carbon forms carbides with Cr which acts as the primary means for alloy strengthening. Since the crystalline structure of Co is HCP, it does not possess good ductility (Bernstein *et al.*, 1993, 2006; Castelli, 1996). The addition of Ni

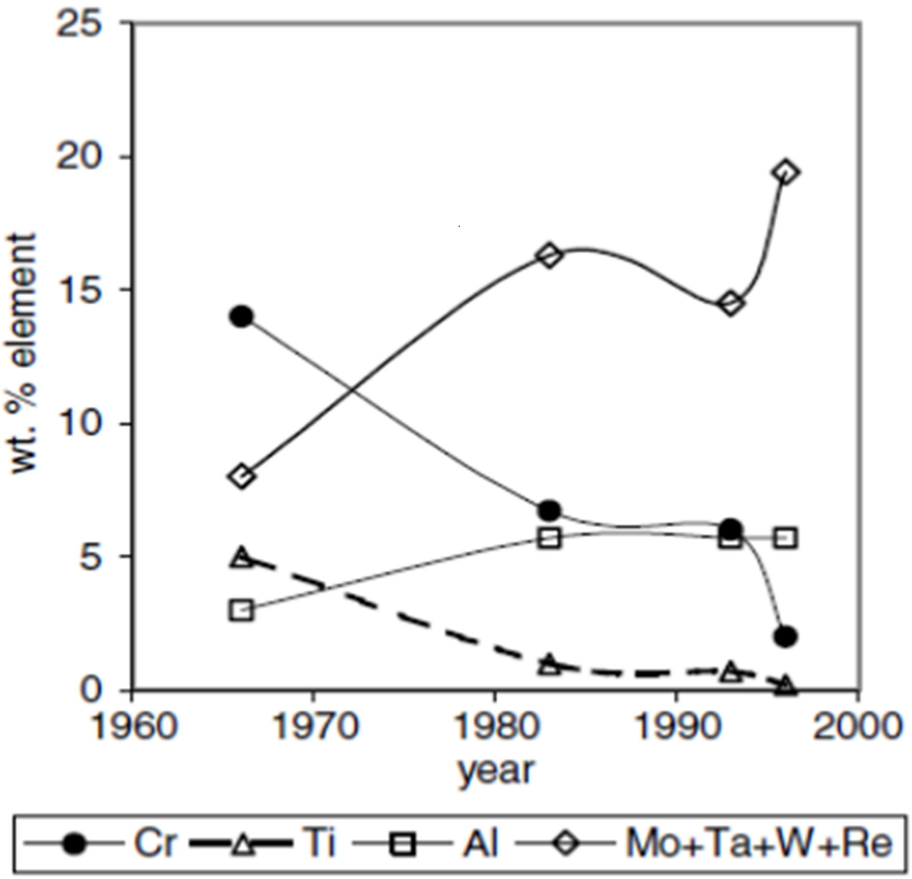

Figure 2.1: Variations in alloying element additions to Ni based alloys (Pomeroy, 2005; Rajendran, 2012)

helps Co-based superalloy to maintain FCC crystal structure and hence provides ductility.

Iron base superalloys such as Fe-(25-27 % Ni), 13.5 to 16 wt % Cr with the addition of Mo, Si, Ti & Al are used at lower operating temperatures, as their strength rapidly reduces above 650°C (Castelli, 1996).

Titanium alloys have been increasingly used in aerospace, biomedical, and chemical industries due to their very high strength to weight ratio, good fatigue strength, biocompatibility, and high corrosion resistance. Although titanium-based alloys exhibit good corrosion resistance due to the formation of Titania on its surface, the nature, composition and thickness of the protective oxide scales are also dependent on environmental conditions (Anuwar *et al.*, 2007).

Development of these alloys has been made to improve mechanical properties to be sustained in a high-temperature environment. However, low Al content in the alloy composition does not have the necessary intrinsic resistance to oxidation and corrosion which is required for the long-term operation associated with gas turbine and boiler operation. To overcome these problems there is a need for surface modification, in terms of coating. Material and coating techniques have been selected based on the environment in which component has to perform its intended function. The substrate material provides necessary mechanical strength to the component. The coating protects the component effectively from a variety of environmental degradation factors such as abrasion, erosion, wear, fretting, oxidation and corrosion. Literature indicates that there is no single coating that meets all the environmental degradation issues (Rajendran, 2012).

2.2 Surface coatings (thin films)

Surface engineering is done to modify or improve the properties of the surface and near-surface region in a desirable way. Surface engineering involves an overlay process or a surface modification process. One such method to improve the life of the surface is by providing coating on the surface. The composition and the coating techniques are chosen to improve the corrosion, erosion wear and oxidation of the surfaces against the various thermal conditions prevailing in the industrial applications. Among the many coating techniques, physical vapor depositions (PVD) techniques are most preferred for cutting tools, wear resistant surfaces and also for any high-temperature applications. This technique has shown good ability for different types of coating materials.

To increase the performance of the tool, reduce tool wear and to increase its life PVD coating is preferred. Powell, Oxley and Blocher first penned the term physical vapour deposition in their book “Vapor deposition” during 1966. PVD processes were developed much earlier (Mattox, 2010); evolution of plasma, laser, and vapor deposition technologies is represented in Figure 2.2 (Halling, 1976).

PVD coatings are relatively hard surfaces and hence are called hard coatings. The thickness

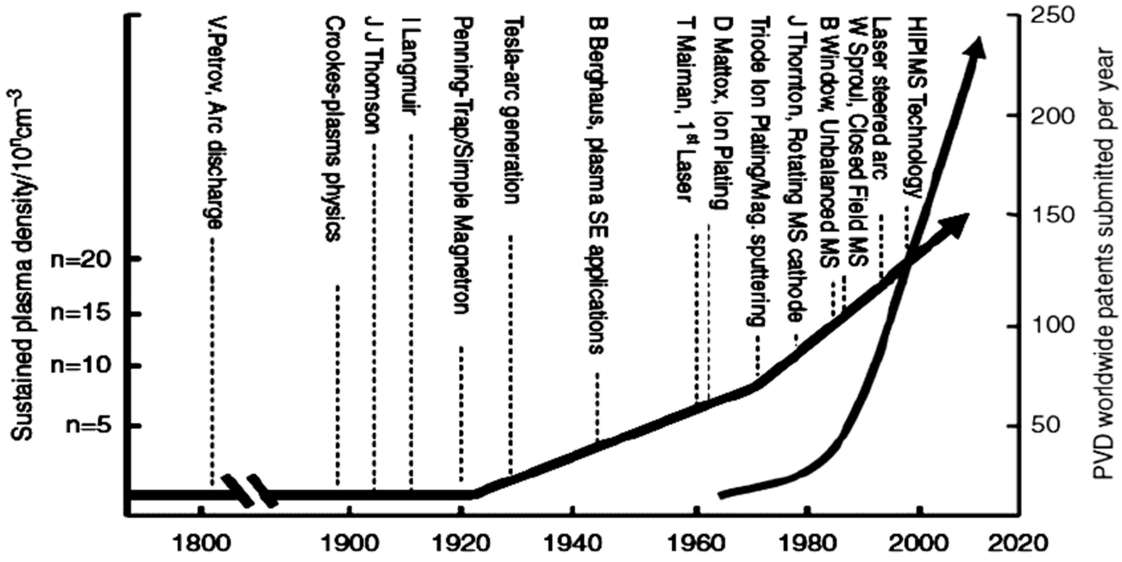

Figure 2.2: Evolution of plasma, laser, and vapor deposition technologies (Halling, 1976)

of the coatings is less than 10 μm, so they are also termed as thin film coatings.

2.3 Physical vapour deposition

In physical vapour deposition technique, the target material (material to be coated) is vaporized and vapors are transported on to the substrate in vacuum. The vapour gets condensed on the substrate surface. Singh *et al.* (1999) have listed numerous types of processes under PVD coating techniques.

- Thermal evaporation
- Electron beam evaporation
- Sputtering
- Balanced and unbalanced magnetron sputtering
- Direct current diode sputtering
- Radio frequency sputtering
- Triode-assisted PVD
- Cathodic Arc/ Vacuum arc deposition

Among the types of PVD coatings, vacuum arc deposition has been reported to be versatile technology and proved to be a successful, reliable and cost-effective solution for many industrial problems (Prabhakara). The coatings of CrN and CaAlN was developed on the Cu alloys substrate and its tribological properties and characterization of coating studied by (Wilson *et al.*, 2012).

The coatings of monolayer thin and multilayered TiN/CrN, TiN/MoN, TiN/NbN and TiN/ TaN were developed on cemented carbide using a hybrid PVD process consisting of deposition of TiN by ion plating and CrN, MoN, NbN and TaN by magnetron sputtering (Nordin *et al.*, 1999*a*,*b*) . It is evident from their reported results that mechanical properties and the abrasive wear resistance were beneficially improved for the multilayered structure of thin hard PVD coatings.

Dearnley et al (2001) have claimed that TiC and TiN coatings could be developed by using $TiCl_4$ as a target material (Brookes, 2018; Dearnley, 2007; Halling, 1976). The chemical exchange reactions are shown below.

$$TiCl_4 + (H_2) + CH_4 \rightarrow TiC + 4HCl + H_2$$
$$TiCl_4 + C + 2H_2 \rightarrow TiC + 4HCl$$
$$2TiCl_4 + N_2 + 4H_2 \rightarrow TiN + 8HCl$$
$$2TiCl_4 + 2C + N_2 + 4H_2 \rightarrow 2Ti(C+N) + 8HCl$$

CrN coatings are gaining much importance because of its widespread industrial applications. CrN coatings were developed using the low voltage thermionic arc sputtering technique. At a temperature of 480°C CrN coatings were developed for H11 steel mold and the properties of the mould surface showed remarkable improvement (Navinšek *et al.*, 1997). For the enhancement of hardness of single crystal, super-lattice films were made by sputtering of polycrystalline nitride super-lattice films on polycrystalline substrate materials. TiN/NbN and TiN/VN coatings have been developed. Nitride super-lattice films such as TiN/VN and TiN/NbN have hardness that matches the hardness of cubic boron nitride which is known to be the second hardest material (Ono *et al.*, 2008).

Harlin *et al.* (2006) developed TiN and WC/C coatings high-speed steel (ASP 2023) samples prepared by powder metallurgy route. The substrate surface was prepared by grinding with different grade polishing papers and then the TiN and WC/C coatings were developed on HSS samples. Pre-coated surface topography and coated substrate topography studies under SEM showed that the polished surface has better surface adhesion. Authors have reported no adhesive or cohesive failure in the load range of 0-100 N, except cracking within the scratch track and minor chipping.

Plasma nitriding was the pre-treatment process used for the improvement of corrosion resistance of PVD coatings on low alloy steel. PVD coatings of graded zirconium carbide layers (ZrCg) and graded chromium carbide layers (CrCg) are developed on heat treatable low steel alloy protect against corrosion and wear. These PVD coatings for corrosion resistance should have very smooth surface and plasma nitriding is also recommended for that. From the wear test results, it was inferred that there was no influence of nitriding (Durst *et al.*, 2008).

Jao et al, deposited Ti-Cu-DLC onto the Si substrate using the cathodic arc evaporation process in which alloy of titanium and copper was used as the target material. Acetylene gas was used as the carbon sources, which was activated at 180^{o} C at 20 mTorr. Substrate bias voltage was varied between 80-205 V and used to provide the (Ti: Cu)-DLC structure. The deposited (Ti: Cu)-DLC films had a multi-layered structure where nanocrystalline Cu-layers alternated with amorphous Ti-DLC layers. The films deposited at 150 V exhibited the highest hardness (Jao *et al.*, 2010).

Ti–C–N films were deposited on silicon (100) and W6Mo5Cr4V2 steel substrates in a PBAIP system. In the coating system, circular graphite and Ti cathodes were placed opposite side of the chamber wall. The surfaces of the substrate surface were polished to the surface roughness of 50nm with the help of diamond paste. The bias voltage of the coating system was varied from $-100V to -700V$. With the applied bias voltage of $-300V$ the formation of a typical nanocomposite structure of Ti(C, N) nanocrystallites embedded in a DLC matrix was observed, leading to a relatively high film hardness (Zhang *et al.*,

2014).

CrN & TiCN coatings were developed on Ti-6Al-4V substrate by Marin *et al.* (2016). Thermal diffusive treatments: Nitriding and carburizing were implemented with the coating process. Morphological studies clearly showed that there was an increase in surface roughness of the coatings after thermal treatment with a subsequent increase in TiC and TiN rich layers and a consequent volume increase. Improvement in hardness has been observed with the results of carburizing and nitriding.

2.4 Characterization of thin films

In the PVD coating process, adhesion of the coating to the substrate is the most important factor to be considered. Valli (1986) has explained various methods to measure the adhesion which include direct pull off, body force method, acoustic method, scratch test and so on. From various trails and experiments Valli (1986) has concluded that the scratch test appears to be the most suitable practical method to study the adhesion of hard tribological coatings.

Ti and TiN coatings were developed on the Aluminium-Silicon alloys. The substrate was thoroughly polished and degreased before the coating process. Coatings were developed by a conventional ion plating process under different discharge current densities. The adhesion test adapted was very similar to the standard scratch hardness test. The tests were conducted on a microhardness tester using 120° diamond indenter. The test technique was to plough the diamond indenter on the coating using various loads (0.05 N - 5 N). With the increase in loading, the scratch became wider and at a certain critical load chipping of the coating took place at the rim of the groove (Ashrafizadeh, 2000).

To prevent the delamination's of DLC coating layer, intermediate TiCN layer was coated on Ti-6Al-4V using the filtered arc method. The presence of TiCN interlayer is exhibited the better hardness, elastic modulus, and interface bonding of the thin film (Kang *et al.*, 2015).

Ti-6Al-4V was coated with Ta-O ceramic layers using PVD magnetron sputtering. The

coated samples were heat treated at 300, 400 and 500 °C to investigate the enhancement in the adhesion strength. The study revealed the coating to be more sensitive to the thermal surface treatment. The highest adhesion strength was observed at 500°C C. The formation of Ta_2O_5 during thermal treatment was cited as the reason for the increase of the adhesion strength (Rahmati *et al.*, 2015).

CrN and TiN hard coatings were developed on steel, sapphire and alumina substrates using a plasma beam sputtering process. The microstructure of the surface of the coating was observed under STEM. Cross-sections of the coatings were observed using SEM microscopy, hardness of the coatings was measured using the Vickers hardness tester (Milošev *et al.*, 1997).

TiN and TiAlN coatings were developed on a V820 nitridable steel and hardness of the coating was determined using nanoindentation. From the indentation test, it was found that coatings remained intact during deformation at the indented region. Cracks were observed with columnar in the TiN coating and shear steps were observed at the steel-coated substrate (Ma *et al.*, 2006).

Coating hardness and Young's modulus were determined by nanoindentation for TiN and TaN coatings developed on the HSS substrate. It is reported that the experimentally measured hardness was higher than the hardness value suggested by the simple rule of mixture (Nordin *et al.*, 1999*b*).

TiN/TiAlN coatings were developed on steel substrate, TiN/TiAlN single layers were polycrystalline, exhibiting diffraction peaks with the preferred orientation along (1 1 1) plane. Diffraction peaks of (1 1 1), (2 0 0), (2 2 0), (2 2 2) for TiN and (1 1 1), (2 2 0) and (2 2 2) for TiAlN peaks respectively, were observed in the XRD pattern. The close observation using SEM and TEM resulted smaller particle size of TiN/TiAlN. Raman spectra for the single and multilayer coatings were studied, TiN coatings exhibited the characteristic peaks at 209 and 318 cm^{-1} and TiAlN coating exhibited the characteristic peaks at 253 and 673 cm^{-1} (Ananthakumar *et al.*, 2012).

2.5 Studies on wear of thin films

Many researchers have investigated on the wear behaviour of thin films deposited by PVD technique. TiN and TaN coatings were developed on the HSS substrate. Coatings were developed by the Balzers BAI640R apparatus by magnetron sputtering. Tribological studies with abrasive and erosive wear were conducted for multi-layered coatings. From the performance studies of coatings, it was witnessed that multi-layered coatings were more wear resistant compared to single layer coating (Nordin *et al.*, 1999*b*).

Hsu *et al.* (2013) developed Ti-N-O coatings on AISI 304 SS substrate considering the variation in the oxygen and nitrogen gas content. Wear tests were conducted by using the ball-on-disc tribometer. The counterface material was a WC-6 % Co ball (1780Hv). Tests were conducted with speed of 0.2 m/s, load of 5 N without lubricant at 25°C (3 trials each) and total travel distance was 600 m. The friction coefficient was measured continuously during tests and wear rate was measured by weight loss method.

Study on the frictional behaviours of the TiN/TiAlN coatings under a normal load of 3.924 N showed that multilayer coated film exhibits a relatively lower coefficient of friction compared with single layer and substrate. The enhanced wear resistance of TiN/TiAlN multilayer coatings can be attributed to factors such as high hardness and decreases in the coefficient of friction. The interfaces in the multilayer coating act as crack inhibitors, thereby increasing the fracture resistance due to crack deflection at the interfaces, crack tip shielding by plastic deformation (Ananthakumar *et al.*, 2012).

The wear performances of PVD Ti/TiN multilayer coatings were investigated under two different types of wear tests; body abrasion and particle erosion using diamond slurry and silicon carbide particles as an abrasive medium. Increase in the amount of metallic Ti in the Ti/TiN multilayer coating resulted in an increase in abrasive wear rate. In erosion, the lowest wear rate was recorded for the homogeneous TiN coating. For the Ti/TiN multilayer coatings, the erosion rate was found to decrease with an increasing relative amount of metallic Ti in the coatings (Bromark *et al.*, 1997).

CrN, (Ti, Al) N and CrC/C DLC-based coatings were developed on high-speed steel. Tribological properties of the coatings have been investigated using pin-on-disk tribometer under sliding contact and lubrication. In the wear studies, the hardness of the substrate was observed to have a strong influence on the friction characteristics and galling resistance of the substrate. Chances of chipping are more in the brittle coatings due to low hardness of the substrate. For the coatings investigated, it is reported that the cracking tendency increased with increasing coating hardness (brittleness), i.e. in the order CrC/C–CrN–(Ti, Al)N (Eriksson and Olsson, 2011).

Fretting wear is the technique used to evaluate the performance of the cyclic wear mechanism which occurs between mating surfaces (thin solid films) (Benea *et al.*, 2015; Kreines *et al.*, 2004). Diamond film developed on a steel surface with CrN interlayer resulted in a linear relation between its life span and coatings thickness. Wear rate of the coatings was independent of the coating thickness (Kreines *et al.*, 2004).DLC layer as a topcoat on the SiCN layer provided protection against mechanical damage and helped in insulating from defects while SiCN sublayer acted as a barrier layer. Wear resistance of TiN particles, were linearly dependent on its surface morphology and uniformity of distribution in Al medium. Al/TiN layer experienced both abrasive and adhesive wear (Hashemi and Hussain, 2015). Wear counter face and wear scar for the coatings were measured by the amount of deformed area after the wear test. Wear measurements were carried out using electron microscopy and profilometry techniques. As per literature Al-based thin films are very minimal in number, namely AlN, Al-Cr, Al-Cr-(N), Al-Ti coatings. These are developed by using RF magnetron sputtering. Electrical, structural properties were investigated for the solar concentrator application. AlN coated on Si/quartz showed good electrical conductivity. AlN films deposited on Cu using an Al underlay showed good electrical insulation which can be helpful for solar applications. In Al-based coatings, corrosion resistance is strongly dependent on the Cr content in the coatings (Creus *et al.*, 2004; Kale *et al.*, 2012; Sanchette *et al.*, 1995).

2.6 Machinability studies of materials using thin film coated cutting tools

In manufacturing industries, turning operations have been reported as more flexile among the different machining processes. All of the manufacturing processes need to be optimized and standardized for better productivity and also to reduce the capital investment. Machining process has been improved over the time by through various optimisation techniques and proper selection of cutting parameters. Tool wear, machined surface texture, surface roughness characteristics and cutting forces are the prime factors considered for the improvisation (Chabbi *et al.*, 2017; Das *et al.*, 2018, 2015; Grzesik *et al.*, 2018; Kumar and Chauhan, 2015; Mia and Dhar, 2016; Musfirah *et al.*, 2017; Suresh *et al.*, 2015, 2012; Zhang *et al.*, 2015). Machining of hard-to-machine materials which include Incoloy, Inconel and other superalloys require proper selection of cutting tool combination. Physical vapor deposition (PVD) coated tools provide solutions for problems associated with machining of the hard-to-machine materials (Arulkirubakaran and Senthilkumar, 2017; Kıvak, 2014) . Performance of the PVD coated tools has been evaluated using the machinability characteristics (Coelho *et al.*, 2007; Das *et al.*, 2015; Grzesik *et al.*, 2018; Sahoo and Sahoo, 2013*a*,*b*; Scheerer *et al.*, 2005; Zhang *et al.*, 2015). Machinability characteristics provide a correlation between process parameters and responses. Statistical and parametric techniques help in optimisation, validation and error analysis of the machinability characteristics (Anderson and Whitcomb, 2016; Hanief *et al.*, 2017; Hirano and Yoshikawa, 2012; Malghan *et al.*, 2017; Manjaiah *et al.*, 2016).

Highly alloyed steel finds wide usage in the aerospace and defense industry as a material for turbine blades and turbine shaft. It is a well-known fact that turbine materials are subjected to several types of tribological failures. With proper alloying, mechanical properties of the turbine materials are tailored for such applications; however, they become hard-to-machine materials with increased strength and hardness. PVD/CVD coated inserts provide an answer to these problems; with the presence of hard metallic carbide, metallic nitride

and DLC in the coatings. Various researchers have worked on PVD coated steel substrates and experimented for wear resistant studies of the coating (Badiger *et al.*, 2017; Cheng and Zheng, 2007; Kreines *et al.*, 2004; Li *et al.*, 2013; Miyoshi, 1996). Generally, most of the material failure originate on the surface of the material. Surface engineering provides an answer to the problems related to surface degradation and failures. PVD is state of art technique using which little modification of the surface leads to tremendous improvement in life (Ibrahim *et al.*, 2015).

Under PVD coating technique numerous types have been developed over the time which include cathodic arc evaporation, magnetron sputtering, direct sputtering and so on (Efeoglu and Bulbul, 2005).Various researchers have concluded that cathodic arc evaporation is most reliable coating technique. Using cathodic ion plating pre-treatment for the substrate was done with plasma nitriding techniques for the development of AlCrSiN, CrSiBN, and TiAlN coatings (Abusuilik, 2015). Plasma nitriding pre-treatment on substrates resulted in the superior quality of adhesion for AlCrSiN coatings. Advanced characterization techniques were used to evaluate the mechanical properties, crystal structure, and morphology of the coatings was calculated using the nanoindentation, GAXRD and FESEM-EDS (Badiger *et al.*, 2017; Cheng and Zheng, 2007; Ibrahim *et al.*, 2015; Tkadletz *et al.*, 2016).

The main aim of industries intending to use thin films on cutting tools is to improve the life of cutting tools without affecting the performance. Kennametal, Sumitomo, Sandvik Tools, Rohith tools and many more are the companies which manufacture the cutting tool inserts. These manufacturers coat Ti, Al, N, Al_2O_3 and its combinations on inserts before they supply the products to market. Some researchers have worked on the performance of the coated inserts against the conventional inserts. Important findings in the field of coating on the cutting tools and its performances are explained below.

WC inserts were coated with Nano carbon particles /carbides by CVD and their machinability and scratch wear resistance were investigated. The coating increases the tool life by protecting the insert from crater wear and flank wear and break away of edge.

The surface finish at a spindle speed of 90 m/min, a depth of cut of 0.2 mm and a feed rate of 0.1 mm was found to be excellent with a roughness of R_aa = 0.64 μ m. The R_a value was lower by 0.8 μ m as compared with the commercial insert (Pazhanivel *et al.*, 2015).

Dry machining of aluminum and Al-Si alloys were carried using the coated inserts. Mono or multilayer coated carbide tools with a top coating of TiC, TiN, TiAlN, Al_2O_3, TiB_2, MoS_2 on WC–Co inserts has already made a breakthrough in dry machining of ferrous materials. WC based uncoated tools and coated tools with a coating of TiC, TiN, Al_2O_3 , TiB_2 and AlN are reported to be capable of machining ferrous materials, however the same tool was found to be not effective while dry machining aluminium and built-up edge was observed on the face and flank of the cutting edge. The edge built-up not only increased the cutting forces substantially but also affected surface finish of the work-piece adversely. A similar observation was also made during machining of Al–12% Si alloy (Roy *et al.*, 2009).

Suresh *et al.* (2012) studied the dry machining of AISI4340 high strength low alloy steel using (TiN/MT-TiCN/A_2O_3) coated insert. Experiments were planned to use full factorial design and influence of machinability parameters were analysed using response surface methodology RSM. From the parametric analysis, it was revealed that the combination of lower feed rate, lower depth of cut and high cutting speed is appeared beneficial for minimizing the machining force and surface roughness. It was observed that the cutting tool wear increases with increase in cutting speed for all values of feed rates and sensitive to feed rate variations for all values of cutting speed specified. Tool wear was also sensitive to variations in depth of cut at lower values of cutting speed. The authors have claimed that the tool wear can be minimized by employing lower values of cutting speed, feed rate, depth of cut and machining time.

TiC_xN_{1-x} single-layer $(x = 0–1.0)$ and TiC/$TiC_{0.5}N_{0.5}$/TiN multilayer coatings were prepared by using the hollow cathode discharge ion plating method was investigated to study improvement in the mechanical performance of high-speed steel cutting tools. The TiC/TiCN/TiN coatings showed better mechanical performance of cutting tools (Yasuoka *et al.*, 2012).

AlCrN nanocomposite coatings of 3 μm thickness were developed on tungsten carbide using arc-PVD. Screening machinability tests were carried out on Ti6Al4V alloy as per ISO 8688-2 standard. The authors also investigated AlCrN-T coating and have concluded that AlCrN-T has wide potential for tribological applications under the condition of sliding wear. This tool can be used in machining of aerospace and biomedical components with larger span of process parameters and acceptable levels of productivity (Cadena *et al.*, 2013).

TiCN and TiCN/ZrN coatings were developed on the WC-Co cutting tools by using cathodic arc PVD method. The coefficient of friction of a coating was found to be strongly depended on its lubricity properties than its surface roughness. Ti-based hard coating also significantly improve the surface hardness of cutting tools. The surface hardness of the in-house developed TiCN/ZrN and TiCN coatings was lower than that of commercial TiCN coating but higher than that of commercial TiN coating (Siow *et al.*, 2013).

Multilayer TiN/TiCN/Al_2O_3/TiN hard surface coatings were developed on the carbide insert by Sahoo and Sahoo (2012, 2013*a*,*b*). This tool was used to machine the AISI4340 steel (HRC of 47 ± 1) under dry environment. Parametric influences on turning forces were also analysed. A better machining performance was observed in case of TiN coated inserts due to a lubricious TiN coated layer which reduces the friction and prevents the interface temperature at higher cutting speed. Multilayer TiN coated carbide inserts produced better surface quality and also within recommendable range of 1.6 μm which is comparable to cylindrical grinding.

TiN was coated on the ceramic inserts made of Al_2O_3+TiCN and the coated tool was used to machine AISI4140 steel under dry environment. The authors investigated the machined surface, tool wear mechanism and chip morphology. Mathematical models for surface roughness and flank wear were also developed. By adopting techniques such as orthogonal array and analysis of variance, the consequences of cutting parameters (cutting speed, feed and depth of cut) on surface roughness and flank wear (V_{bc}) were explored. From the ANOVA results and the main effect plot that, the authors have inferred as cutting speed

is the major cutting parameter affecting flank wear (V_b) with a contribution of 25.35%. The extensive experimental research showed the effectiveness and potential of PVD-TiN coated Al_2O_3 + TiCN mixed ceramic tool for hard turning process under the dry machining conditions to be productive and cost-effective option to replace the cylindrical grinding operations (Das *et al.*, 2015).

There is trend of developing surface treatments like DLC coatings to produce low COF and wear resistant surfaces. The use of diamond in coatings is extensively increased in the coating industries due to its exceptional properties. Metal-carbon nitrides, metallic carbides and metallic nitrides show superior combinational properties like the high hardness of carbides and high ductility of nitrides; Ti and Si combined with carbides and nitrides result in high hardness of coatings. Nondoped DLC coatings are shown better performance as compared to Cr-doped DLC coatings. As Cr-doped films showed poor adhesion which resulted in the failure of coatings. Fretting wear is a phenomenon occurring under a relative cyclic motion of lower amplitude between the two surfaces and is useful in studying the cyclic frictional performance. TiSiCN, TiCrSiCN, CrSiCN were deposited on WC/Co alloys, for studying the comparative performance TiCrSiCN coating exhibited higher hardness compared to CrSiCN. Highest adhesion was witnessed in CrSiCN coating while all the three coatings exhibited relatively better dry sliding wear resistance compared to WC/Co alloys. Ti-based coatings exhibited wear accelerated corrosion consequently resulting in poor wear and frictional performance. A significant increase in the fretting fatigue life of 210 % to 798 % is witnessed in multilayer coatings of TiAlN/CrN and monolayer TiAlN coating respectively. TiAlN/CrN coatings exhibited better mechanical properties compared to monolayer TiAlN coatings (Ibrahim *et al.*, 2015). Cu/Ni multilayers(10-15nm) which consist of sub-layers of Cu and Ni exhibited comparatively better fretting wear resistance with reduced thickness as against its monolayers.

Musfirah *et al.* (2017) in his work, have discussed tool wear, wear mechanism, cutting force and surface roughness during machining of Inconel 718 using TiAlN/AlCrN coated tool.

The tool experienced adhesion and abrasion type of wear during dry and cryo-machining.

Kıvak (2014)employed Taguchi optimisation and regression modeling techniques to evaluate the machinability of Hadfield steel while using PVD and CVD coated cutting tool. Statistical analysis showed that the feed rate significantly influences the surface roughness whereas flank wear is mainly influenced by cutting speed.

Grzesik *et al.* (2018), in his work measured the tool wear progress continuously for AlTiN, TiAlN TiN and (Ti, Al) N_2 coated inserts during machining of Inconel-718. The authors have reported that the enhanced thermal resistance of AlTiN and TiAlN and thermal barrier effect increase the tool life. Abrasive and built-up-edge types of tool wear were observed.

Kumar and Chauhan (2015), studied the influence of machining parameters for turning of Al 7075/10/SiC_p and Al 7075 hybrid composites. Response surface methodology (RSM) and artificial neural network (ANN) methods were used to develop predictive models and compare with the experimental work. ANN model was found to be more adequate in the prediction of results. Feed rate was found to significantly influence cutting forces than speed and approach angle.

Hanief *et al.* (2017), used predictive ANN modeling and full factorial design of experiments for predicting cutting forces during machining of red brass. Tool life was greatly influenced by cutting forces and optimizing the cutting forces helped in improvement of tool life.

Combination of RSM and ANN techniques were used by M. Nouioua et al for analysing Minimum quantity lubrication (MQL), dry and wet turning of X210Cr12 steel using multilayer coated tool. Experiments were planned based on Box-Behnken design, RSM and ANN techniques were used for modeling and validation of experiments. ANN method was concluded as the best method for the predictive modeling and building correlation coefficients (Nouioua *et al.*, 2017).

Particle swarm optimization (PSO) is a computational method that optimizes a problem by iteratively trying to improve a candidate solution with regard to a given measure of quality (Malghan et al. 2017; Onwubolu 2006; Parsopoulos and Vrahatis 2010; Rao 2011; Taha, Zahari, Rostam 2006). Ciurana *et al.* (2009)suggested a multiobjective PSO

technique for optimizing process parameters in micromachining of hardened AISI H13 steel. Hence, PSO and ANN techniques combinedly are capable of providing efficient results of optimisation and models for the prediction. Swarm optimization proved as an evolutionary computational approach for optimization of process parameters irrespective of the field.

Saravanan *et al.* (2005),has also explain that due to the high complexity of the machining optimization problem, PSO technique proved more beneficial among all the other algorithms.

Kong *et al.* (2018)observed that the addition of CrN/CrCN coatings to the HSS and WC substrates enhanced tool life significantly due to high hardness and low coefficient of friction of the coatings. Bushlya *et al.* (2017)explain that uncoated WC tools face the diffusion of cobalt binder into the chips and minor cross diffusion of copper and zinc during the machining of CuZn21Si3P and CuZn39Pb3 brass. Subsequent to this, pull out of WC grains occurs due to loss of adhesion. By coating the WC tools with (Ti, V, Zr, Nb, Hf, Ta) N coating the diffusion tool wear was prevented and the same was attributed to the formation of stable amorphous SiO_2 and SiAlON layers.

Aouici *et al.* (2012)explain mathematical modeling for surface roughness and cutting forces developed using RSM. Cutting forces were found to be influenced by depth of cut and workpiece hardness. Surface roughness is influenced by feed rate and workpiece hardness. With the combination of lower feed rate and the highest permissible cutting speed lower surface roughness was achieved. Das *et al.* (2018) reported that the feed rate and cutting speed influence surface roughness during machining of Al 7075/SiC_p.

Kumar *et al.* (2013) used multiple regression analysis and artificial neural network to predict the results and develop the mathematical models for the same purpose. Their analysis suggested that neural network has better capability for prediction and is an efficient modeling technique.

Chabbi *et al.* (2017) used full factorial design (L_{27}) for the experimentation and response surface methodology (RSM) and artificial neural network (ANN) for the modeling of the

output responses. Using statistical analysis correlation between process parameters and output responses was established. Based on the determination coefficients, ANN method proved to be more robust and efficient modeling technique.

Gaitonde and Karnik (2012)used PSO technique and ANN technique for minimizing burr size and optimization of the process parameters during drilling of AISI316. Multiobjective optimization using PSO technique suggested that the experimental conditions for the minimum burr height and burr thickness.

Malghan *et al.* (2017) carried out similar approach of PSO technique for the optimization of cutting force, surface roughness and power consumption during face milling of the Al composites.

Grzesik *et al.* (2018) in his work on machining of Inconel 718 has explained about tool wear measurements. TiAlN/AlTiN coatings were developed on cutting tools and the performance of the coatings was evaluated using tool wear results. Abrasive wear and built-up-edge were experienced during machining.

Aslantas *et al.* (2012) studied tool wear of Al_2O_3–TiCN coated insert during machining of AISI 52100. Crater wear was dominant in both coated and uncoated tool, coated tool experienced built-up-edge, whereas crater formed on uncoated tool transformed into chipping.

Hanief *et al.* (2017) combined regression and ANN modeling for cutting forces during machining of red brass and validated experimentally. Anova was capable of predicting the results but ANN model was found to be more accurate than the regression model.

Ciurana *et al.* (2009) used the artificial neural network (ANN) and multiobjective particle swarm optimization (MOPSO) for optimization and modeling of process parameters during micromachining of hardened AISI H13 steel. Resulting in least surface roughness obtained at the highest pulse frequency and highest scanning speed combination. Results of PSO and ANN indicate that the proposed techniques were efficient for optimization and prediction.

Kumar *et al.* (2013) explained the use of response surface methodology (RSM) combined with a neural network for the modeling and prediction of rock properties during drilling.

Coelho *et al.* (2007)have reported that TiAlN-nanocoating performed better in terms of minimizing the tool wear and surface roughness during turning of hardened AISI 4340 steel as compared to TiAlN, TiAlN-nanocoating and AlCrN coating. TiAlN-nanocoating outperforms due to its high hardness and oxidation resistance at high temperature.

Table 2.1: Literature review on coating materials

Referred Literature	**Coating Composition**	**Coating Process**	**Substrate**	**Journal Title**	**Remarks**
Wilson *et al.* (2012)	CrN & TiCN	Vacuum arc deposition	Copper	Tribological applications	Wear resistance of the substrate is increased remarkably
Nordin *et al.* (1999*a*,*b*)	TiN/CrN, TiN/MoN, TiN/NbNTiN/TaN	PVD	Cemented carbide	Cutting tool	Mechanical properties and the abrasive wear resistance were beneficially improved for the multilayered structure of thin hard PVD coatings
Milošev *et al.* (1997)	CrN	low voltage thermionic arc sputtering technique	H11 Steel mould	Industrial applications	The industrial application where TiN coatings is compared with CrN coatings from the results it is evident that the for tribological systems TiN coatings can be replaced with CrN coatings
Ono *et al.* (2008)	TiN/NbN	sputtering	polycrystalline substrate	Cutting tools	Nitride super- lattice films such as TiN/VN and TiN/NbN have harnesses that match the hardness of cubic boron nitride, the second hardest known material
	TiN/VN				

Table 2.1 Literature review on coating materials

Referred Literature	Coating Composition	Coating Process	Substrate	Applications	Remarks
Harlin *et al.* (2006)	TiN and WC/C	PVD	HSS	cutting tools	It is found that the polished surface has better surface adhesion. No adhesive or cohesive failure in the load range of 100N.
Durst *et al.* (2008)	ZrCg CrCg	Plasma Nitriding	Low steel alloy	Corrosion resistance applications	ZrCg and CrCg coatings resulted that improvement in corrosion resistance and plasma nitriding is also recommended.
Harlin *et al.* (2006)	TiN and WC/C	Arc deposition	HSS	Cutting tools	The influence of surface topography of PVD coatings on the initial material transfer tendency and friction characteristics in dry sliding contact conditions has been investigated.
Jao *et al.* (2010)	(Ti: Cu)-DLC	Cathodic Arc evaporation process	Silicon wafers	Cutting tools	The films deposited at 150V exhibited highest hardness.

Table 2.1 Literature review on coating materials

Referred Literature	Coating Composition	Coating Process	Substrate	Applications	Remarks
Eriksson and Olsson (2011)	CrN, (Ti, Al)N CrC/C DLC	arc evaporation	HSS	Tribological applications	In the wear studies the hardness of the substrate has a strong influence and consequently on the friction characteristics and galling resistance of the coating/substrate composite.
Zhang *et al.* (2014)	Ti–C–N	pulsed bias arc ion plating was	silicon & W6Mo5Cr4V2 steel	Nano composites applications	With the application bias voltage of 300V the formation of a typical nanocomposite structure of Ti(C, N) is applied. Nanocrystallites embedded in a DLC matrix, which led to a relatively high film hardness.
Marin *et al.* (2016)	CrN & TiCN	PVD	Ti-6Al-4V	Tribological applications	Morphological studies clearly shown that there is increase in surface roughness of the coatings after thermal treatment with subsequent increase in TiC and TiN rich layers and a consequent volume increase.

Table 2.1 Literature review on coating materials

Referred Literature	Coating Composition	Coating Process	Substrate	Applications	Remarks
Nordin *et al.* (1999*a*,*b*)	TiN and WC/C TaN	magnetron sputtering	HSS	Tribological applications	From the results of coatings, it was witnessed that multilayered coatings were wear resistant compared with single layered coatings.
Hsu *et al.* (2013)	Ti-N-O	cathodic arc plasma deposition system	AISI 304 SS	Tribological applications	Microstructure and tribological behavior of the Ti–N–O film deposited by the CAPD system could be controlled through a proper adjustment of the O2/N2 ratio.
Ananthakumar *et al.* (2012)	TiN/TiAlN	DC magnetron sputtering	MS, Glass	Corrosion applications	TiN/TiAlN multilayer coatings show the lowest average friction coefficient against steel compared to single layer coated substrate and bare substrate. The TiN/TiAlN multilayered coating shows the highest protective efficiency of 96.4%.

Table 2.1 Literature review on coating materials

Referred Literature	Coating Composition	Coating Process	Substrate	Applications	Remarks
Bromark *et al.* (1997)	Ti/TiN	PVD	ASP2030	Tribological applications	The wear performances of PVD Ti/TiN multilayer coatings subjected to two-different types of wear tests respectively body abrasion and particle erosion using diamond slurry and silicon carbide particles as abrasive medium and erodent. Ti/TiN multilayer coatings resulted in increase in abrasive wear rate with the increase in relative amount of metallic Ti in the coatings.

Table 2.1 Literature review on coating materials

Referred Literature	**Coating Composition**	**Coating Process**	**Substrate**	**Applications**	**Remarks**
Pazhanivel *et al.* (2015)	Nano carbons/ carbides	CVD	WC	Machinability	The surface coating increased tool life and its surface finish while its adherence protects the insert from crater wear and flank wear and break away of edge the surface finish at a spindle speed of 90 m/min, a depth of cut of 0.2 mm and a feed rate of 0.1 mm was found to be excellent, resulted in roughness of $R_a = 0.64\mu m$. The R_a value is lower by 0.8 m as compared with the commercial insert

Table 2.2: Literature on fretting wear and adhesive wear studies

Coating material	Coating method	Performance studies	Remarks
Ni/nano-WC	Electro deposition (Benea *et al.*, 2015)	Fretting and wear behaviours	The fretting and wear behaviors of Ni/nano-WC composite coatings were studied at different applied loads in dry or wet conditions. The results show that Ni/nano-WC composite coatings exhibited a low friction coefficient, high Nano hardness and wear resistance compared with pure Ni coatings under similar experimental conditions.
Ti(Cr)SiCN	Plasma enhanced magnetron sputtering (Li *et al.*, 2013)	Microstructure and tribological properties	TiSiCN, TiCrSiCN, CrSiCN were deposited on WC/Co alloys, TiCrSiCN coating exhibited high hardness compared to CrSiCN. Highest adhesion was witnessed in CrSiCN coating and all the three coatings exhibited relatively better dry sliding wear resistance compared to WC/Co alloys.
AlCrSiN, CrSiBN and TiAlN	Plasma nitriding (Abusuilik, 2015)	Performance for forming and cutting tools	Using cathodic ion plating pretreatment for substrate was done with plasma Nitriding techniques for the development of AlCrSiN, CrSiBN, and TiAlN coatings. Plasma Nitriding pre-treatment on substrates resulted in superior quality of adhesion for AlCrSiN coatings.

Table 2.2 Literature on fretting wear and adhesive wear studies

Coating material	Coating method	Performance studies	Remarks
Ti-6Al-4V	Ultrasonic nano crystalline surface modification (Amanov *et al.*, 2013)	Fretting wear	Fretting wear and friction characteristics of commercially pure titanium (CP Ti) and Ti–6Al–4V alloy by using an ultrasonic Nano crystalline surface modification (UNSM) technique was studied. Lubricated fretting wear and friction tests were conducted on untreated and UNSM-treated specimens using silicon nitride (Si3N4) balls. The results showed that the fretting wear and friction coefficient characteristics of the UNSM-treated specimens were improved compared to those of the untreated specimens.
SiCN/DLC	PACVD (Pech *et al.*, 2009)	Fretting-corrosion resistance	Amorphous hydrogenated SiC, SiCN, SiC/DLC and SiCN/DLC were deposited on steel substrates by a plasma assisted chemical vapour deposition (PACVD) technique. It was found that the combination of a SiCN-based PACVD sub-layer with a DLC topcoat could provide an enhanced solution to withstand both fretting and corrosion.

Table 2.2 Literature on fretting wear and adhesive wear studies

Coating material	Coating method	Performance studies	Remarks
Al/Cr multilayers	DC magnetron sputtering (Creus *et al.*, 2004)	Mechanical and corrosion properties	The Nano layer coating presents the highest intrinsic corrosion resistance but multilayer and Nano layer Al/Cr coatings become nobler than the steel substrate. The corrosion resistance of the coated steel is then strongly dependent on the microscopic coating defects which act as preferential pathways for the corrosive solution.
AlN films	RF magnetron sputtering (Kale *et al.*, 2012)	Structural and electrical properties	AlN coating deposited with and without an Al interlayer, on various substrates like Si, quartz, and copper using RF magnetron sputtering. Films deposited on copper without Al interlayer showed presence of voids or micro cracks and poor electrical properties.
AlN thin films	RF magnetron sputtering (Kim *et al.*, 2011)	Thermal conductivity	Aluminum nitride (AlN) film, which is being investigated as a possible passivation layer in inkjet print heads, was deposited on a Si substrate by radio frequency (RF) magnetron sputtering using an AlN ceramic target. High Al–N bonding ratio in AlN film is considered the most important factor for higher thermal conductivity.

Table 2.3: Machinability studies using coated inserts

Method	Coating Used	Machined material	Remarks
CNC single point turning	TiCN	High-speed tool steel (Downey *et al.*, 2014)	Analysis of audible sound energy emissions during single point machining. The experiments demonstrated consistent acoustic signatures, which are specific to the tool in a known good cutting state, and distinct, but also consistent sound energy signatures, in a known bad cutting state. The experimental measurements replicated the audible range of human hearing and sought to determine what encouraged experienced machinists to declare a machining process to be in a state of degradation.
Lathe	Uncoated and coated carbide inserts (Roy *et al.*, 2009)	Pure Al & Al–12% Si	An investigation has been undertaken to study the compatibility of cutting materials in dry machining of aluminum and Al-Si alloys.

Table 2.3 Machinability studies using coated inserts

Method	Coating Used	Machined material	Remarks
Ball on disk test	TiCN and TiCN/ZrN (Siow *et al.*, 2013)	Not shared	The mechanical properties of TiCN and TiCN/ZrN were investigated using a ball on disk test. The substrate material made from a carbide-based cutting tool was also developed in-house. The analysis showed that the performances of TiCN and TiCN/ZrN coatings were found to be comparable to that of the commercial TiN-coated carbide-based cutting tool. Both the in-house and commercial coated inserts have a significantly lower coefficient of friction than uncoated inserts, and the friction coefficient of TiCN coatings was constantly slightly lower than that of TiN coatings.
CNC Lathe	carbon-coated WC inserts (Pazhanivel *et al.*, 2015)	SS316 austenitic steel	Cemented tungsten carbide inserts were coated with Nano carbons/carbides by chemical vapor deposition and their machinability and scratch wear resistance were investigated. The hardness and surface conditions of the WC substrate were studied before and after coating.
Lathe	coated carbide insert Suresh *et al.* (2012)	AISI 4340	An attempt has been made to analyse the influence of cutting speed, feed rate, depth of cut and machining time on machinability characteristics such as machining force, surface roughness and tool wear using response surface methodology based second order mathematical models during turning of AISI 4340 high strength low alloy steel using coated carbide inserts.

Table 2.3 Machinability studies using coated inserts

Method	Coating Used	Machined material	Remarks
Endmill	AlCrN Coating (Cadena *et al.*, 2013)	Ti6Al4V alloy	The mechanical behavior of the AlCrN coating was evaluated through hardness test and tribology with pin-on-disk to quantify the friction coefficient and wear rate. Machinability tests using coated tungsten carbide cutting tools were executed to determine its performance through wear resistance, which is a key issue of cutting tools in high-end cutting at elevated temperatures. It was demonstrated that the specimen (with lower friction coefficient than previous research) is more efficient in machining Ti6Al4V alloys.

2.7 Summary

The literature survey emphasizes that significant effort has been made to develop wear resistant coating using physical vapour deposition and the progress made for applications involving cutting tools like inserts, cermet's, drill bits etc. In most of the instances wear rate and coefficient of friction are considered in the estimation of the tool life performances. It is clear from the literature (Table 2.1- 2.3) that the coatings presently used in machine tools have either wear resistance or better mechanical properties. It is of utmost importance to formulate coatings which are resistant to wear with better enhancement of mechanical properties on its surface. Also, there is a need, not only to formulate and test new coatings but also to understand behavior of coating and its performances under real-time conditions.

2.8 Identification of problem

Based upon the available literature, it appears that not many investigations done to quantify the development of iron and aluminium based PVD coatings and its tribological behavior. Hence, objectives of this study includes development of iron, aluminium and titanium based (monolayer and multilayer) coatings, and conduct characterization and performance evaluation. Furthermore, to study adhesive wear and fretting wear behaviour of the coatings. From section 2.6 it is evident that the machinability studies carried out using the coated inserts are minimal. Hence, coatings are to be developed on the tool inserts for the investigation of tool wear (flank wear).

2.9 Objectives of proposed work

The objectives of the present investigation are:

1. Development of carbides and nitrides of titanium, aluminium and iron-based coatings by plasma assisted cathodic arc evaporation technique on substrates of MDN 121 and SNMG120408 tungsten carbide tool inserts.
2. Characterization of developed coatings using glancing angle X-ray diffractometer

(GAXRD), field emission scanning electron microscope (FESEM) attached with energy dispersive spectroscopy (EDS), Raman spectroscope and nanoindenter techniques.

3. Evaluation of fretting wear performance of thin films using nano-scratch tester [ISO 14577-4].
4. Evaluation of adhesive wear performance (wear rate and coefficient of friction) of thin films using nanotribometer [ASTM G133].
5. Evaluation of machinability of highly alloyed steel using coated inserts and assessment of tool wear [ISO-3685:1993]. Optimisation of cutting parameters with respect to output responses of cutting forces and surface roughness [ISO 468:1982] using full factorial design-based approach and particle swarm optimization (PSO).

Chapter 3

METHODOLOGY

This chapter describes the equipment and various characterization techniques used for studying microstructural features, mechanical properties, fretting wear, adhesive wear and machinability using coated inserts.

The plan of experimentation and characterization for evaluating mechanical and physical properties of coatings is shown in Figure 3.1

3.1 Substrate materials

Following materials are used as substrate fir depositing different coatings,

1. Special Steel MDN121
2. SNMG120408 WC inserts

Alloyed steel (MDN 121) [AISI equivalent – 121], are the materials used for manufacturing components of steam gas turbine, steam turbine and aero engine. The materials were procured from M/S MIDHANI, Hyderabad who have proven credentials in terms of material quality. The specimens with appropriate dimensions of $12.5mm \times 12.5mm \times 5mm$ are used for experiments. The composition of substrate materials are determined by spectroscopy and is mentioned in Table 3.1. Uncoated SNMG120408 tungsten carbide with chip breaker inserts manufactured by Kennametal Germany is planned for the proposed

machining work. SNMG120408 is having 8 cutting edges and is known to process better tool life compared to other brands available in the market.

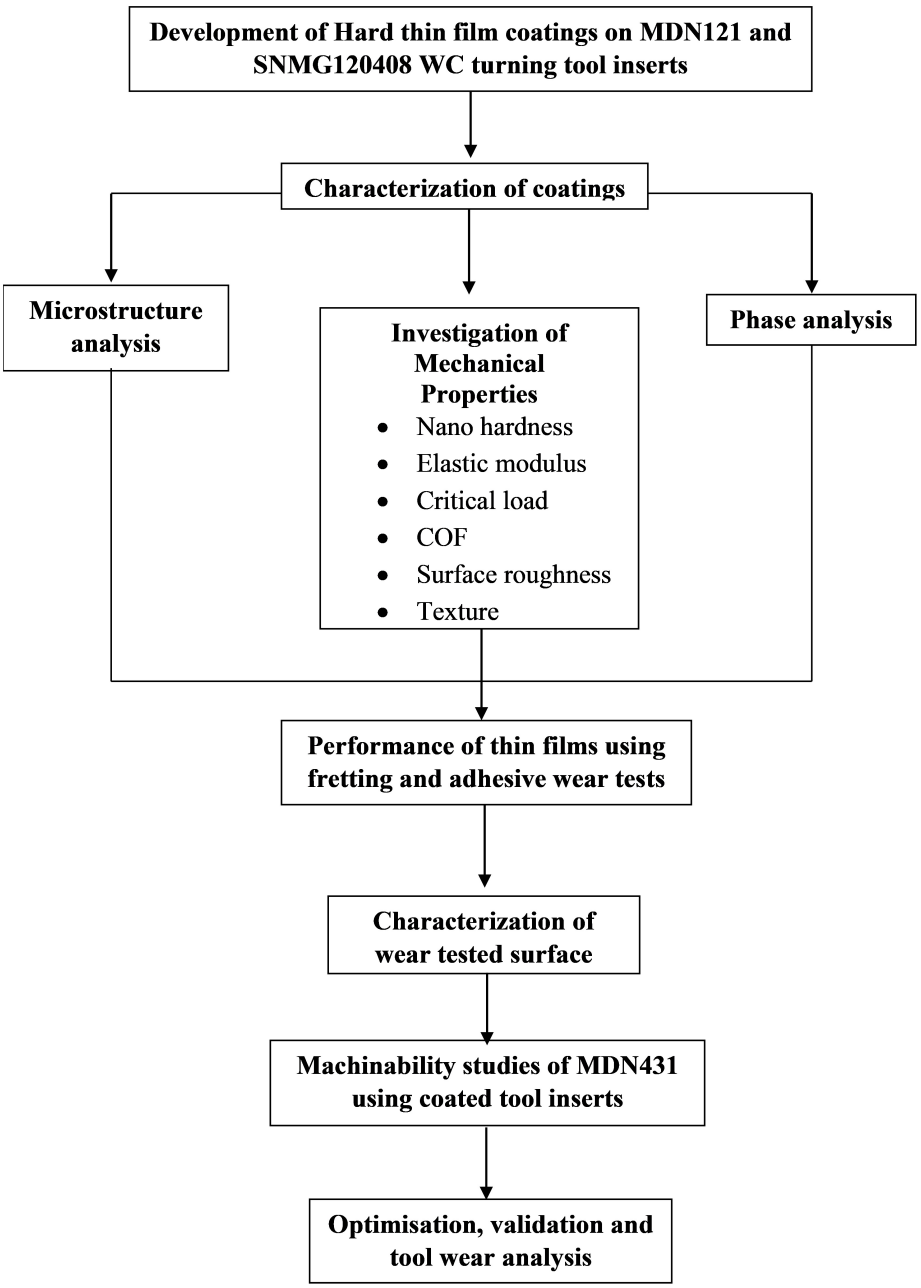

Figure 3.1: Work flow chart

Table 3.1: Composition of substrates

Substrate material	Chemical composition (wt %)
MDN121 Grade: X22 CrMoV121	C-0.2, Mn-0.6, Si-0.25, Cr-12, Mo-1, Ni-0.8 and Fe-Bal

3.2 Coating materials and deposition of coatings

Three types of target material are used in the form of solid slab and deposited using cathodic arc vapor deposition on two different substrate metals. The chemical composition of the target material is reported in Table 3.2. Cathodic arc deposition is carried out using coating chamber setup developed by M/s Bangalore Plasmatek Pvt. Ltd.

Table 3.2: Chemical composition target material

Target material	Chemical composition (wt %)
Stainless Steel 304	C-0.08, Mn-2.0, P-0.045, S-0.030, Si-1.0, Cr-19, Ni-9.2 and Fe-Bal
Pure Aluminium	Mn-0.05, Fe-0.4, Cu-0.05, Mg-0.05, Si-0.25, Zn-0.07, Ti-0.05 and Al-Bal
Grade 2 Titanium	C-0.005, Fe-0.05, H-0.0009, N-0.03, O-0.19 and Ti-Bal

3.3 Cathodic arc evoporation

In a vacuum arc deposition system, thin films are developed on the finely finished surface of the substrate. Samples are cleaned ultrasonically and loaded into the coating chamber initially maintained at 200-300^{o}C. This initial temperature maintained in the coating chamber will enhance the coating adhesion. Coatings obtained from cathodic arc sources are very dense and adhesion to the substrates is also good. The films are free of voids. Reactive deposition is more efficient as the ions are energetic and ionized unlike in magnetron sputtering. Schematic diagram of cathodic arc deposition setup and coating

chamber are shown in Figure 3.2 and Figure 3.3 respectively.

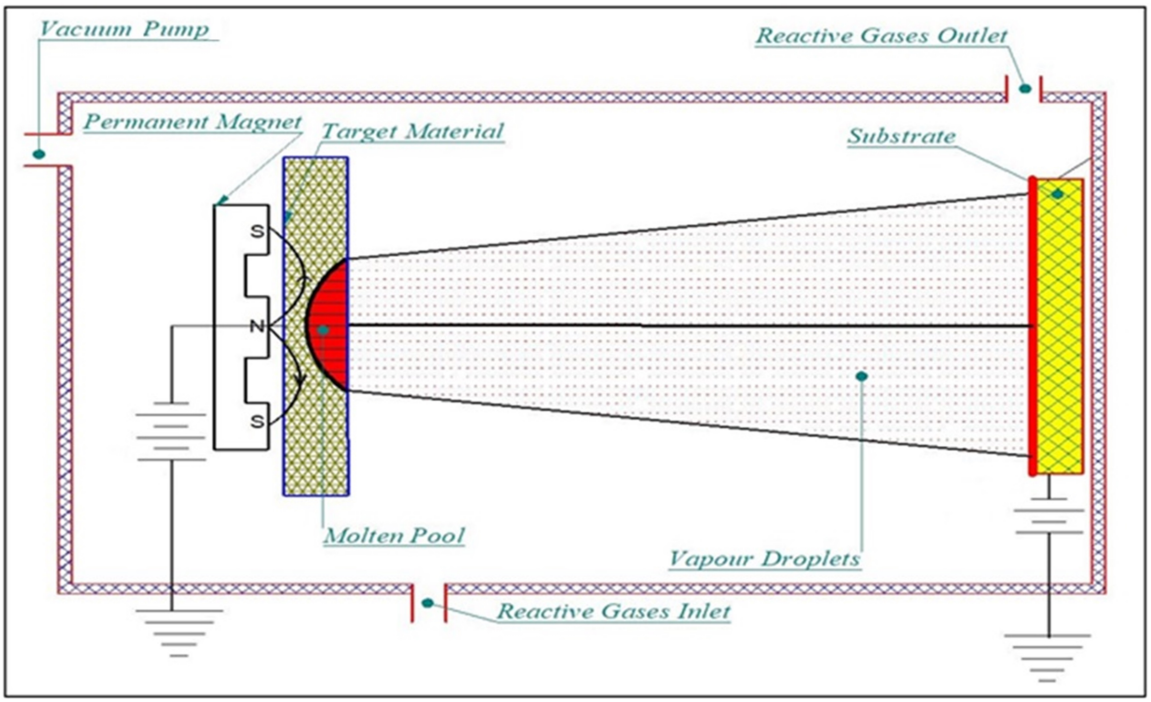

Figure 3.2: Cathodic arc deposition setup

There are 3 important stages in the development of thin film coatings. namely,

1. Creation of vapor phase,
2. Transport from target to substrate and
3. Film growth on the substrate.

Which are explained below in detail:

Step1: Creation of vapor phase An electric arc is generated when the flow of current is suddenly interrupted. During the arc, the electrode material evaporates and reacts with reactive gases in the vacuum and deposited as a compound on the substrate. It is more likely that reaction takes place on the surface of the substrate. Target material is used as a cathode as shown in Figure 3.2. Voltage applied between the cathode and the anode (substrate) is connected to the wall of the vacuum chamber. The cathode is brought in contact with the anode by using the igniter. Withdrawing of igniter creates large current flow, thus the arc is

generated on the cathode surface. A few tens of amperes to a few kilo amperes of current are maintained in the circuit. The temperature in cathode arc spot increases so that the region of the arc spot starts melting corresponding area is called a molten pool of cathode.

Figure 3.3: Coating chamber

Step 2: Transportation of vapours from target to substrate

The vapor particles produced were transported from target to substrate. While transporting, some of the atoms can be ionized creating plasma. From the molten pool of target, electrons are emitted by field emission process. The emitted electrons ionize the vapors of cathode which are coming from the pool. Thus, the high-density plasma is created near the cathode this expands towards the substrate which leads to improvement in the adhesion of the coating, film quality improves, and crystal orientation also controlled. Some of the ions from the plasma are attracted to the cathode, which leads to exertion of pressure on molten pool. The emitted ions are accelerated to energies up to 150 eV. This is more than the cathode voltage of about 25 V. Further, the ions are multiplied ionized; these energetic ions are further accelerated at the substrate by the bias voltage. Thus, the substrate is applied

with the bias voltage. Thus, the substrate is bombarded with high energy ions during the growth of the film. This improves the density of the film and reduces or suppresses the formation voids in film and thus the integrity of the film is good.

Step 3: Film Growth on the substrate

Table 3.3: Coating parameters of cathodic arc deposition process

Arc parameters	Vacuum Pressure	10^{-4}-10^{-3} mbar
	Voltage	30-40 V
Reactive Gases		Nitrogen and Acetylene
Voltage at substrate		50-500 V
Temperature		250^{o}C
Stand of Distance		180-330 mm

In this step the vapor gets condensed on the substrate and develops thin film by nucleation and growth process. The nucleation and growth process are strongly influenced by approach of new ions or vapor particles which result in a change in microstructure, composition, impurities and residual stresses. The process utilizes the arc to melt the target; the arc is initiated by breaking a current path. Coating is carried out in plasma medium with a vacuum pressure of 10^{-4} to 10^{-3} mbar. All the coating parameters associated during cathodic arc deposition are listed in Table 3.3. All the process parameters, including the stand of distance, are held constant throughout the coating process. To develop a coating on the surface it must be fully mirror finish with a surface roughness $R_{\mathrm{a}} < 0.1\mu m$. The samples are ground to surface roughness of $0.3\mu m$ and then lapping is done to decrease the roughness value to $0.08\mu m$. Then substrate samples are degreased with aqueous solution cleaning in the ultrasonic system to avoid any defects during development of coating and to improve adhesion between substrate and coating. All the sides of samples are coated. In the present study, three different target materials namely Ti-based Al-based and Fe-alloy based are used in cathodic arc evaporation technique to form coatings on MDN 121 and SNMG120408 WC substrates. Here the coating is produced by evaporation

and condensation of vapors droplets of target materials in the form of thin layers. With the consideration of the above discussion, the fretting wear (ISO-145774) and adhesive wear (ASTM G-99-05) studies are conducted on the coatings developed on the MDN121 substrate. Machinability studies of MDN431 is carried out using coated inserts.

3.4 Microstructure and elemental compositions analysis

Cross section along the thickness of the coated samples was taken, and then cold mounted with the help of acrylic powder and resins. The specimen was polished with up to 2000 grit SiC paper and final polishing was done using superfine diamond paste embedded cloth. The microstructures of the specimen were examined using an optical microscope (OM) and field emission scanning electron microscope (FESEM). Energy-dispersive spectroscopy (EDS) was used to study the surface morphology and localized elemental composition.

Glancing angle X-ray diffraction (GAXRD) with Cu-Kα radiation was used to identify the distinct phases in the coating at the angle of 2°. X-ray diffraction patterns were recorded with a Bragg–Brentano geometry using Cu-Kα radiation. Experiments were carried with 2θ angle ranging from 20-100°, results were further analysed for the compositional changes, phases and compounds formed in the coatings.

RAMAN spectral analysis was carried out on the surface with monochrome laser of 514nm wavelength attached with CCD detector. Raman analysis was carried out for the range of $50-2000cm^{-1}$. Presence of DLC and phase compounds in the coatings was studied. Diffraction peaks, Gaussian peaks, D/G ratio and 2D/G ratio were calculated to evaluate the number of graphene (DLC) layers present in the coating. The results are further compared with the standard Raman database.

3.5 Nano-indentation studies

Mechanical properties of the coatings are evaluated using nanoindentation test and nano scratch test. Performance of coatings were investigated using Fretting test. Agilent G200 USA nanoindenter equipment (Figure 3.4) was used in the present study. Tests were

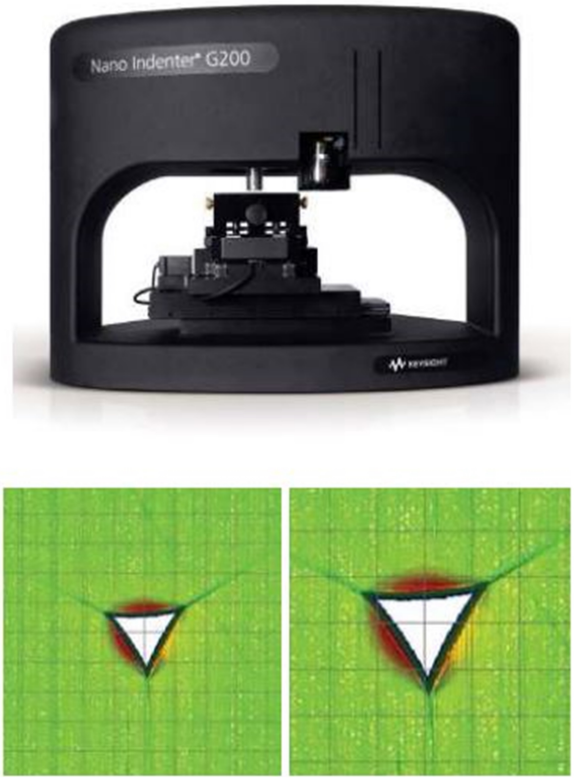

Figure 3.4: Agilent G200 nanoindenter

conducted as per ISO 14577-4 and ASTM E2546 under clean room conditions. Fretting wear tests were done with a constant velocity of 20 $\mu m/s$, wear track length of 300 μm for different loads of 20 mN, 40 mN and 60 mN. During the nanoindentation, Berkovich indenter was used. During the fretting wear test after each cycle, the amount of area deformed due wear track was measured. Wear resistance $(R_{w(M)})$ for the coatings is calculated using the formula as(3.1) as mentioned by Kreines *et al.* (2004).

$$R_{w(M)} = \frac{N_T - N_R}{H - h_R} (3.1)$$

Here N_T– Total number of cycles, N_R- number of friction cycles during running-in period, H-initial thickness of the coating and h_R- wear depth at the end of running-in period.

3.6 Thickness and adhesion studies

Calo test is a spherical abrasion test method. To this end, a small crater is ground into a coating with a ball of known geometry, providing a tapered cross-section of the film when viewed under an optical microscope. In the present work Calo test was used to measure the coating thickness of the thin film coating. Coated surface was cleaned with IPA solution. Steel ball is run against the surface at 200 rpm for the period of 120-180 sec with the presence of diamond paste as lubricant. Wear scar created on the surface after the Calo test is analysed using microscope and coating thickness is calculated with its built-in software. Calo test rig (Figure 3.5) and VDI3198 test rig located in Oerlikon Balzers Bangalore is used for the present studies.

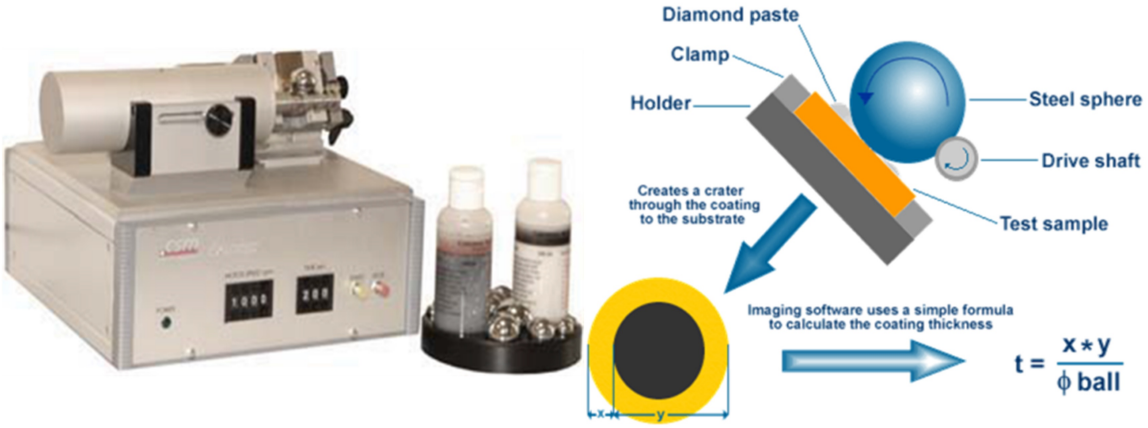

Figure 3.5: CSM calo test equipment

VDI3198 test was used for the qualitative analysis of adhesion of coatings. Using a Brinell hardness machine (ball indenter) with the load of 100 kg for the constant dwell time, indentation is created. Deformed coatings after indentation are cross-referred with the standards mentioned in Figure 3.6 to draw conclusions on the results.

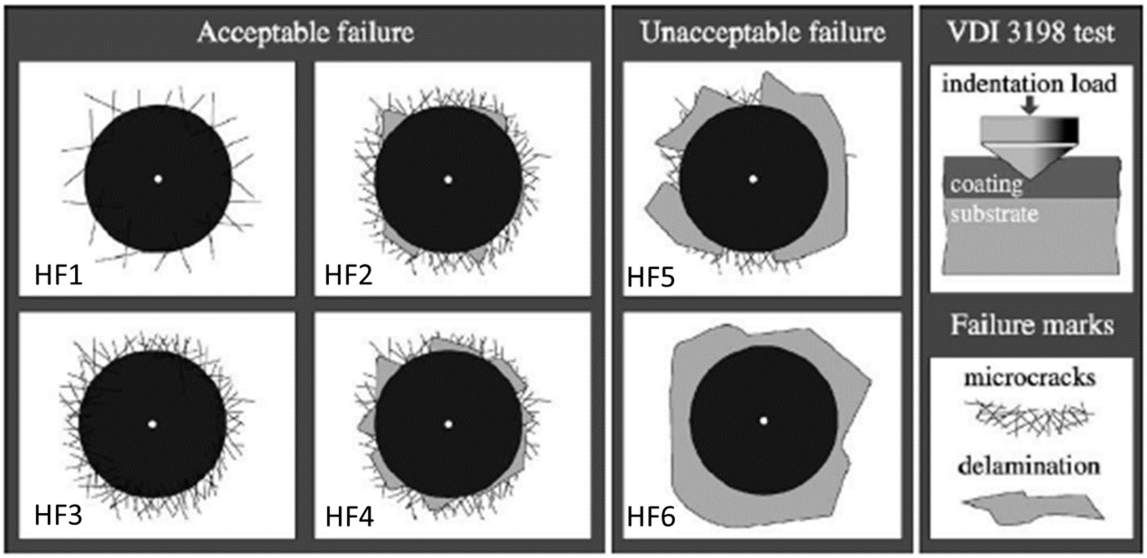

Figure 3.6: VDI 3198 reference chart

3.7 Topographical studies

Figure 3.7: Scanning tunnelling microscope

Surface topography and surface roughness studies were done using a scanning tunnelling microscope (Figure 3.7) (i2N technologies, IISC make). 5 nA tunnelling current was used to analyse the surface topography. Surface area $25nm \times 25nm$ is considered for the study. Surface mean area roughnesses were calculated using GWYDDION software.

3.7.1 Surface profile studies

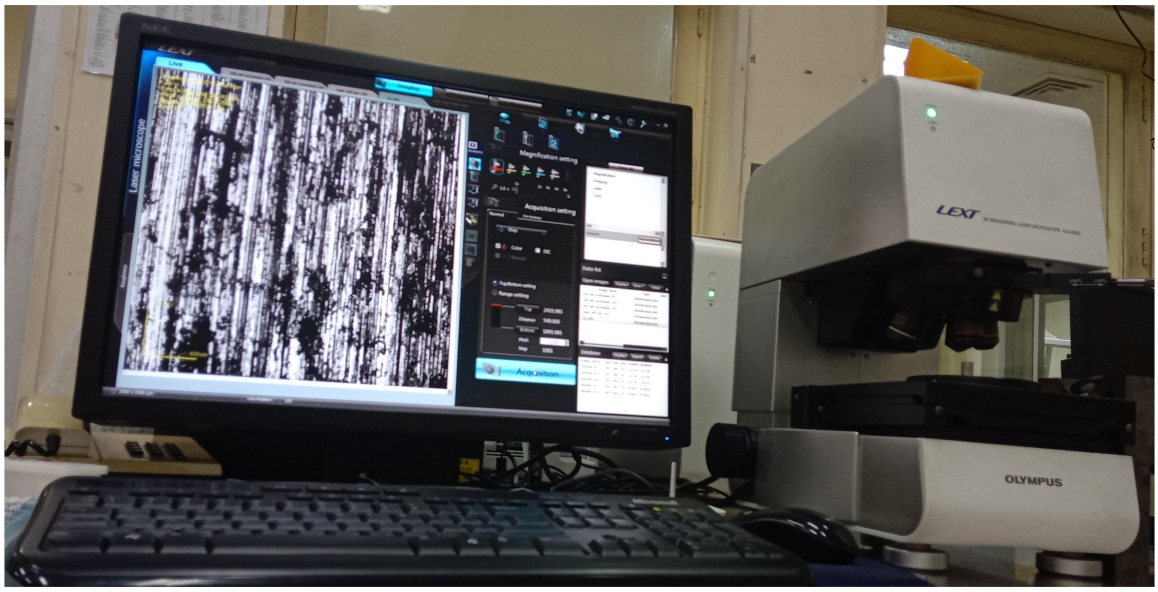

Figure 3.8: Confocal microscope

A confocal microscope (Figure 3.8) (Olympus LEXT 4000, Japan) was used to examine the profile of the machined surface topography, tool wear measurement, indented surface and fretting worn surface. It uses a monochromatic laser to build the 3D profile of surface. The height, width and depth of the worn surfaces were measured and analysed.

3.8 Nano tribometer studies

During the wear test, after each cycle, the amount of area deformed on wear track was measured with a built-in facility in the equipment. Adhesive wear tests were conducted using Anton-Paar make Nano-Tribometer (NTR^3) as shown in Figure 3.9 as per ASTM G99 and ASTM G133. Nano tribometer works based on an elastic double beam cantilever

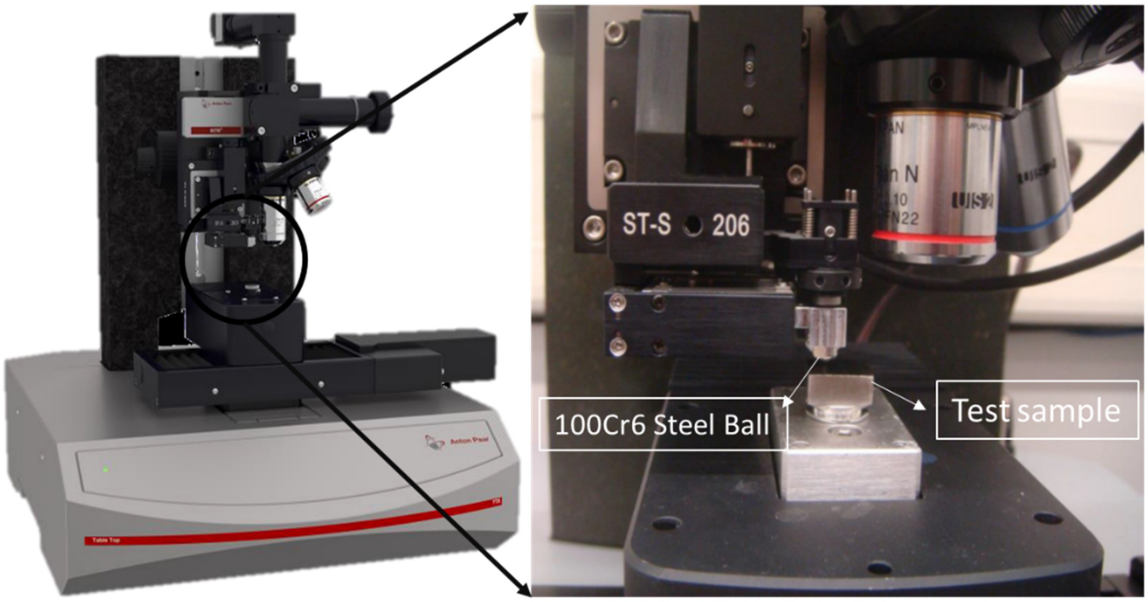

Figure 3.9: Anton paar nano-tribometer (NTR^3)

combined with high-resolution capacitive sensors, the applications of a standard Pin-on-Disk tribometer were extended for such cases where force is in the range of mN and displacements in the range of microns were required. Adhesive wear tests were conducted at the laboratory condition of temperature 25°C and humidity 42%. Test conditions are linear displacement motion, speed 0.47 cm/s, normal loads of 20 mN, 40 mN and 60 mN for 1000 cycles. A 100Cr6 steel ball of 2 mm diameter was used as counter body during the wear test.

3.9 Machinability studies

Tool life and its performance tests are conducted as per the ISO-3685:1993(E) using the coated insert. Machinability studies Figure 3.10 are being conducted using highly alloyed steel MDN431. MDN 431 [EN equivalent – 57/AISI431], which are currently the materials used for making of aircraft shafts and pump components in aero engines. The round bar specimens with length of 200 mm and 32 mm diameter range of 30-40 mm are planned to be used for experiments. Table 3.4 shows chemical composition of MDN431. Three-jaw self-centered panther lathe machine tool was used for experimental work sown in Figure

3.11. Kennametal German-make SNMG120408 tungsten carbide tool insert was attached to the DSSNR2020K12 tool holder. Experiments for each combination are repeated to minimize the errors to ensure the accurate readings.

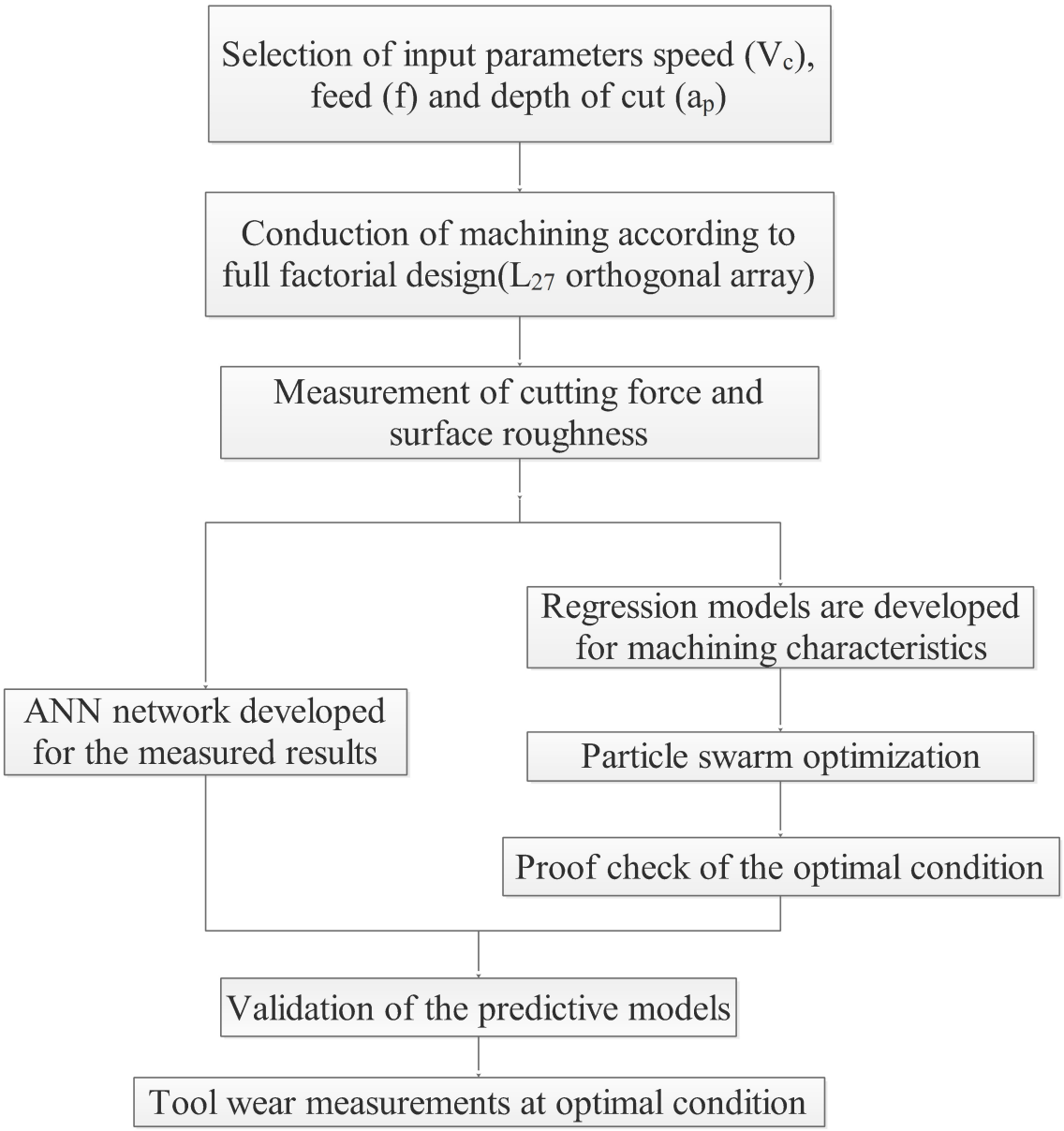

Figure 3.10: Machinability study flow chart

Figure 3.11: Machinability experimental setup

Table 3.4: Chemical composition (wt %) for MDN 431 stainless steel

Type of substrate	Grade	C	Mn	Si	Cr	Ni	Fe
MDN 431	AISI431, EN57,14X17H2	0.15	0.7	0.7	17	2.5	Balance

3.9.1 Cutting force studies

Cutting forces are measured using Kistler 9257B piezoelectric dynamometer mounted on the tool post with the help of Kistler Dynoware software 2825D-02 data acquisition system shown in Figure 3.12. Kistler Dynamometer 9257B is used to measure the cutting forces during the machining studies. Kistler Dynamometer 9257B (technical specification given in Table 3.5) equipped with 5070A charge amplifier is connected to computer with A2D Board and is controlled by Kistler 2825 DYNOWARE software.

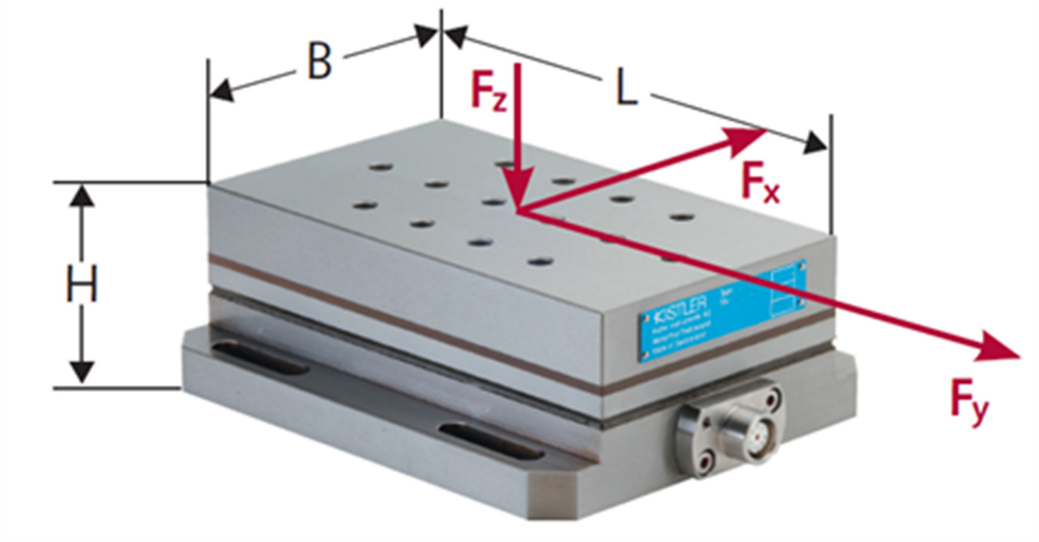

Figure 3.12: Kistler 9257B dynamometer

Table 3.5: Technical specifications of Kistler 9257B dynamometer

Technical Data	**Type**	**9257B**	
Measuring range	Fx, Fy	kN	–5 ... 5
	Fz	kN	–5 ... 10
Calibrated measuring range	Fx, Fy	kN	0 ... 5
	Fz	kN	0 ... 10
Sensitivity	Fx, Fy	pC/N	≈–7.5
	Fz	pC/N	≈–3.7
Natural frequency	fn(x), fn(y)	kHz	≈2.3
	fn(z)	kHz	≈3.5
Pretensioning direction			vertical
Operating temperature range		°C	0 ... 70
LxWxH		mm	170x100x60
Weight		kg	7.3

3.9.2 Surface roughness tester

Machined surface roughness is measured by the Mitutoyo Talysurf SJ201 surface roughness tester. Machined surface having vertical deviation, if the deviations are

Figure 3.13: Mitutoyo SJ301 surface roughness tester

large, roughness of surface be high. If deviations are small, the surface is smooth. Surface roughness plays a vital role in determining how a machine interacts with its real environment. Wear is usually faster in rough surfaces and smooth surfaces during coefficient of friction are very high. Average surface roughness(R_a) was considered there are many different roughness parameters in use, but R_a arithmetic mean roughness is by far the most common. Other common parameters include: R_Z ten points mean roughness, and R_t is the maximum height of the surface profile measured according to Standard ISO 468:1982: five measurements were taken for R_a of each machined sample with a cut off length (λ) of 4 mm and average values are considered. Figure 3.13 shows the Mitutoyo surface roughness tester:

3.10 Regression analyis

In the present study on machinability using coated tools, speed, feed rate and depth of cut are the input variables used to develop the experimental design. Full factorial design of experiments was used for design and analysis of experiments. FFD L_{27} array for distinct levels of input variables shown in the present study, speed, feed rate and depth

of cut are the input variables used to develop experimental design Table 3.6 shows the experimental conditions. In regression analysis, the correlation between input parameters and output responses are established using quadratic mathematical regression model. Using the mathematical regression model, results are predicted for the combination of 27 experiments. The predicted results and experimental results are compared. Multi-objective optimization for the output responses are carried out using desirability approach for minimization function (smaller is better). Desirability approach was initially introduced by Suich and Deringer in 1980. The desirability approach finds experimental conditions "*targeted*" as the most advisable response value.

Table 3.6: Experimental conditions

Levels	**Unit**	**Level 1**	**Level 2**	**Level 3**
Speed	m/min	59	75	118
Feed rate	mm/rev	0.062	0.093	0.125
Depth of cut	mm	0.2	0.3	0.4

3.11 Multi-objective particle swarm optimization

The optimal process parameters are achieved by employing the multi-objective particle swarm optimization (MOPSO) technique. Minitab software tool was used for desirability approach and MOPSO was implemented using MATLAB software. The parameters of MOPSO algorithms are represented in Table 3.7 and the working conditions for the MOPSO model are illustrated in Figure 3.14. Parameters indicated in the table(3.7) play a vital role in obtaining finer convergence of characteristics. If the population of particle increases, the learning rate increases. In turn, the number of iterations increases in the search space. Velocity of the particles is kept within the boundary range of variables. The particle movements are governed by the mathematical functions (3.2- 3.3).

$$x_i^{t+1} = x_i^t + v_i^t \tag{3.2}$$

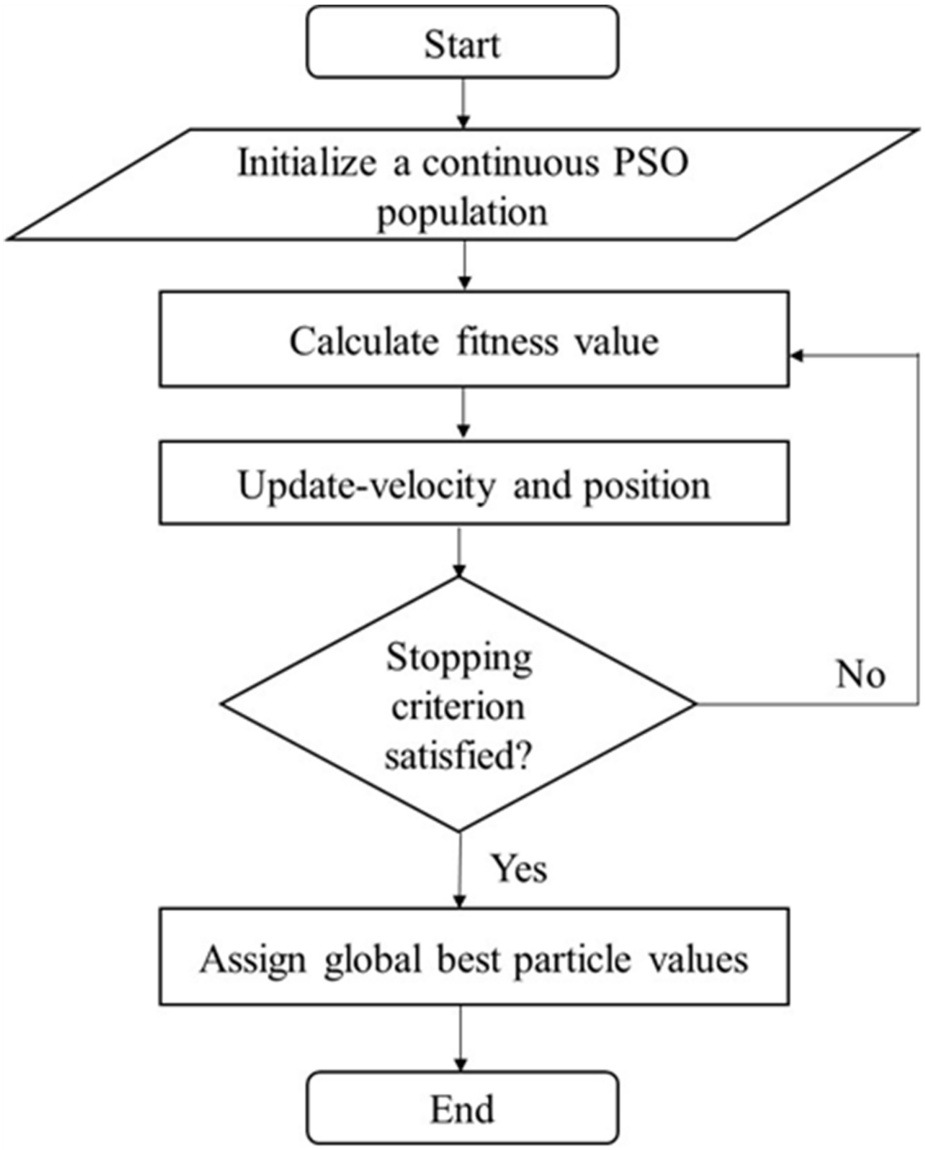

Figure 3.14: Principle of the particle swarm optimization

$$v_i^t = v_i^{t-1} + c_1 r_1 (pbest^t - x_i^{t-1}) + c_2 r_2 (gbest^t - x_i^{t-1}) \tag{3.3}$$

Where,

x_i^t and x_i^{t+1} are the position of the particle i in steps t and $t+1$,

v_i^t is the velocity of the particle i in time t,

x_i^{t-1} and v_i^{t-1} are the position and velocity in the (t-1) time,

c_1 and c_2 are the acceleration factors, r_1 and r_2 are the randomized vectors for the particle

direction and pbest is the local best solution of the particle i in time t. and gbest is the global best solution among all the particle i.

MOPSO algorithm:

1. Initialize the population of particles (n) randomly.
2. For every particle, the fitness value(f) is evaluated.
3. If the calculated fitness value of the particle is better than the best fitness value (*pbest*) in history, then the present value is assigned as new best fitness value (new *pbest*).
4. Choose the particle with the best fitness value among all the pbest which are considered to be the global best (*gbest*).
5. The velocity (v_i^t) and position (x_i^t) of each particle are calculated.
6. Each particle velocities are stored to a maximum velocity. If the sum of the acceleration causes the velocity on that dimension to surpass the specified range set by the user, then velocity needs to be limited.
7. Terminate if minimum error condition is reached or the maximum iteration is reached; else go to step 2.

Table 3.7: Parameters of MOPSO

Number of parameters(m)	3
Number of iterations(i)	1000
Number of particles(n)	100
Acceleration factor c_1	2
Acceleration factor c_2	2
Lower bounds of variables (LB)	[59 0.062 0.2]
Upper bounds of variables (UB)	[118 0.125 0.4]

3.12 Artificial neural network modeling

ANN modeling consists of the three steps; training, testing and validation. ANN modeling developed according to the training parameters mentioned in Table 3.8. Architecture of

ANN network shown in Figure 3.15. The trained ANN was used to predict the results for error and accuracy by presenting 27 input process parameter combinations. For every input training combination, the predicted results of cutting forces and surface roughness are compared with corresponding experimental results.

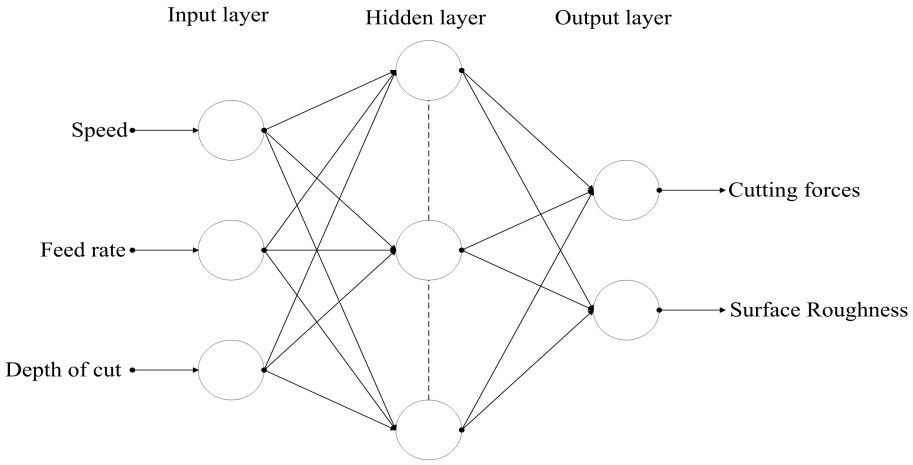

Figure 3.15: Architecture of ANN network

Table 3.8: ANN training parameters

Learning rate (α)	0.10
Learning rate increment	10
Momentum constant (β)	0.90
Maximum number of epochs	1000

Chapter 4

RESULTS AND DISCUSSION

This chapter delineates the results and discussion on the performance of the coatings developed in this research work. The results of microstructure, mechanical properties, physical properties, quality characteristics, fretting wear behavior, adhesive wear behavior, wear track deformation studies and machinability characteristics are discussed.

4.1 Microstructure and elemental compositions analysis

Results of FESEM morphology and elemental compositions of TiC-C, Ti/TiN/TiCN/TiN/TiCN, AlCN/AlC and FeCrN thin solid films are represented in Figure 4.1, 4.3, 4.5 and 4.7 respectively. Cross section of the coated samples was considered for morphology and coating thickness measurement. The EDS mapping was carried out on the coated surface for elemental mapping of the elements.

Figure 4.1 (a) shows that the developed TiC-C coating is uniform and dense; droplets formed during the coating as-measured from SEM image using Image J software are in the size range of1 μm to 20 μm. For this coating, the surface roughness measured using roughness tester (Mitutoyo Talysurf) was 0.42μm. Ibrahim *et al.* (2015), in their work on TiAlN coating, have reported the development of dense coating showing a roughness of about 0.17 μm and have attributed it to a smaller droplet size.

Figure 4.1 (b) represents the EDS spectral analysis of TiC-C coating, where the presence

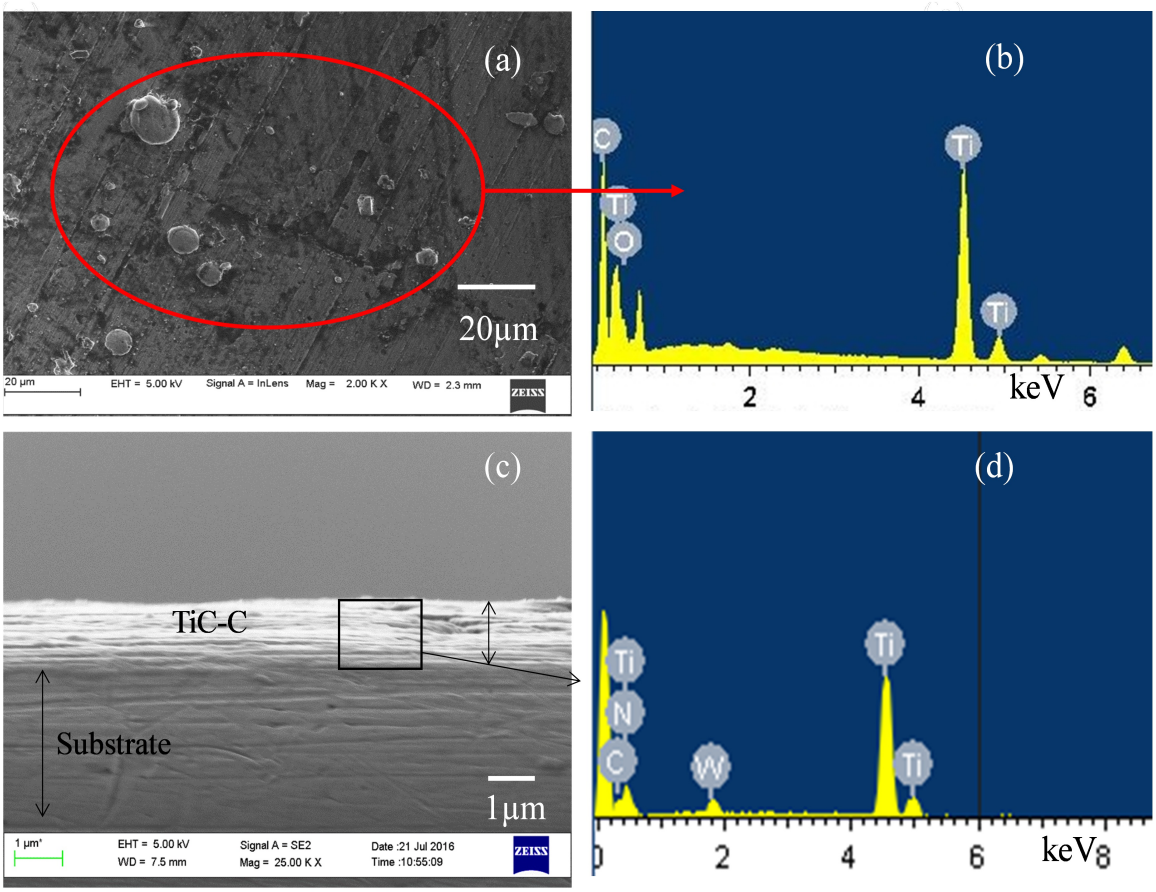

Figure 4.1: (a) FESEM micrograph on surface, (b) EDS spectrum on surface,(c)FESEM cross-section micrograph and (d) EDS spectrum on cross section of TIC-C coating

of Ti and C peaks confirms that the coating is developed successfully with the required composition.

Figure 4.1 (c-d) shows the developed TiC-C thin solid film is of thickness 1.3050 μm and EDS analysis on cross-section confirms the presence of Ti and C.

Figure 4.2 represents the elemental mapping of TiC-C coating with Ti mapped inside the droplet and C mapped as covering for the droplet which clearly indicates that Ti ions are covered with C ions leading to TiC-C coating.

Figure 4.3 (a) represents the coated morphology of Ti/TiN/TiCN/TiN/TiC coating. This micrograph represents the droplets formed during condensation. Majority of the droplets are formed in the size ranging from 1-10 μm. The coating showed a surface roughness of

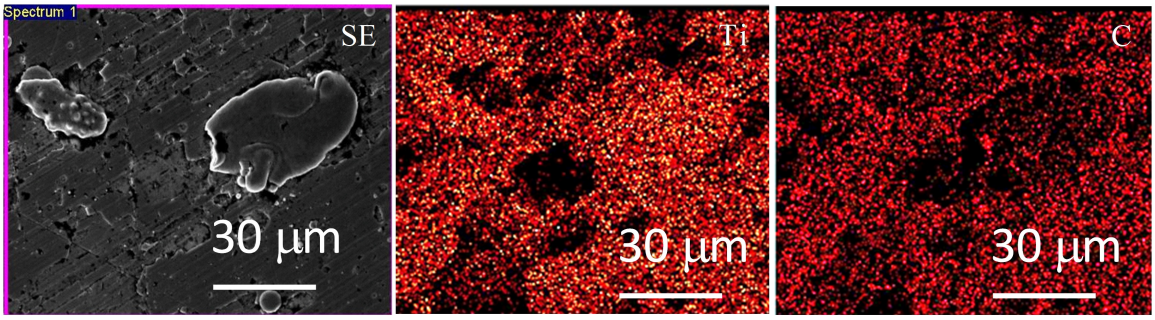

Figure 4.2: Elemental mapping of TiC-C coating

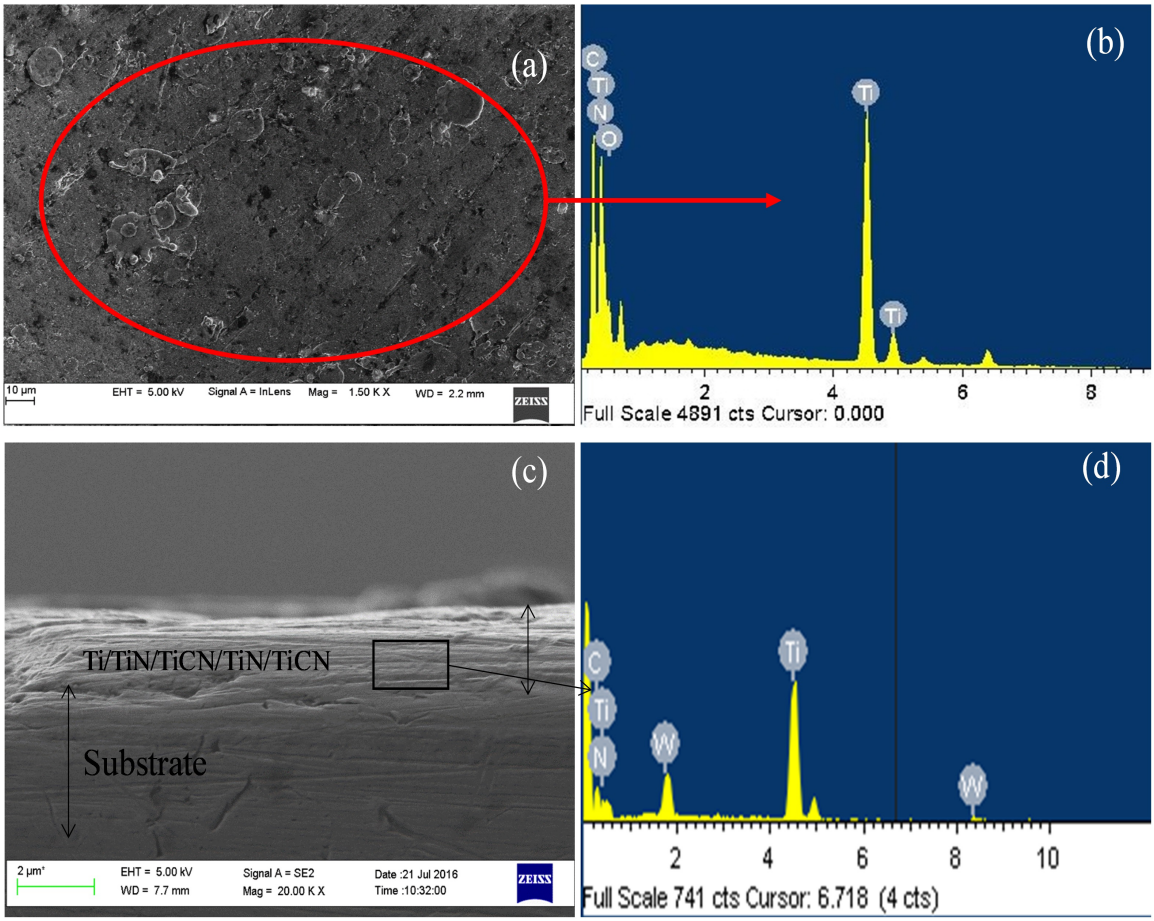

Figure 4.3: (a) FESEM micrograph on surface, (b) EDS spectrum on surface,(c)FESEM cross-section micrograph and (d) EDS spectrum on cross section of Ti/TiN/TiCN/TiN/TiCN coating

0.34 μm. This indicates that droplet size in multilayer coating is smaller than monolayer coating.

This is evident from the denser micrograph in Figure 4.3 (b) which represents the EDS spectral analysis of Ti/TiN/TiCN/TiN/TiCN coating in which one can observe the Ti, N and C peaks confirming that coating is developed successfully with the required elemental composition.

Figure 4.3 (c-d) shows the developed Ti/TiN/TiCN/TiN/TiCN thin solid film coating is developed for thickness 1.6050 μm and EDS spectral analysis on cross-section confirms the presence of Ti, C and N.

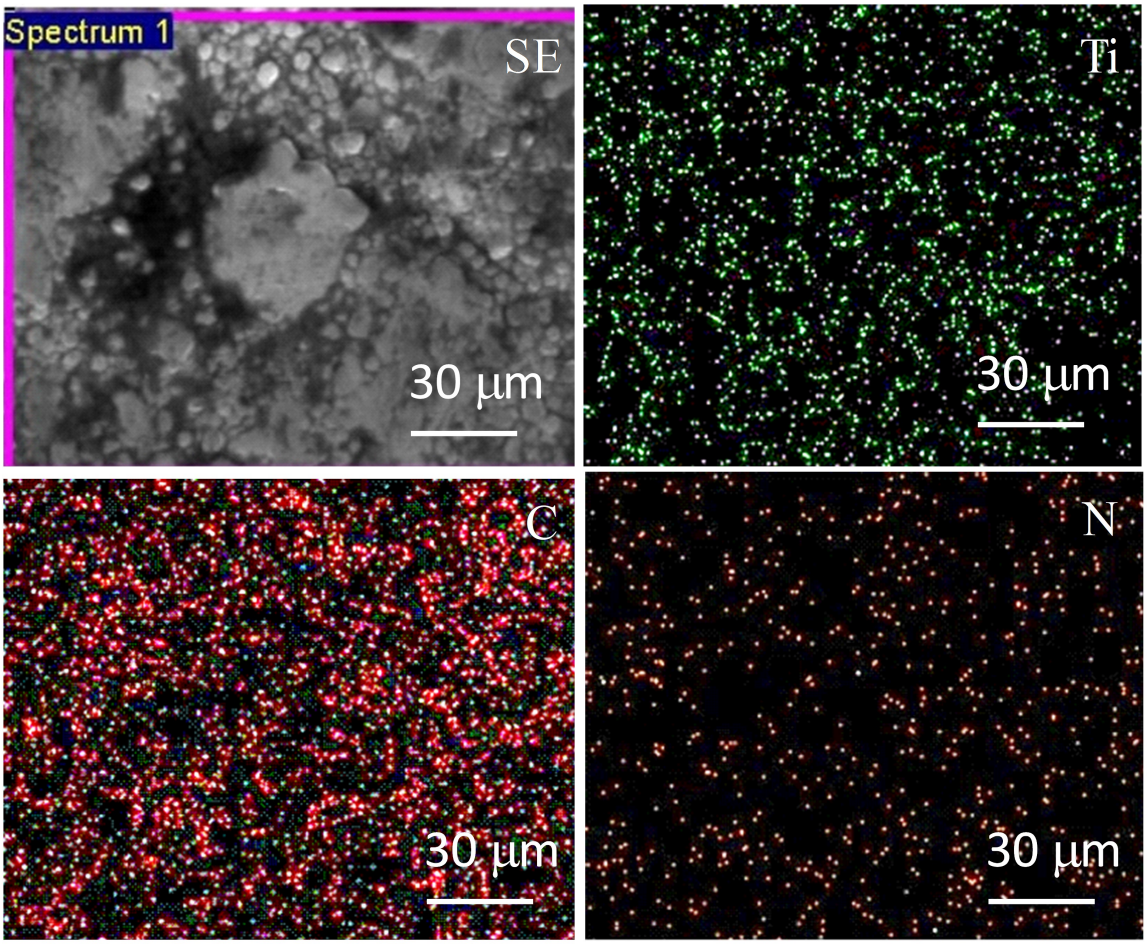

Figure 4.4: Elemental mapping of Ti/TiN/TiCN/TiN/TiCN coating

Figure 4.4 represents elemental mapping of the Ti/TiN/TiCN/TiN/TiCN coating. In the multilayer coating, the average individual layer thickness is found to be Ti= 187 nm, TiN= 571 nm, TiCN= 152 nm, TiN= 226 nm, and TiCN=326 nm. The developed multilayer

coating is a continuous deposition. The initial layer of Ti is added onto the substrate. Over the Ti layer, alternate layers of TiN and TiCN are deposited by the controlled supply of reactive gases. The presence of nitride phase results in the increased hardness of the coating.

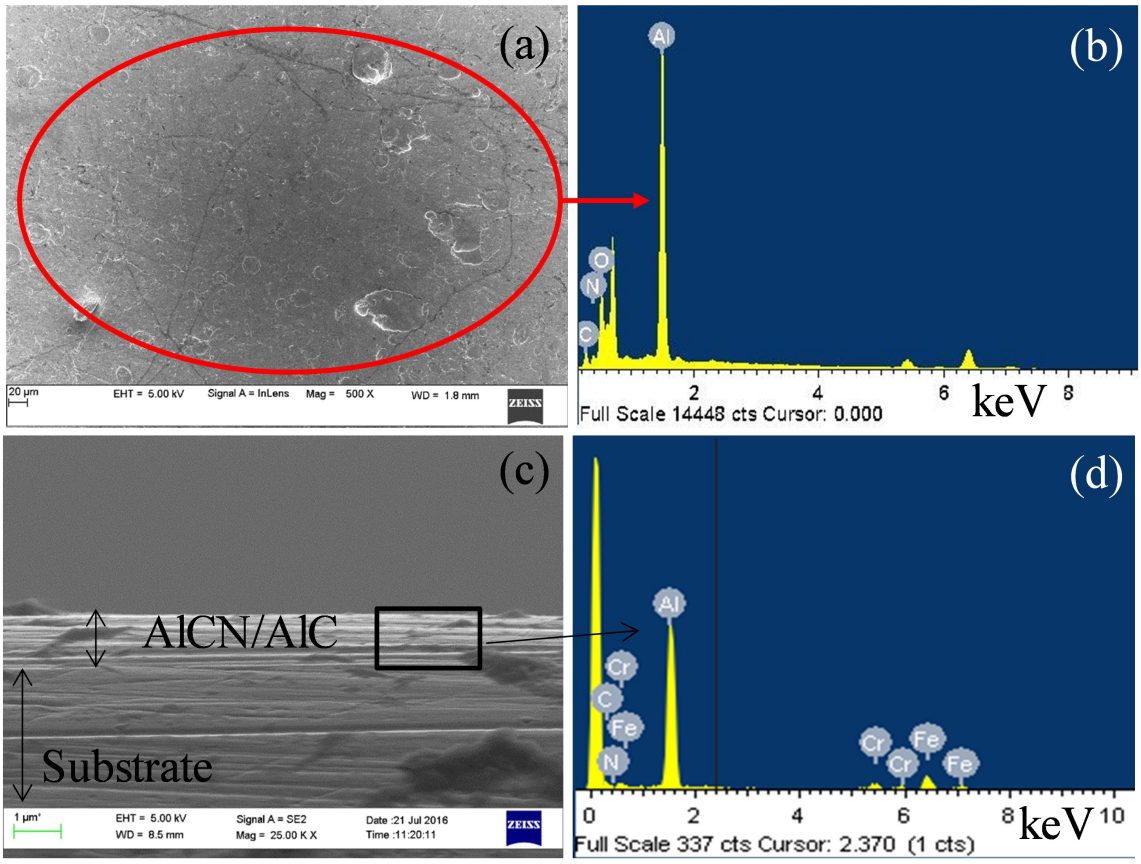

Figure 4.5: (a) FESEM micrograph on surface, (b) EDS spectrum on surface, (c)FESEM cross-section micrograph and (d) EDS spectrum on cross section of AlCN/AlC coating

Figure 4.5 (a) shows that the developed AlCN/AlC coatings are even and dense; droplets formed during the coatings as measured from SEM image using ImageJ software are in the size range of 1 to 20 μm. The surface roughness of the coating is measured using Mitutoyo Talysurf and found to be 0.42 μm.

Figure 4.5 (b) represents the EDS spectral analysis of AlCN/AlC coating, which shows the presence of Al, C and N peaks, confirming that coating is developed successfully with the

required composition.

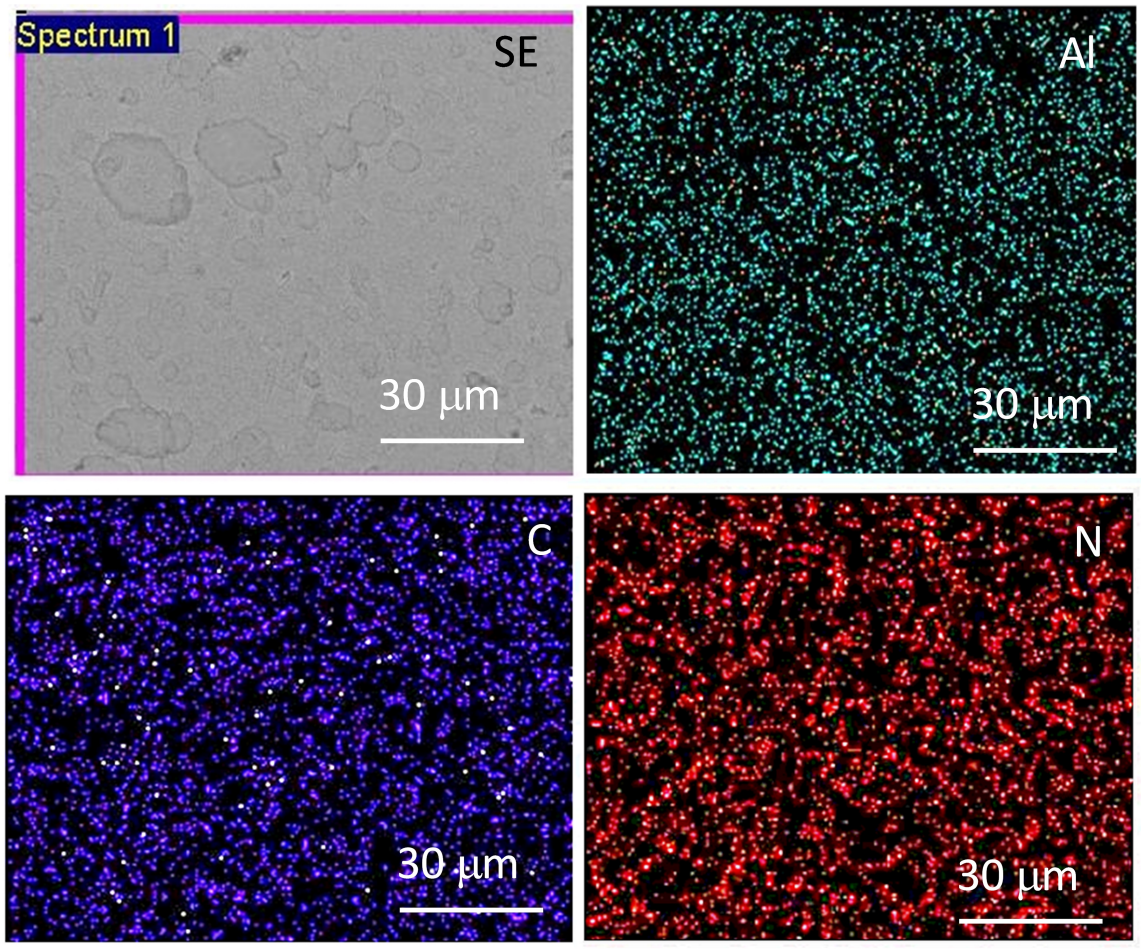

Figure 4.6: Elemental mapping of AlCN/AlC coating

Figure 4.6 represents the elemental mapping of AlCN/AlC coating. From the observations of the mapping results, coexistence of Al with N and C are evident and this confirms the presence of AlCN and AlC.

Figure 4.7 (a) represents FeCrN coating is equally distributed over the surface with droplets formed during condensation. Majority of the droplets are formed in the size ranging from 1-10 μm and the maximum numbers of particles are in 1-3 μm size. The coating showed a surface roughness of 0.48 μm. The micrograph shows cluster like microstructure which are the globules of irons deposited onto the surface.

Figure 4.7 (b) represents the EDS spectral analysis FeCrN coating, the peaks of Fe, Cr,

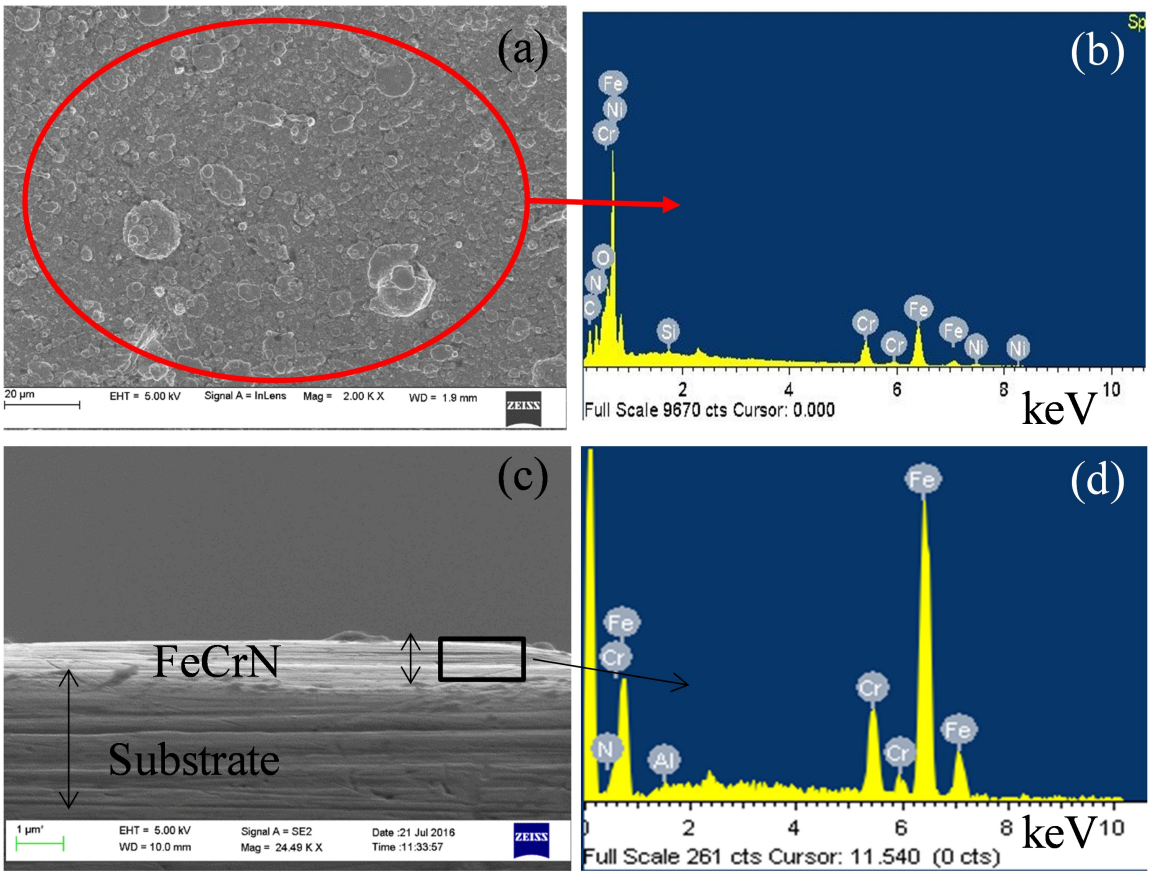

Figure 4.7: (a) FESEM micrograph on surface, (b) EDS spectrum on surface,(c)FESEM cross-section micrograph and (d) EDS spectrum on cross section of FeCrN coating

Ni, C and N are observed which confirming that coating is developed successfully with the required elemental composition.

Figure 4.7 (d) represents the EDS spectral analysis FeCrN coating. The peaks of Fe, Cr, Ni, C and N are observed while confirming that coating is developed successfully with the required elemental composition.

Figure 4.8 represents an elemental mapping of FeCrN coating in which Fe and Cr cluster in the form of globules. N is distributed evenly covering the surface with the co-existence of Fe and Cr, confirming FeCrN coating on the surface.

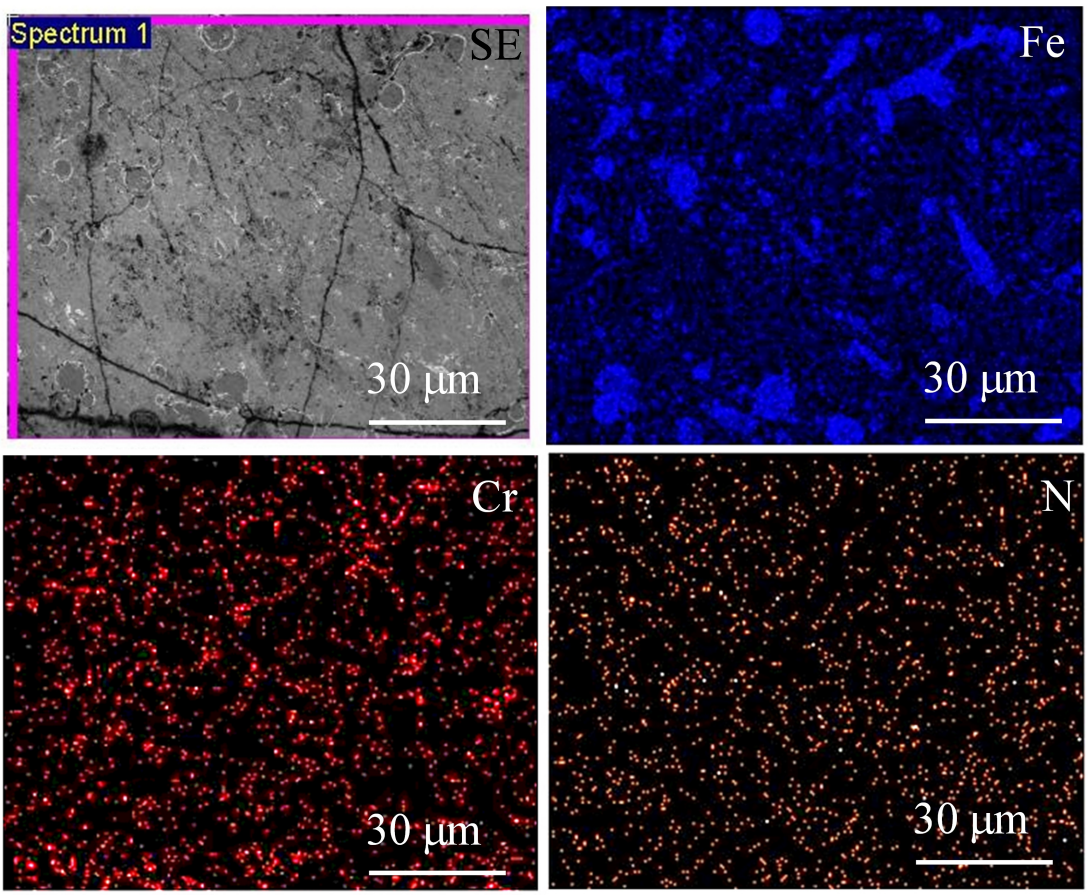

Figure 4.8: Elemental mapping of FeCrN coating

The GAXRD analysis is carried out on the surface at a glancing angle of 2°. Figure 4.9 (a) exhibits the results of XRD analysis of TiC-C coating and Ti/TiN/TiCN/TiN/TiCN. Compounds formed during the coating have the major phase of TiCN, TiC and TiN. Peaks obtained in TiC-C monolayer coating are in correspondence with major phases of TiC peaks in agreement with JCPDS card No 892726. Peaks obtained in Ti/TiN/TiCN/TiN/TiCN multilayer coatings are in correspondence with major phases TiC, TiN and TiCN peaks with the JCPDS card No 892726, 655774 and 861152 respectively. Similar type of XRD peaks are reported for single and multi-layer coatings of TiAlN (PalDey and Deevi, 2003). Results of Raman spectral analysis for TiC-C, Ti/TiN/TiCN/TiN/TiCN coated samples are represented in Figure 4.9 (b). Raman peaks for TiC and TiN compounds are observed at Raman shift value of 426, 605 cm^{-1} and 540, 310, 600 cm^{-1} respectively. Presence of

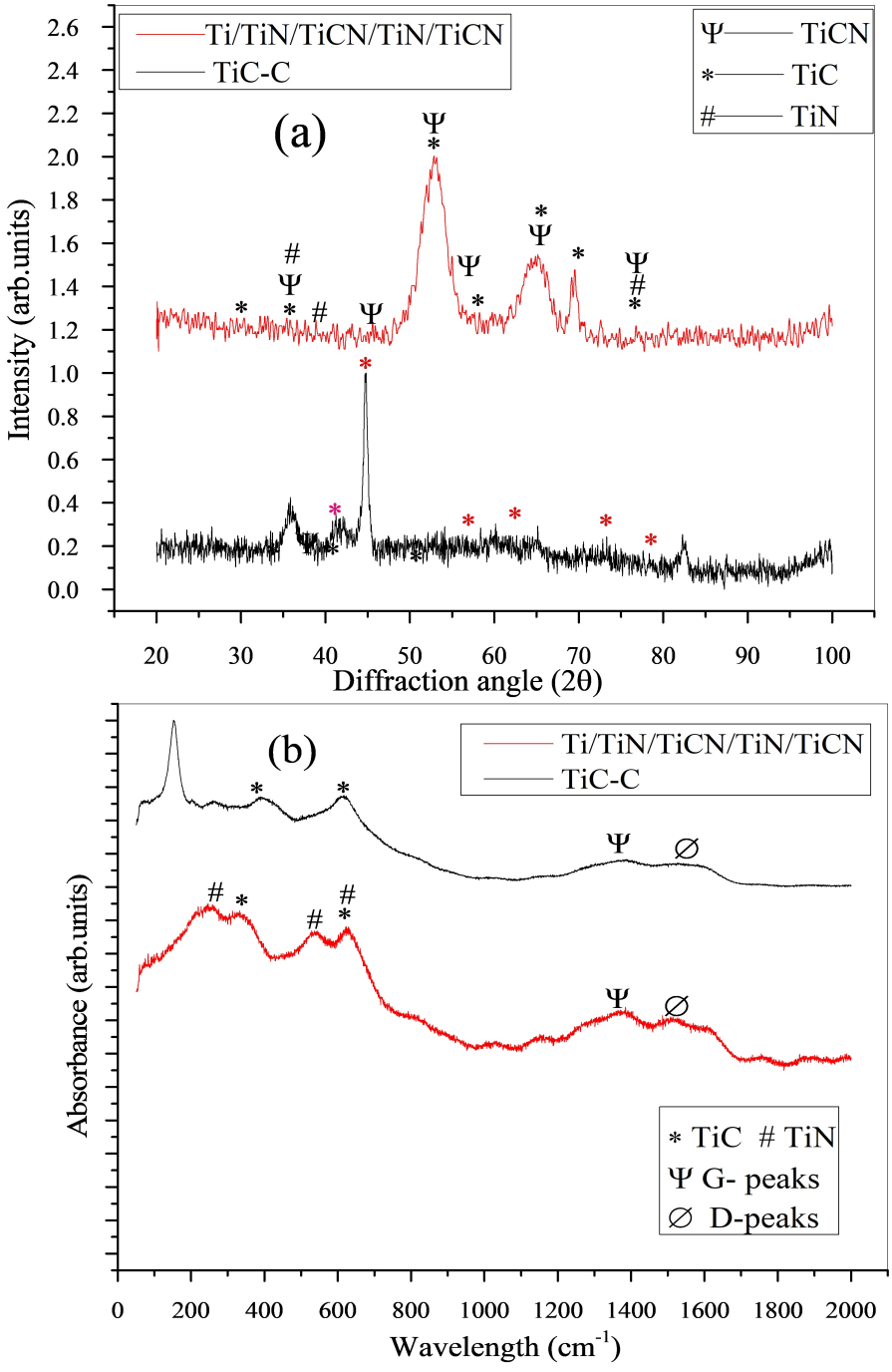

Figure 4.9: (a) GAXRD plots and (b) RAMAN spectral analysis of Ti monolayer and multilayer coatings

DLC is evident in both the Ti coatings, Which is confirmed with the presence of G-peaks (sp^3 hybridized carbon atoms) and D-peaks (sp^2 hybrid carbon atoms) at Raman shift of 1364 and 1583 cm^{-1} for multilayer Ti coatings; 1381 and 1509 cm^{-1} for TiC-C coating respectively.It was reported in earlier research that G and D peaks of DLC coatings appear e at 1335 cm^{-1} and 1580 cm^{-1}, respectively, which are in a close agreement with the results obtained here. The value of 1.1605 for the ratio of D/G for Ti-multilayer coatings indicates the presence of graphene multilayers in the coating. D/G 1.09 for TiC-C which indicates the presence of diamond-like structured graphene layer with sp^3 phase. Significant presence of sp^3 structured carbon atoms is attributed to improvement in mechanical properties as shown in Table 4.1. Hardness of 31.77 and 29.09 GPa are measured in Ti-multilayer and TiC-C monolayer coating respectively. Elastic modulus of 297 GPa and 334 GPa are reported in Ti-multilayer and TiC-C monolayer coating respectively. Similar conclusions have been reported by Ramamoorthy and Yeldose (2009) while investigating adhesion strength of DLC multilayer coating.

Figure 4.10 (a) exhibits the results of XRD analysis for AlCN/AlC coating. Compounds formed during the coating have the major phase of carbides Al_4C_3 in agreement with JCPDS card No 791736 and 712205. Aluminium-carbon-nitrides formed during the coatings are in the form of $Al7C_3N_3$, $Al_8C_3N_4$, $Al_6C_3N_2$ and Al_5C_3N in agreement with JCPDS card No 893201, 850413, 882155 and 712205 respectively.

In FeCrN coating nitrides of Fe and Cr are obtained in different chemical compositions. Cr ions combined with the nitrogen are in correspondence with major phases Cr_2N and CrN peaks with the JCPDS card No 792159. Fe ions combined with the nitrogen are in correspondence with major phases Fe_2N, Fe_3N and Fe_4N peaks with the JCPSDS card No 882153, 893939, 860232 and 860231. Chromium-iron-nitride compound phases are observed $(Cr, Fe)_2N_{1-x}$ peaks with the JCPDS card No 190330.

Results of Raman spectral analysis for AlCN/AlC and FeCrN coated samples are represented in Figure 4.10 (b). Raman peaks for AlC compound are exhibited at Raman shift values of 532 and 785 cm^{-1}. DLC presence is not evident on both AlCN/AlC and

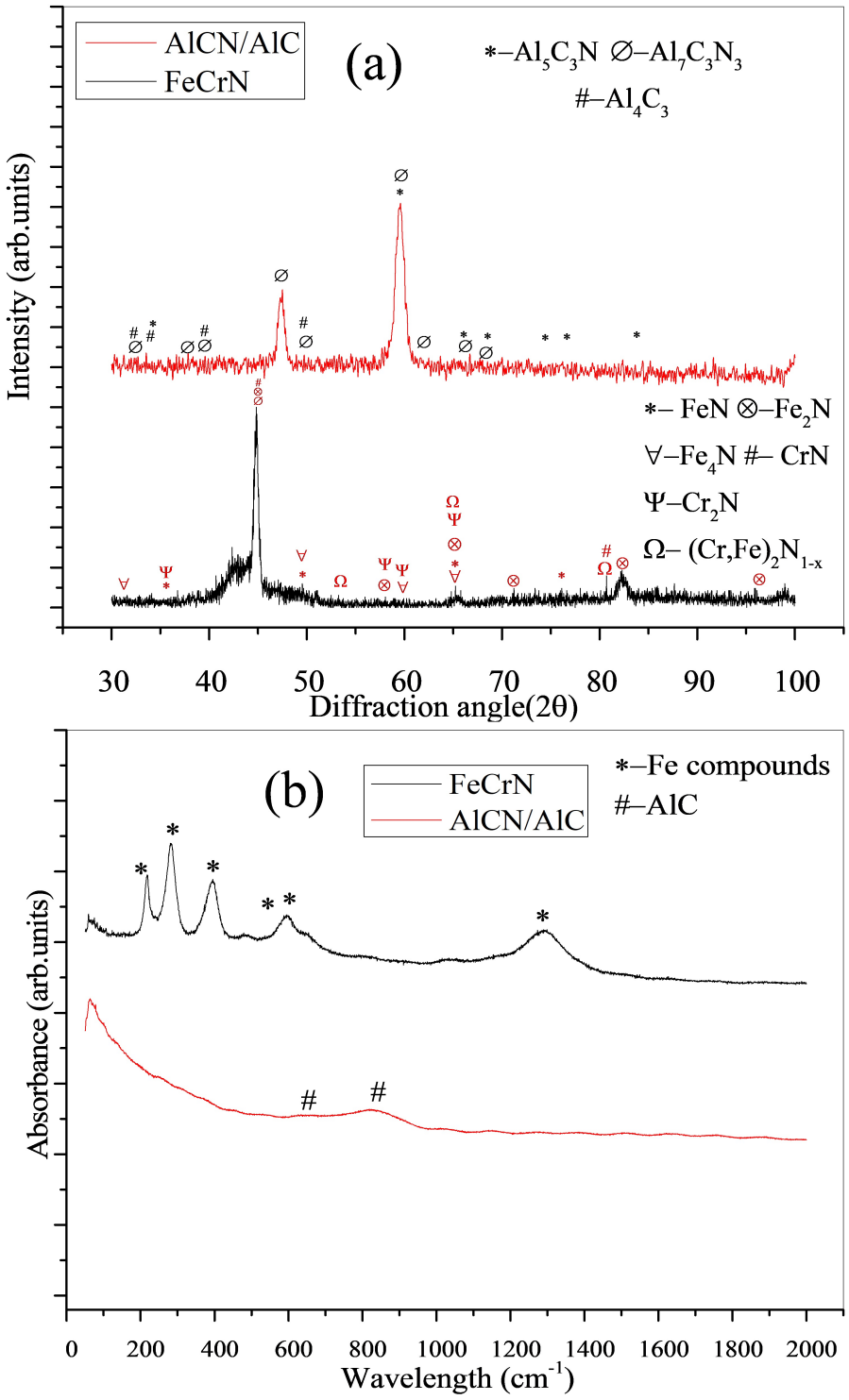

Figure 4.10: (a) GAXRD plots and (b) RAMAN spectral analysis of AlCN/AlC and FeCrN coatings

FeCrN coatings. Raman peaks for Fe compounds are exhibited at Raman shift values of 216, 282, 392, 595, 1291 and 1500 cm^{-1}.

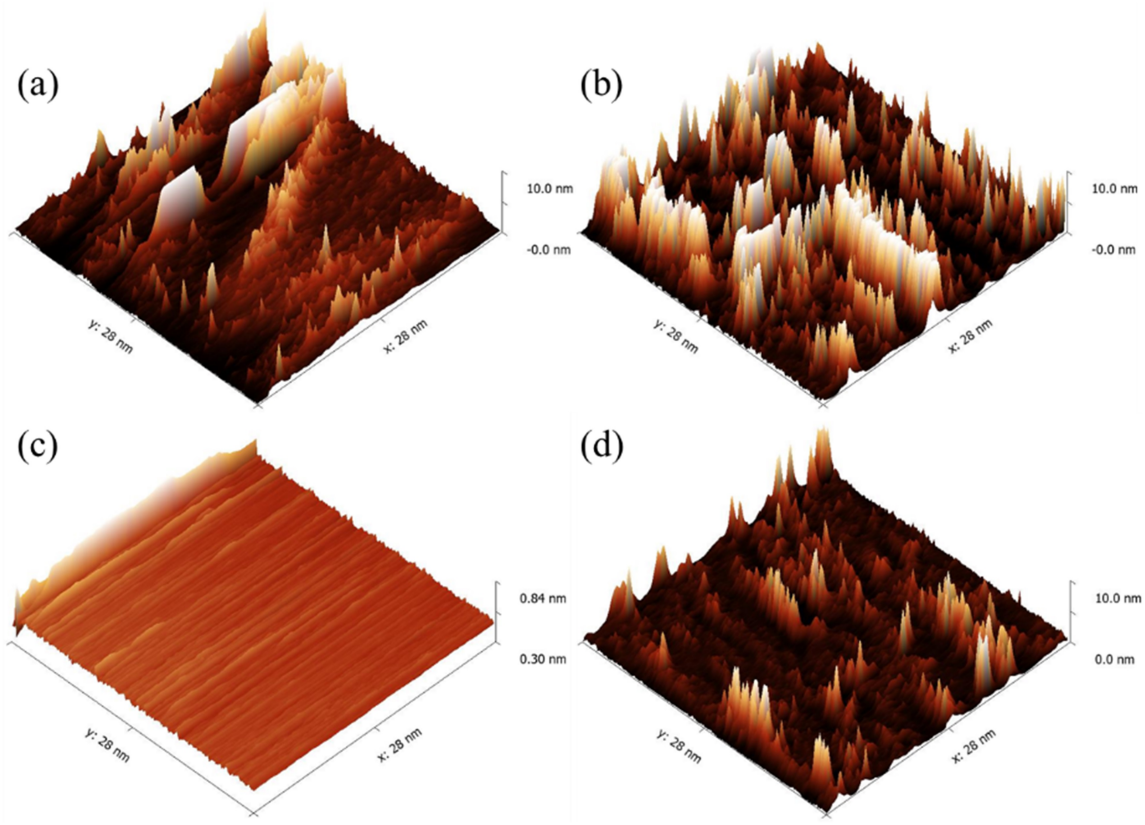

Figure 4.11: STM topography of coatings (a)TiC-C (b) Ti/TiN/TiCN/TiN/TiCN (c) AlCN/AlC and (d)FeCrN

Figure 4.11 represents the surface topography of coatings. Surface topography of the coated samples were studied using scanning tunnelling microscopy at a tunnelling current of 5 nA with a scan area of $28nm \times 28nm$. Atomic arrangement at nano level is observed and the Ra at the atomic scale is found to be 1.37 nm, 1.965 nm, 1.24 nm and 0.907 nm for TiC-C, Ti/TiN/TiCN/TiN/TiCN, AlCN/AlC and FeCrN coatings respectively. The R_a value of the developed coatings are lower than TiCN monolayer and multilayer Ti/TiCN coatings Jao *et al.* (2010). The developed coatings showed uniform columnar crystal structure.

Figure 4.12 and Figure 4.13 show the results of VDI3198 and Calo test. VDI3198 is the industrially accepted qualitative analysis for the adhesion test and Calo test is the

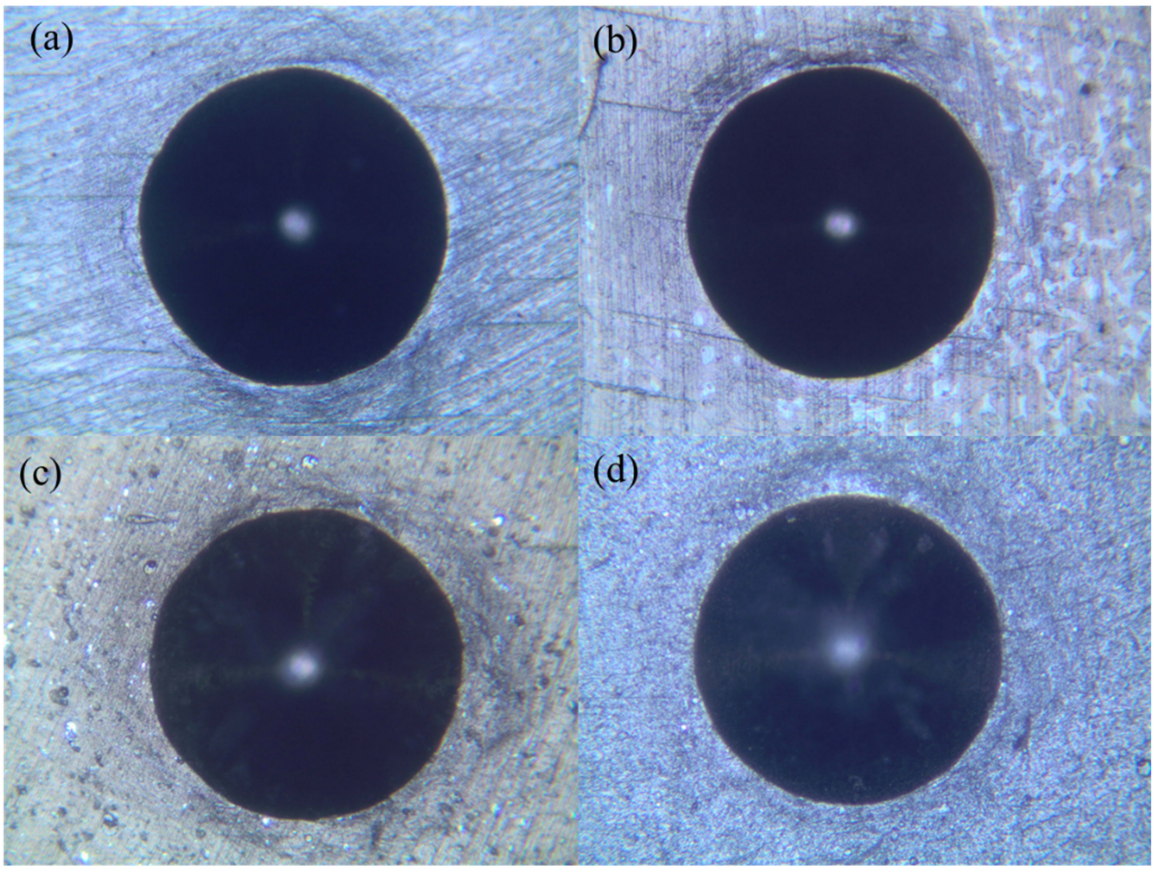

Figure 4.12: VDI3198 results of coatings (a)TiC-C (b) Ti/TiN/TiCN/TiN/TiCN (c) AlCN/AlC and (d)FeCrN

technique used to measure the thickness of the coatings. It is observed from Figure 4.12 that all the coatings exhibited HF1 failures which indicate that developed coatings possesses industrially acceptable adhesion strength. Figure 4.13 represents the results of Calo test showing the coating thickness. In Calo test the metallic (AISI steel) ball rotates against the coated surface at 200 rpm for 120-180 sec, which creates spheroidal grove on the surface. The deformed area is imaged by microscopic and image analyser software calculates the thickness of the coating. The formula (4.1) is used to calculate the coating thickness.

In order to validate the coating thicknesses, it was measured using FESEM and Calo test. Both results are very close to each other and the same is tabulated in Table 4.1. The different thickness calculation methods for these samples are based on ISO EN1071-2.

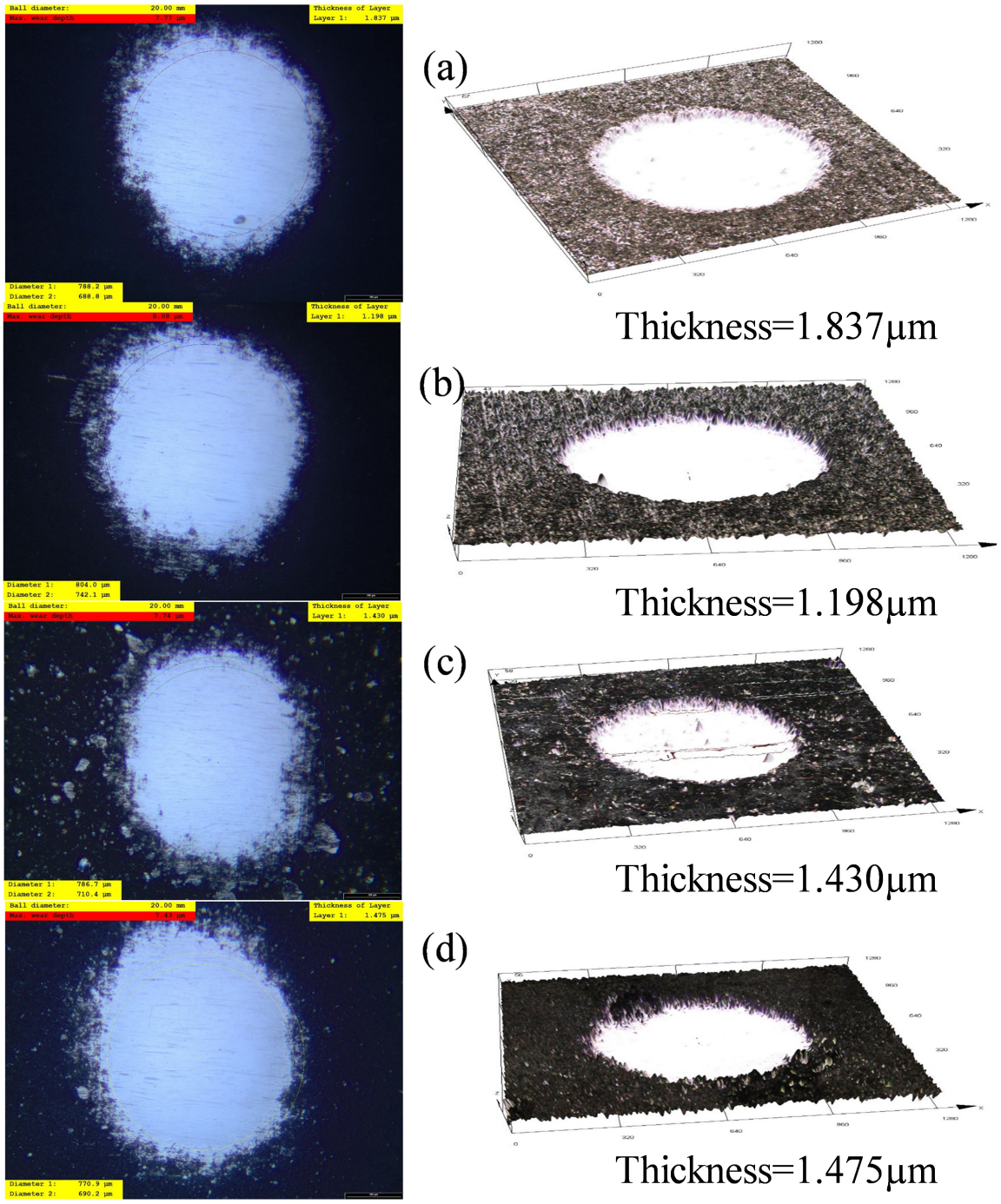

Figure 4.13: Calo test results of coatings (a) TiC-C (b) Ti/TiN/TiCN/TiN/TiCN (c) AlCN/AlC and (d) FeCrN

Calo thickness calculation formula: -

$$t=xy\frac{}{dt=xy\frac{}{dt=xy\frac{}{dt=xy\frac{}{d(4.1)}}}}$$

Here t = coating thickness, d = diameter of the sphere x = difference between the radius of the crater and radius of the part of the crater at the bottom of the coating $x+y$ = diameter of the crater

4.2 Mechanical properties

The hardness and elastic modulus of the deposited coatings are evaluated using nanoindentation technique and the measured values are shown in Table 4.1 . Due to high surface roughness the depth of penetration has been maintained at 60% of coating thickness (As per the standard ISO 14577: 5-10% of surface roughness). The number of experimental trials needs to be conducted is finalised keeping the depth of penetration at 60% of the coating thickness (Bergles et al. 2004). Depths of penetration are kept constant to 60% of the coating thickness, and loading and unloading cycles are carried out using the nanoindenter with the help of Berkovich indenter tip. Each test is repeated at ten distinct locations on the same surface.

Table 4.1: Mechanical properties of coatings

Coating	**Hardness**	**Elastic Modulus**	**Thickness**		**Surface Roughness**	**Critical load**
	(GPa)	**(GPa)**	**(μm)**		**(μm)**	**(mN)**
			FESEM	**Calo**		
MDN121	4.20	317.54	NA	NA	0.03	NA
TiC-C	29.9	334.00	1.30	1.20	0.22	108.40
Ti/TiN/TiCN/TiN/TiCN	31.07	297.60	1.60	1.99	0.33	47.70
AlCN/AlC	26.09	302.00	1.40	1.43	0.40	53.60
FeCrN	36.19	201.00	1.50	1.48	0.42	83.00

Plots of load on sample, hardness and elastic modulus for TIC-C, Ti/TiN/TiCN/TiN/TiCN, AlCN/AlC and FeCrN coatings are represented in Figure 4.14 and Figure 4.15. Results of nanoindentation are tabulated in Table 4.1.

Confocal micrographs taken on the indent spots are represented in the Figure 4.16. The depth of penetration is found to be within the coating thickness. Adhesion of the coatings are found out in qualitative way using the VDI 3198 test. The quantitative analyses of the adhesion of the coatings are measured using the nano scratch test (Figure 4.17) with the nanoindenter. The probe is moved against the surface with the increasing load. When the sudden variation in the plot is observed, it indicates the materialistic properties which in turn ascribed that the probe has reached the substrate. Hence the load at which variation/disturbance occurred is known as failure load and the load just before the failure is termed as a critical load. Critical load for all the coatings is presented in 4.1.
Nano scratch results of coatings (a) TiC-C (b) Ti/TiN/TiCN/TiN/TiCN (c) AlCN/AlC and (d) FeCrN are represented in Figure 4.17.

4.3 Fretting wear behaviour of the coatings

Figure 4.18 and Figure 4.19 exhibit the maximum wear track deformation observed during fretting wear test of the TiC-C, Ti/TiN/TiCN/TiN/TiCN, AlCN/AlC and FeCrN coatings. In each coating, the amount of area deformation has increased with an increase of load.

4.3.1 Fretting wear rate

At 20 mN the magnitude of the area deformation in TiC-C coating shown in Figure 4.18 (a) is higher compared to the multilayer coating shown in Figure 4.18 (b). At higher loads of 40 mN and 60 mN, the amount of increase in deformed area in multilayer coatings is higher compared to monolayer coating. Critical load is the load at deformation of both coating and substrate will always occur. One of the reasons for this could be the critical load of TiCN which is reported to be 40 mN mN (Burnett and Rickerby 1987). Further, the significant difference between elastic properties of interlayers can also cause easy penetration of indenter stylus. In contrast, the maximum wear track deformation in case of monolayer

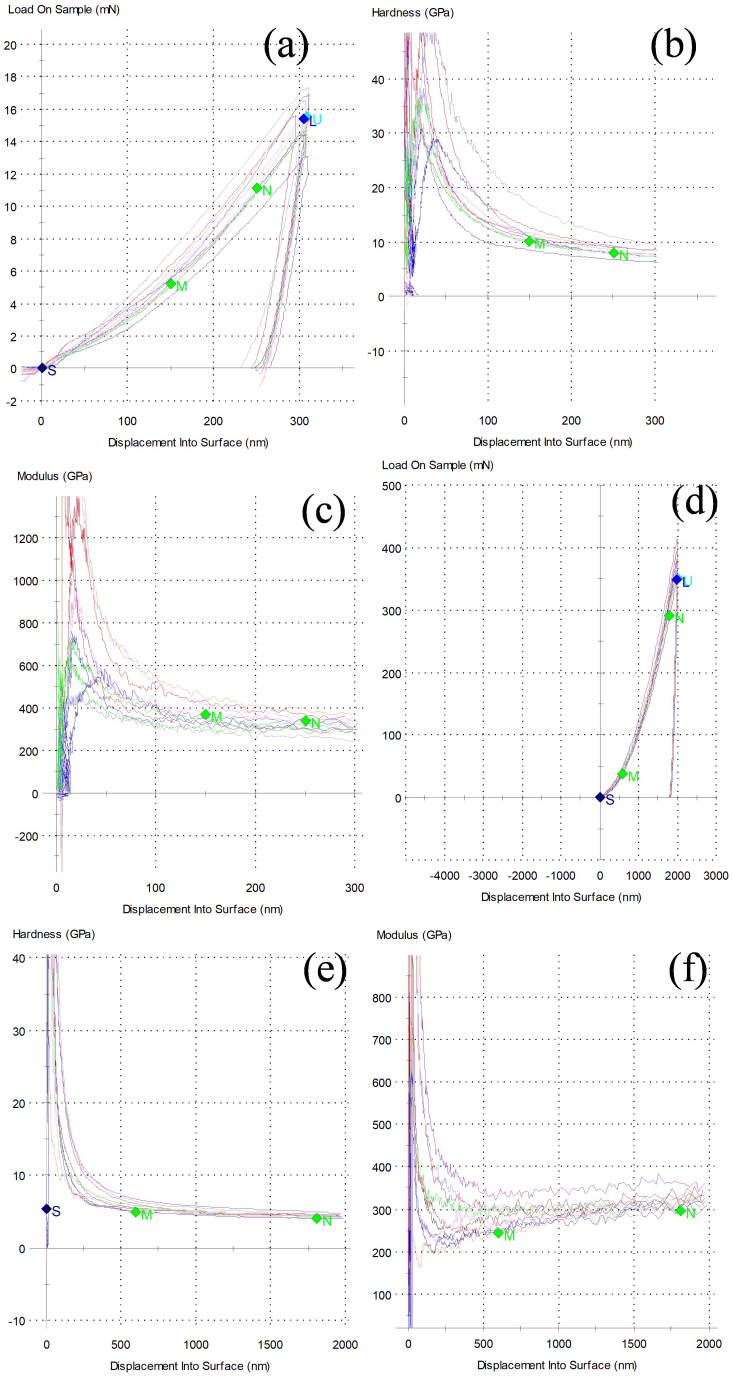

Figure 4.14: Nano Indentation plots of (a-c) TIC-C Coating and (d-f) Ti/TiN/TiCN/TiN/TiCN coatings (a, d) Load on sample, (b, e) Hardness and (c, f) Elastic Modulus

TiC-C at 40mN and 60mN is lower owing to higher critical load. The TiC compound in

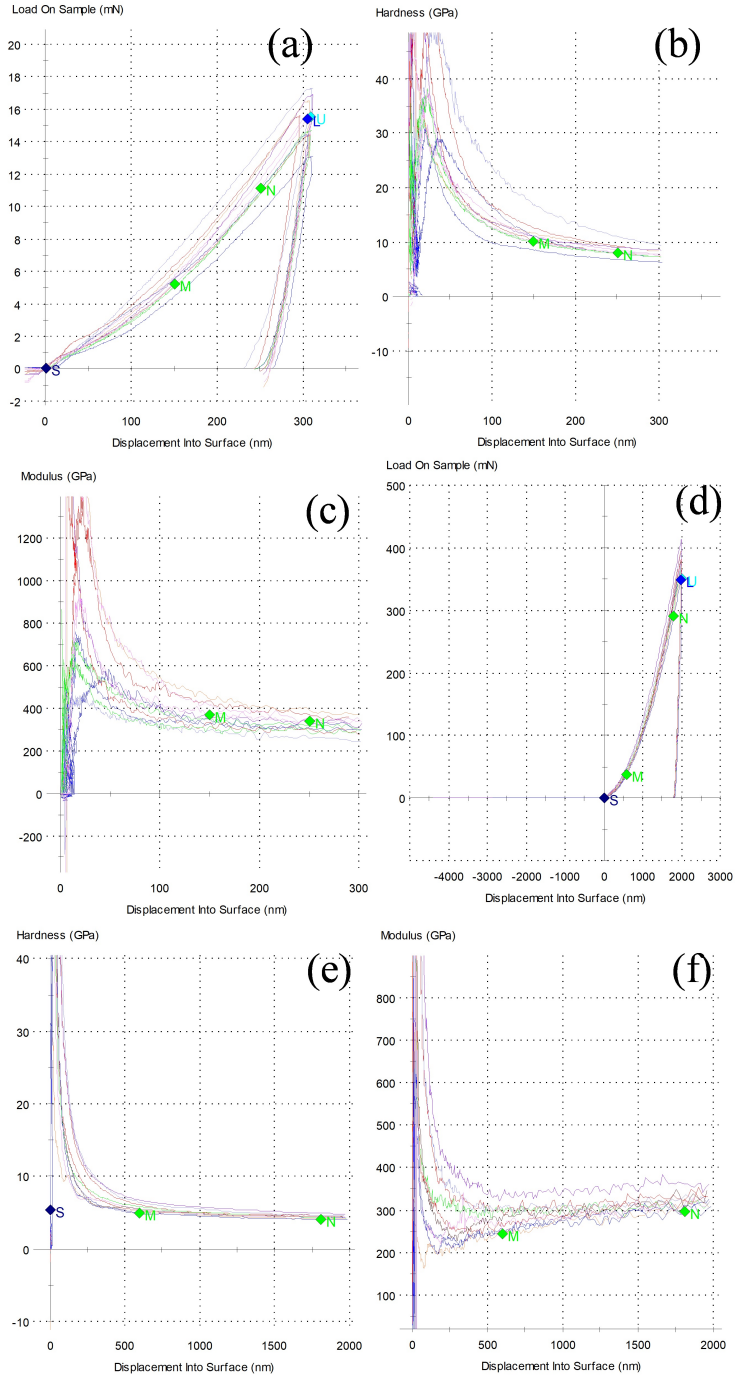

Figure 4.15: Nano Indentation plots of (a-c) AlCN/AlC and (d-f) FeCrN coating (a, d) Load on sample, (b, e) Hardness and (c, f) Elastic Modulus

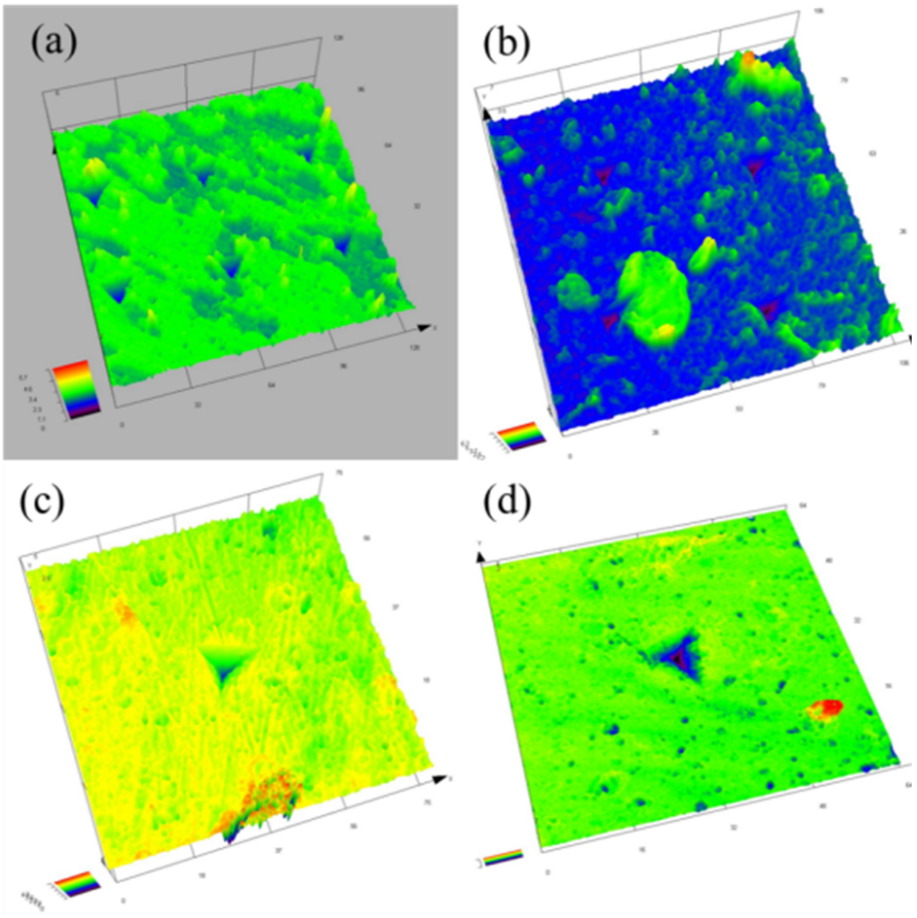

Figure 4.16: Nano indent micrograph of coatings (a) TiC-C (b) Ti/TiN/TiCN/TiN/TiCN (c) AlCN/AlC and (d) FeCrN

the coating is hard in nature which is attributed to non-uniform deformation from cycle to cycle and restricts the wear scar to propagate to the substrate. Rahmati *et al.* (2015) in their investigation of fretting fatigue of TiCr/TiN/CrN have discussed that improvement in surface hardness leads to an abrasive type of wear due to friction.

Figure 4.19 (a) and (b) exhibit the maximum wear track deformation during fretting wear analysis of the AlCN/AlC and FeCrN coatings. In both the coatings, the amount of area deformed has increased with the increase in load. For FeCrN coating it's evident that the

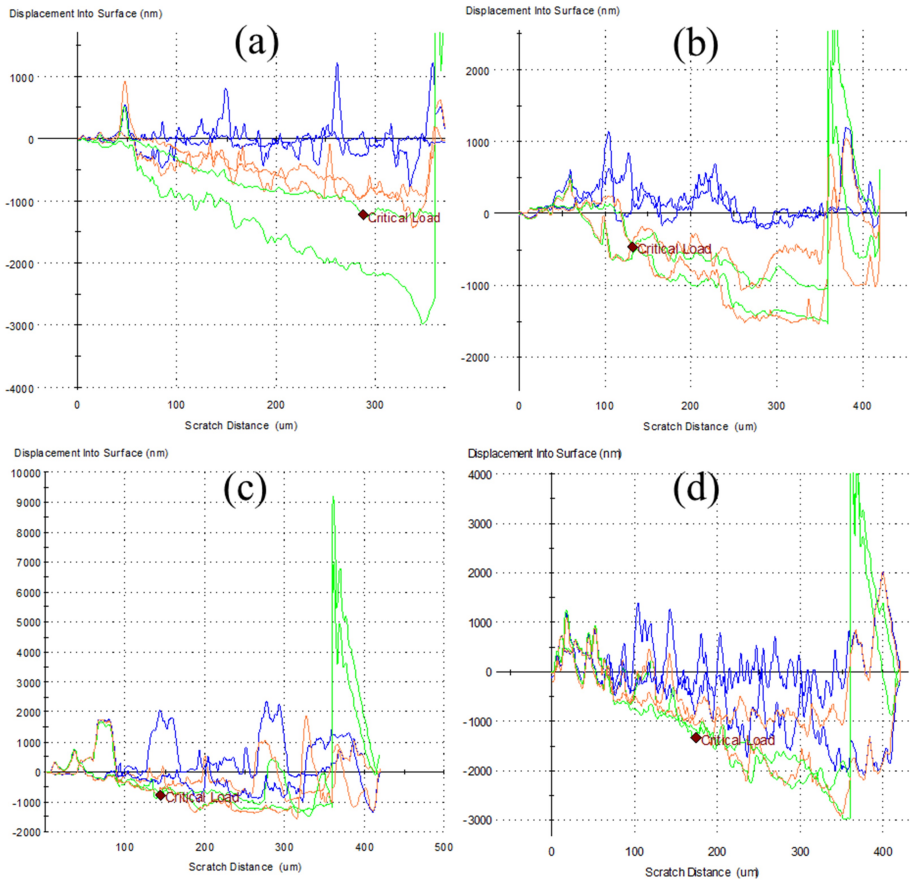

Figure 4.17: Nano Scratch results of coatings (a) TiC-C (b) Ti/TiN/TiCN/TiN/TiCN (c) AlCN/AlC and (d) FeCrN

volume of wear loss during the test is minimum because of ferric nitrides (FeN, Fe_2N, and Fe_4N) and chromium nitrides (CrN and $Cr_2$2N) present on the surface. The presence of ferric nitrides and chromium nitrides lead to an increase in its hardness to 36.19 GPa due to which the volumetric wear loss is reduced.

Figure 4.20 (a) represents the variation of COF for the coatings and the substrate. It is found that the COF after the coating is reduced by 68.49 % in TiC-C, 42.46 % in Ti/TiN/TiCN/TiN/TiCN, 48.65 % in AlCN/AlC and 62.16 % in FeCrN compared to a substrate having COF of 0.75. With the presence of DLC features, lubricating properties of the coatings are improved and hence friction occurring during fretting analysis is reduced in TiC and Ti/TiN/TiCN/TiN/TiCN coatings.

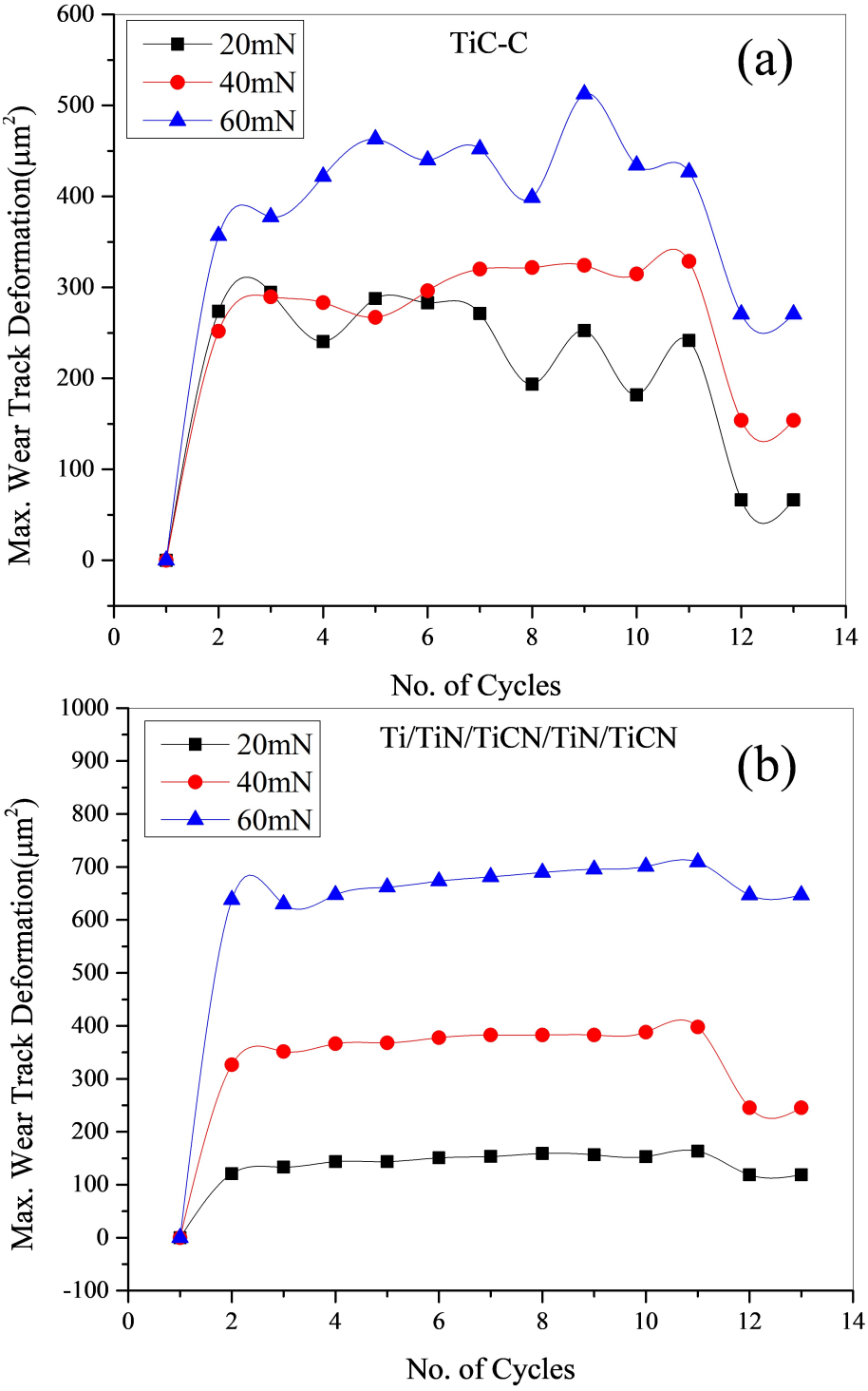

Figure 4.18: Fretting wear analysis of coatings (a) TiC-C and (b) Ti/TiN/TiCN/TiN/TiCN

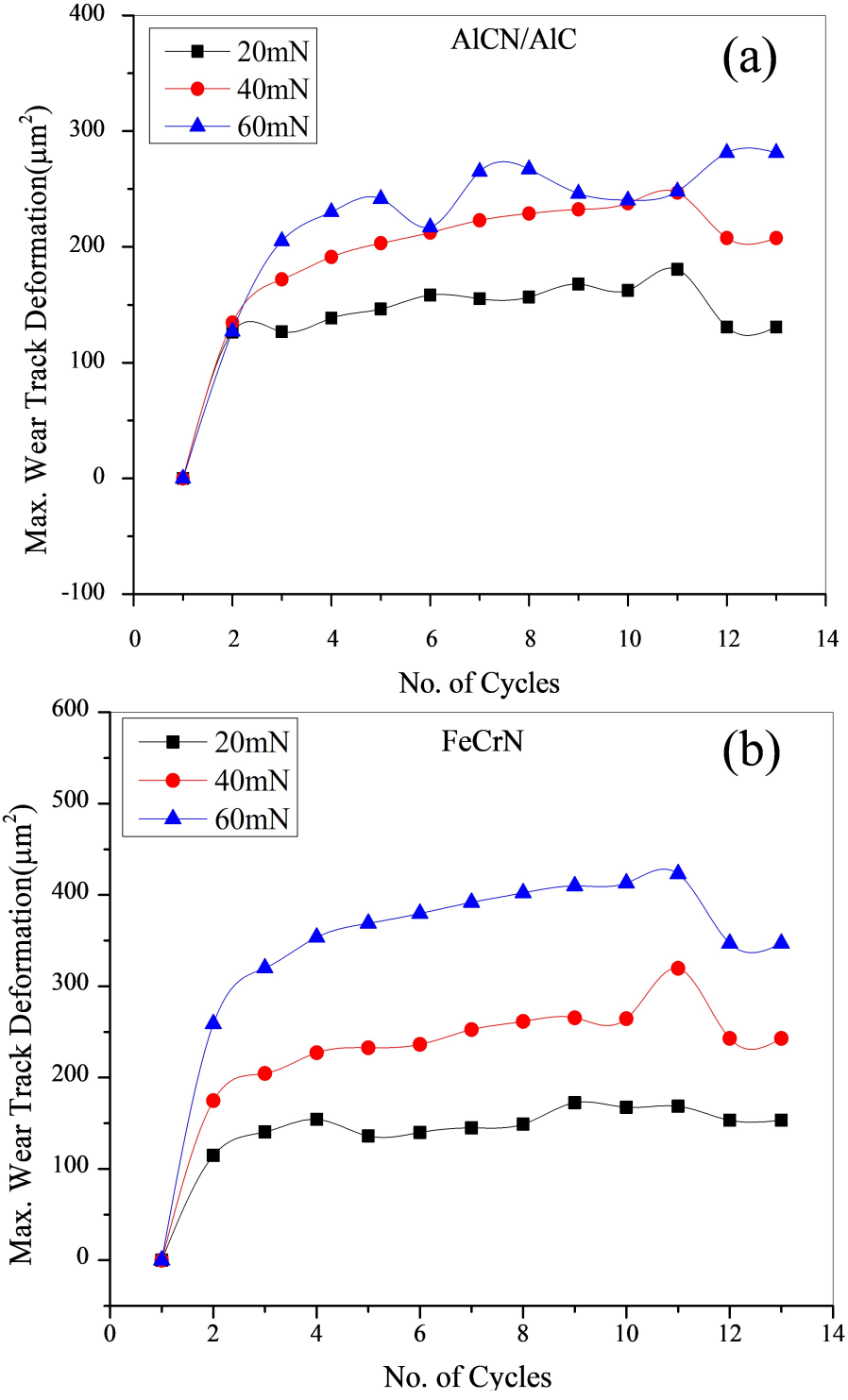

Figure 4.19: Fretting wear analysis of coatings (a) AlCN/AlC and (b) FeCrN

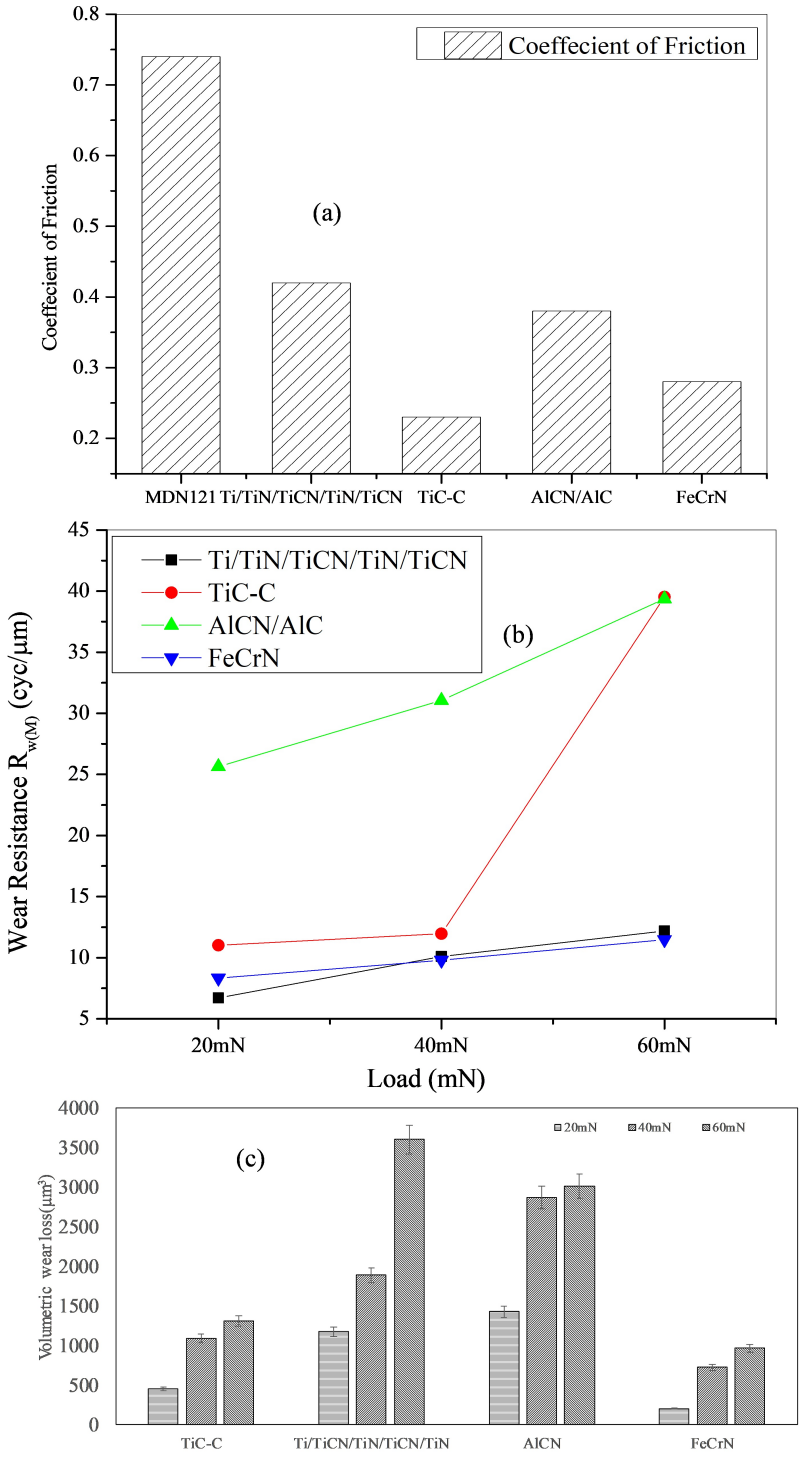

Figure 4.20: (a) Plot of COF, (b) Plot of Wear resistance versus Load and (c) Volumetric loss during wear studies

Figure 4.20 (c) shows the volumetric wear loss experienced during wear test for coated samples. In each coating wear loss has reduced showing an improvement in wear resistance at all of the three loads under the fretting condition.

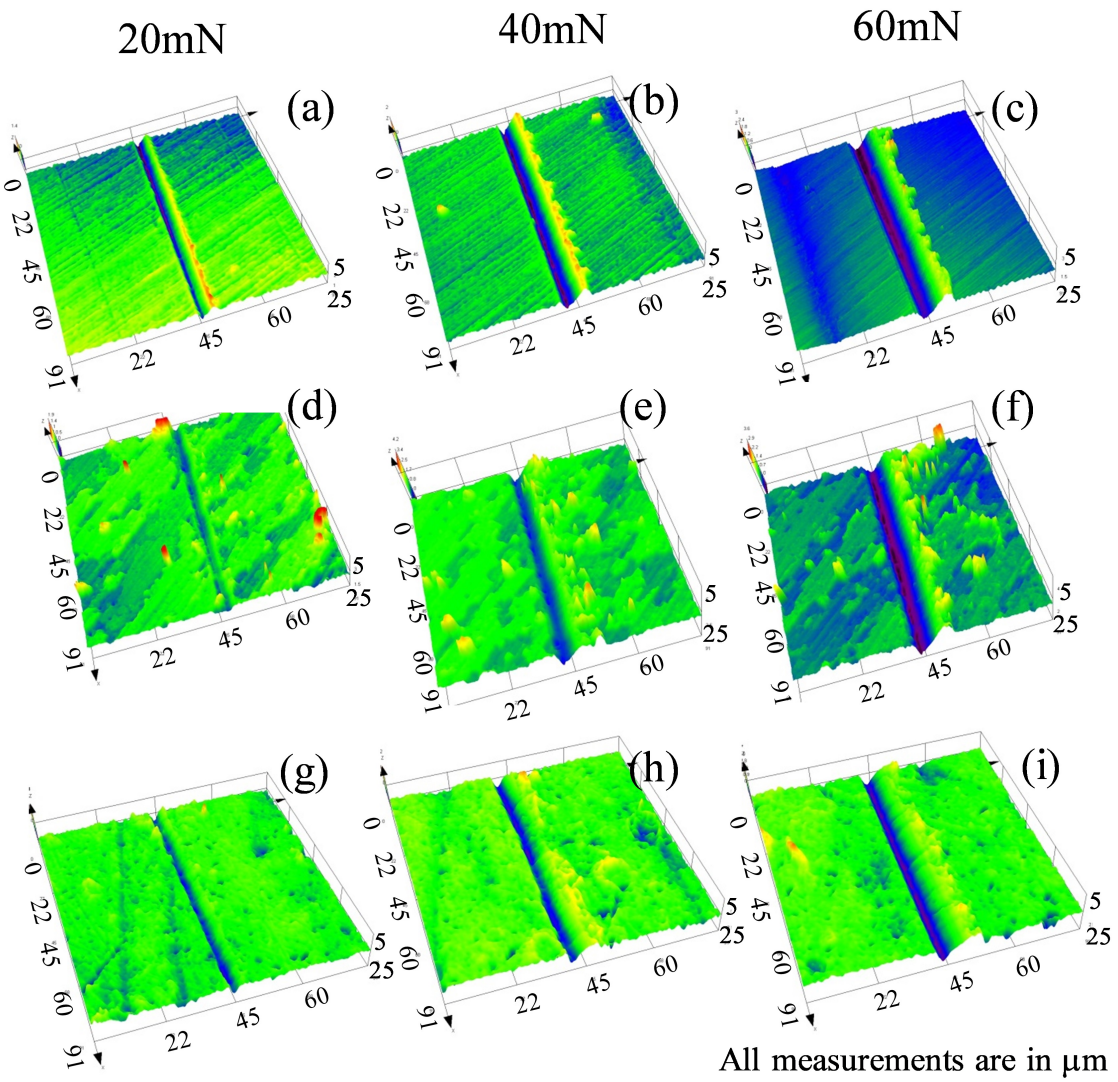

Figure 4.21: Wear tracks deformation at load of 20 mN, 40 mN and 60 mN (a-c) MDN121 (d-f) TiC-C coating (g-i) Ti/TiN/TiCN/TiN/TiCN coating

The confocal micrographs (Figure 4.21 and 4.22) further justify these results with maximum worn material built-up in case of substrate and minimum in case of TiC-C. The presence of DLC in both the coatings are responsible for reduced wear loss. However, there

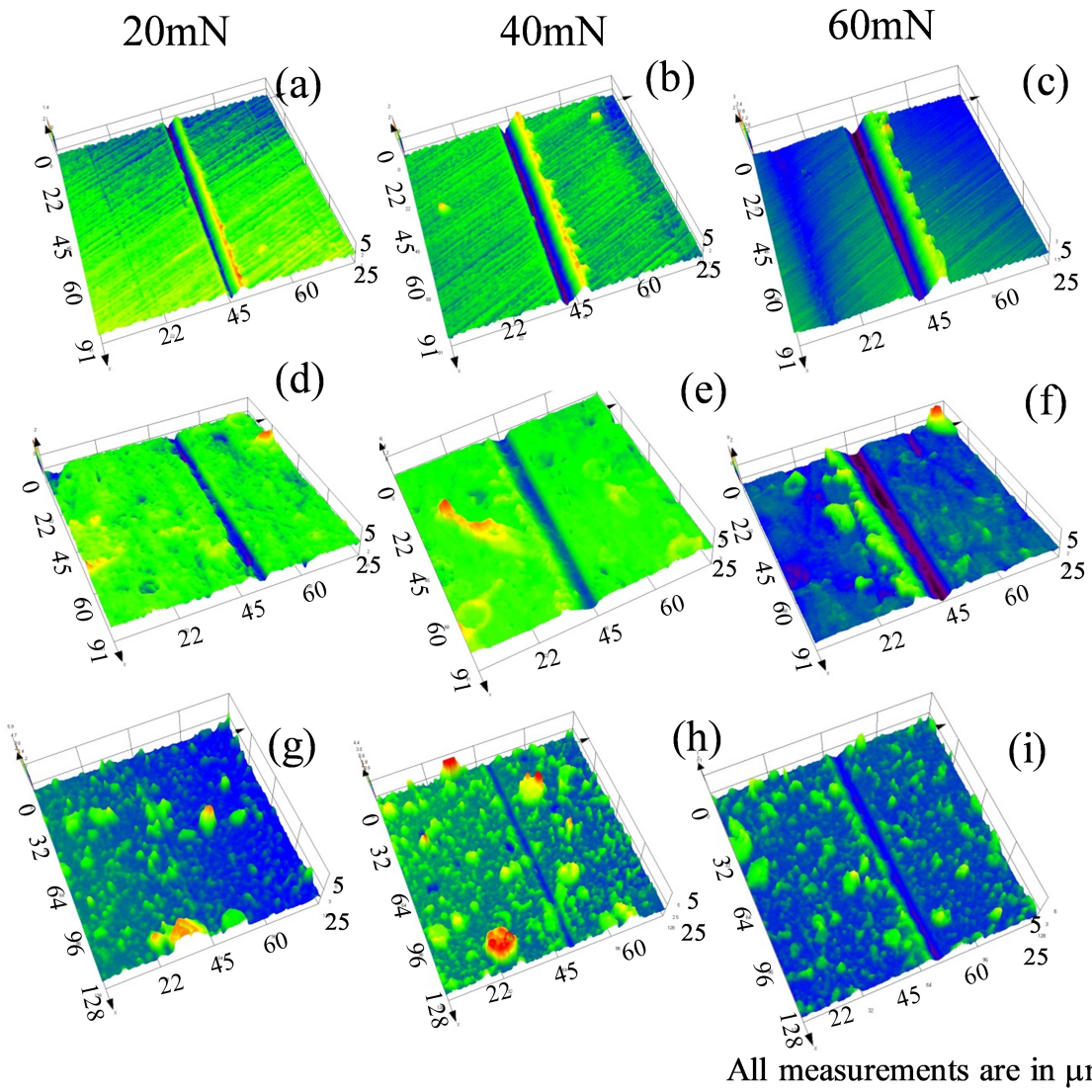

Figure 4.22: Wear tracks deformation at load of 20 mN, 40 mN and 60 mN (a-c) MDN121 (d-f) AlCN/AlC coating (g-i) FrCrN coating

is a significant performance improvement in COF in case of TiC-C coating as compared to Ti/TiN/TiCN/TiN/TiCN multilayer coating. This is attributed to higher hardness and absence of intermediate layers.

Figure 4.20 (b) represents the wear resistance of all the coatings. Increase in wear resistance due to the presence of TiN interlayer is reported by Zalnezhad and Faraji (2017) in their Ti/Cr/TiN/Cr/CrN/TiCrN multilayer coatings (Rahmati *et al.*, 2015). These results reveal

that increase of the wear resistance of the coatings and accordingly the residual thickness $(H - h_R)$ left on the surface at the end of the steady state period is much higher in case of TiC-C as revealed in confocal micrographs Figure 4.22.

4.3.2 Wear track analysis

Morphology of wear tracks for substrate, TiC-C and Ti/TiCN/TiN/TiCN/TIN coatings are represented in Figure 4.23. Figure 4.23 (a) shows galling type of failure in MDN 121 wear track. In case of TiC-C (Figure 4.23 b), Ti/TiCN/TiN/TiCN/TIN (Figure 4.23 c-d), AlCN/AlC (Figure 4.24 b) and FeCrN (Figure 4.24 c-d) coatings wear track, abrasive type of wear is observed during the fretting wear test.

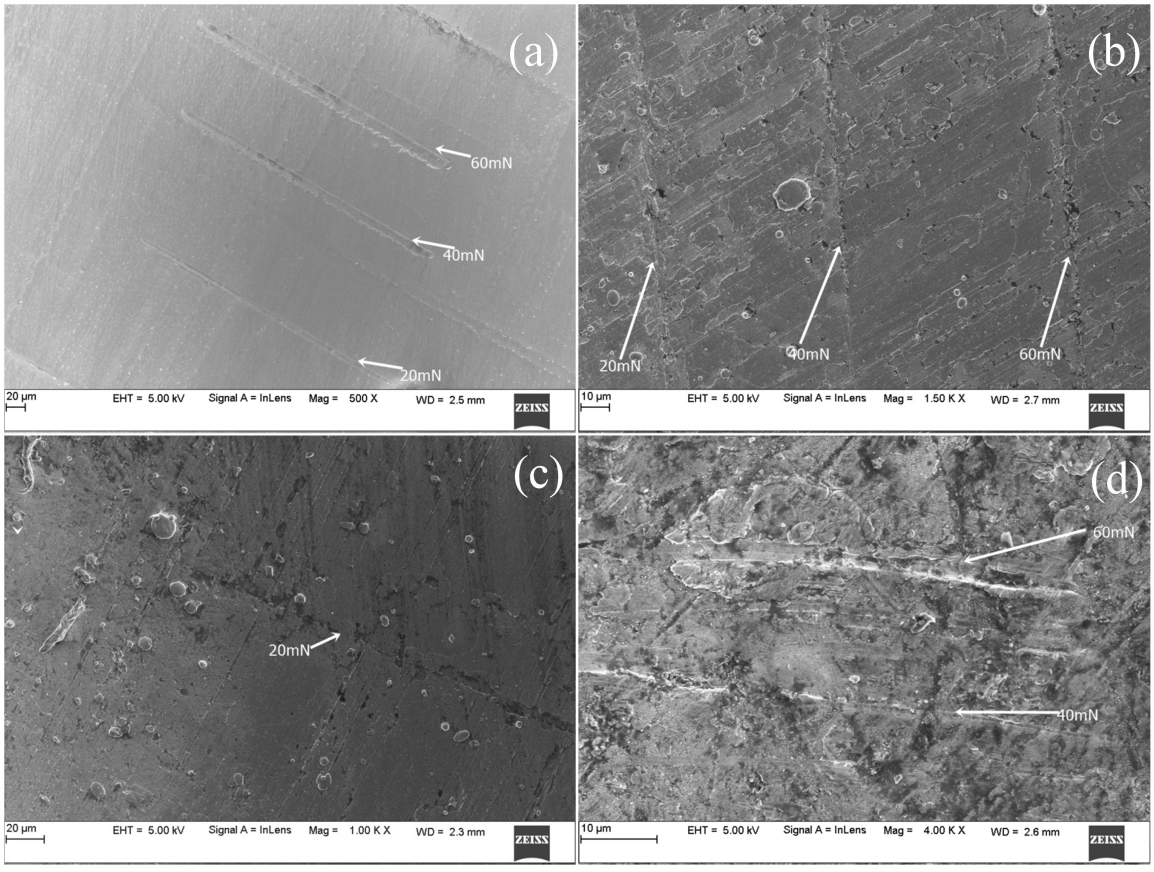

Figure 4.23: Wear tracks on (a)MDN 121, (b) TiC-C coating (c & d) Ti/TiN/TiCN/TiN/TiCN coating

The severity of wear is higher in case of multilayer coating justifying the higher volume loss. Since the measured area of deformation is observed to be maximum at 60 mN for all

the samples, the condition of 60mN wear track is mapped for elemental distribution on the wear track.

Figure 4.25 represents the mapping of TiC-C coating at the load of 60 mN, TiC particles present on the surface that hold the propagation of wear track to its surroundings, confirming the formation of hard phase metallic carbide formed during the coating.

Figure 4.26 represents the elemental mapping of the multilayer TiN/TiCN/TiN/TiCN coating at 60 mN load wear track. TiC particles merge themselves with TiCN compounds which are witnessed in the micrograph (Figure 4.26) . Abrasive type of wear is observed in this coating and from the FESEM micrograph (Figure 4.26) TiCN coating experienced lamella failure. which is due to increased su rface roughness (0.34 μm), and low bonding at the interference between the layers (reduced critical load 47 mN).

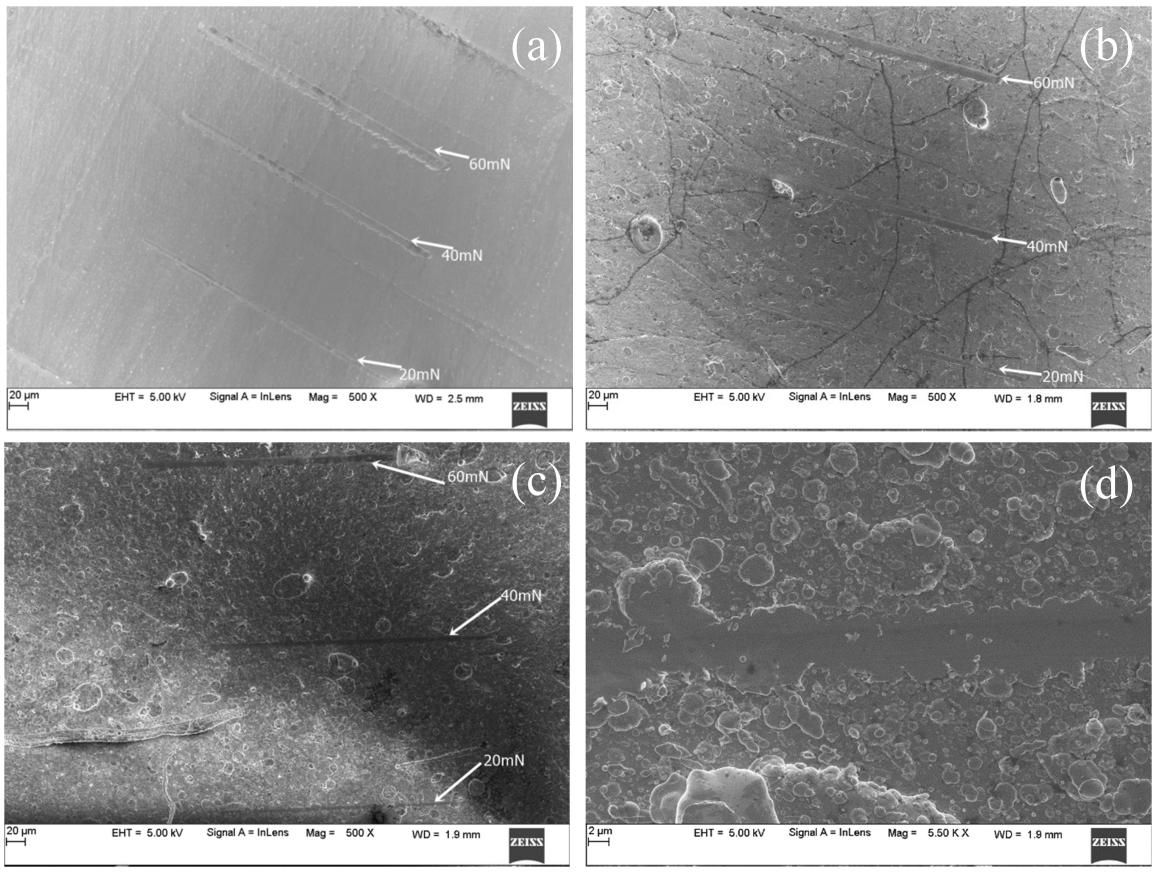

Figure 4.24: Wear tracks on (a) MDN 121 (b) AlCN/AlC coating (c&d) FeCrN coating

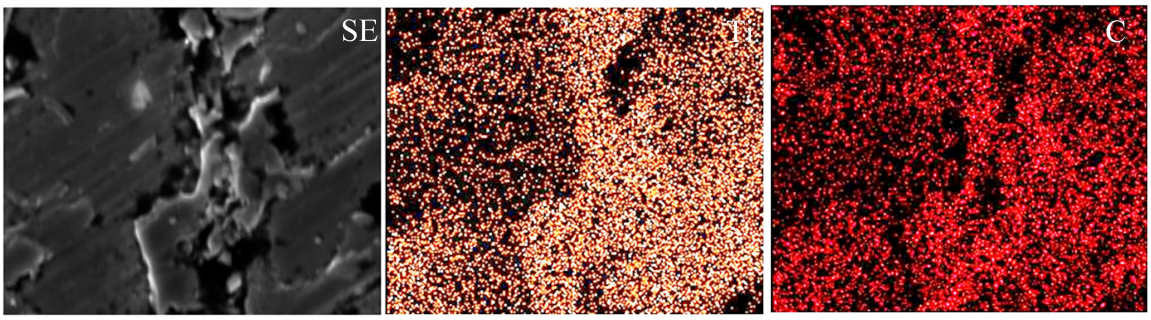

Figure 4.25: Elemental mapping of wear track at 60 mN load for TiC-C coating

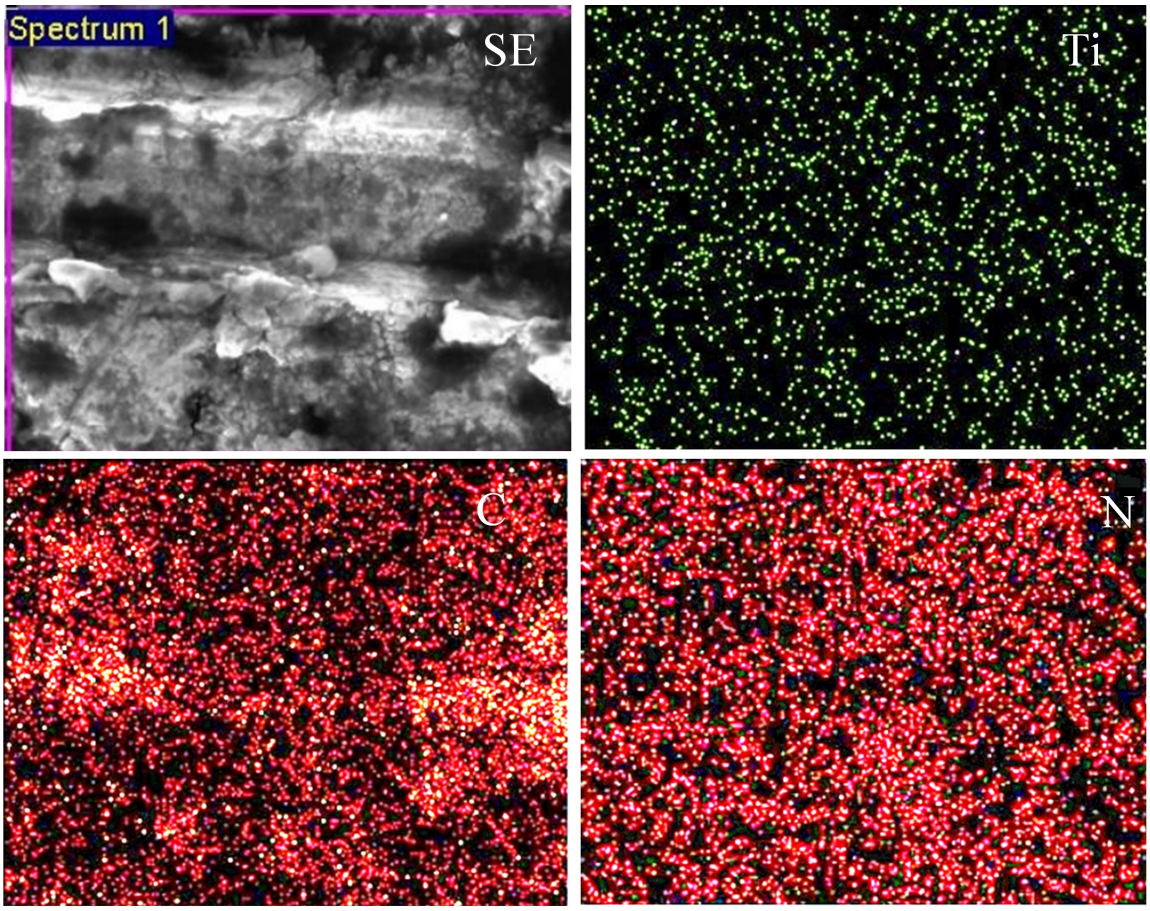

Figure 4.26: Elemental mapping of wear track at 60 mN load for Ti/TiN/TiCN/TiN/TiCN coating

Failures of coatings are better visualized in confocal microscopy; a 3D profile of the wear track was built on the surface. Figure 4.21 (a-c) represents the wear tracks on MDN121 at 20 mN, 40 mN and 60 mN. MDN121 material deforms starts deposited on its adjacent

surface, which is known as the galling type of wear. The amount of the deformed material was measured and proved to be identical to the volumetric wear loss. Figure 4.21 (d-f) represents the wear tracks on TiC-C coating at 20 mN, 40 mN and 60mN respectively. The amount of deformation observed in the TiC-C monolayer coating is least as compared to the substrate and the multilayer coating because of its hardness and dense coating. Figure 4.21 (g-i) represents the wear tracks on Ti/TiN/TiCN/TiN/TiCN coating at 20 mN, 40 mN and 60 mN respectively. The amount of deformation is found to increase due to reduced hardness compared to other PVD coatings Ti(Cr)SiCN, Ti(Cr)N and Ti/TiN (Leoni et al. 1999; Li et al. 2013). COF for the multilayer coatings is in an acceptable range compared to the literature (Bromark *et al.*, 1997) (Adams et al. 2013; Beake et al. 2013; Ibrahim et al. 2015)

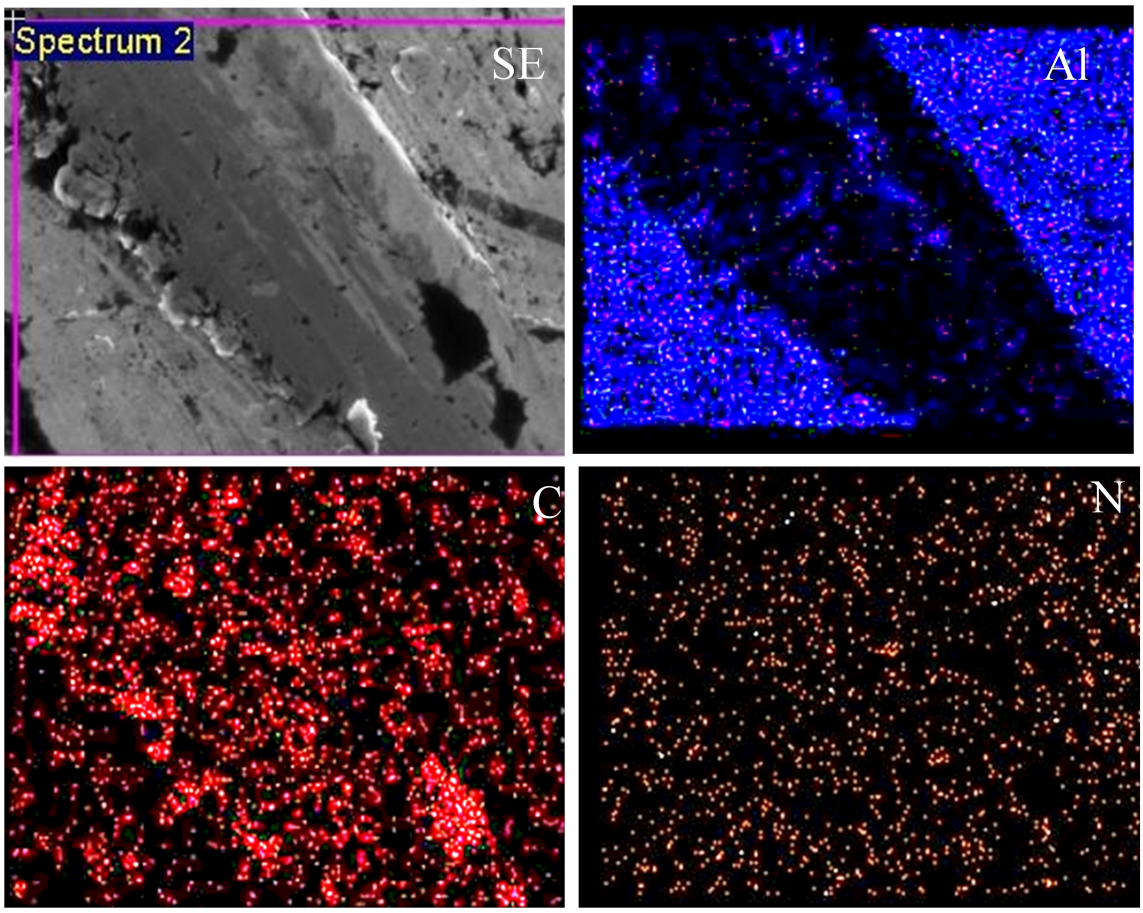

Figure 4.27: Elemental mapping of wear track at 60 mN load for AlCN/AlC coating

TiC-C coating residual thickness at the load 20 mN is 0.959 μm whereas 0.514 μm for Ti/TiN/TiCN/TiN/TiCN coating, which indicates the TiC-C, exhibited better wear resistance compared to Ti/TiN/TiCN/TiN/TiCN coating. At a load of 20 mN life of TiC-C coating is 1.86 times better compared to multilayer coating. Similarly, 1.03 times and 2.05 times better at the load of 40 mN and 60 mN respectively.

Morphology of wear tracks for substrate, AlCN/AlC and FeCrN coatings are represented in Figure 4.24. From FESEM micrograph it can be observed that abrasive type of wear is found during the fretting wear test.

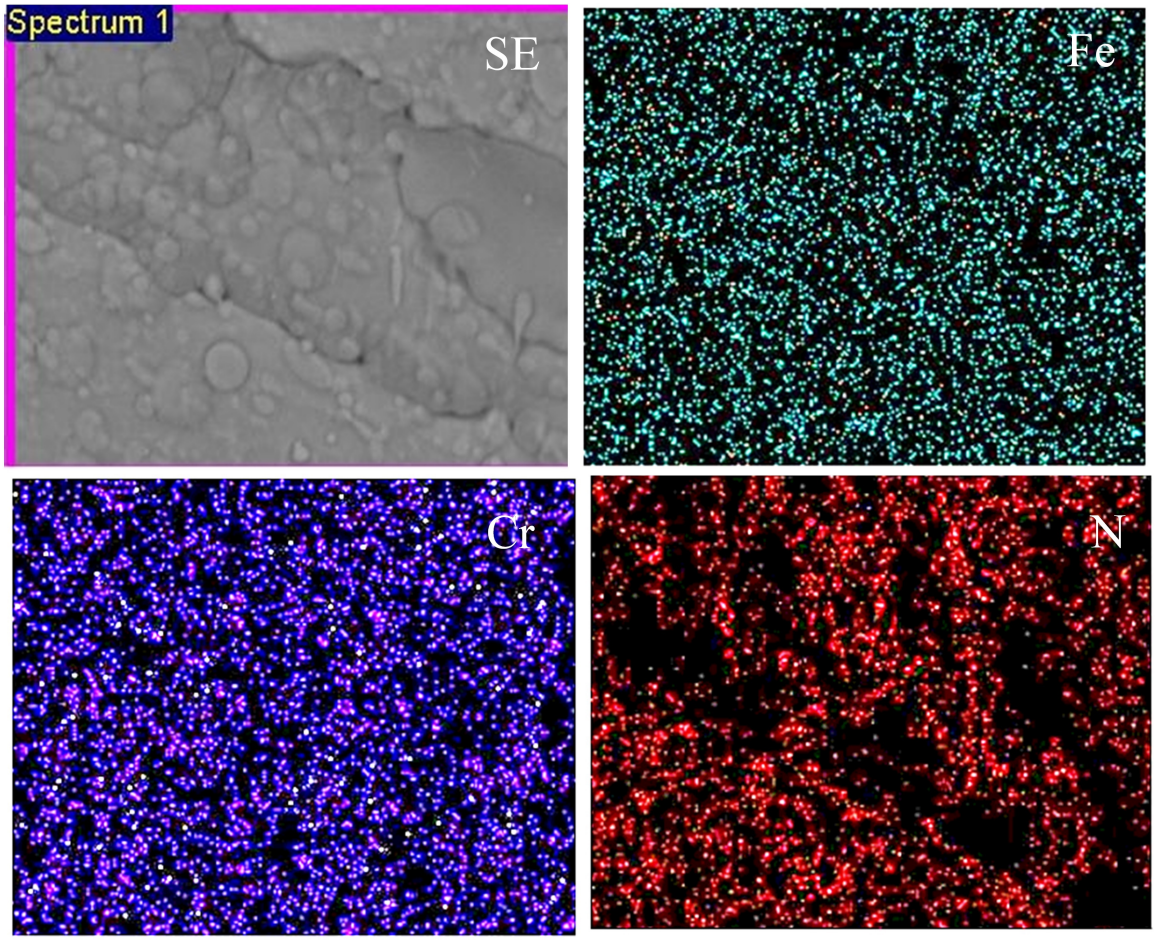

Figure 4.28: Elemental mapping of wear track at 60 mN load for FeCrN coating

Figure 4.28 represents the mapping of AlCN/AlC coating at 60 mN load. And carbon and nitrogen particles present on the surface acting as barriers for the propagation of

wear track to its surroundings. The mapping result shows AlC and AlN compounds are resisting the wear to propagate because of its uniform distribution of C and N. Carbon and nitrogen particles when combined with metallic ions, form hard metallic compounds. Wear resistance of TiN particles are dependent on the uniformity of distribution; similarly, one can observe uniform and dense distribution of N in AlCN/AlC coating.

Figure 4.22 represents the elemental mapping of the FeCrN coating at 60 mN load wear track. The mapping micrograph reveals that the coatings are resistant to the formation of wear scar which is due to the presence of hard CrN and Cr2N compounds. At 60 mN load, the droplets merged together during the wear analysis and least wear loss was observed. AlCN/AlC coating residual thickness at 20 mN load is 0.358 μm whereas it is 0.964 μm for FeCrN coating. Residual coating thickness value indicates the FeCrN exhibited better wear resistance compared to AlCN/AlC. At the load of 20 mN life of FeCrN coating is 1.70 times better. Similarly, at 40 mN it is 1.70 times better and at 60 mN 1.87 times better.

4.4 Adhesive wear behaviour of the coatings

Adhesive wear tests were conducted on TiC-C, Ti/TiN/TiCN/TiN/TiCN, AlCN/AlC and FeCrN thin solid films to evaluate for the coefficient of friction using Nano Tribometer. The Nano Tribometer study provides information about the COF of the coated sample and the amount of worn out area in its tribological counterpart (100Cr6).

4.4.1 Adhesive wear rate

Figure 4.29 to Figure 4.32 show the results of adhesive wear analysis for thin solid films. Wear analysis is carried out under 20 mN, 40 mN and 60 mN load at a constant speed of 0.47 cm/s. Coefficient of friction has been measured throughout the 1000 cycles test duration. After 200 cycles the coefficient of friction was found to be stable till the end of running in period. Figure 4.29 , Figure 4.30 , Figure 4.31 and Figure 4.32 show the results of adhesive wear analysis for TiC-C, Ti/TiN/TiCN/TiN/TiCN, AlCN/AlC and FeCrN thin solid films respectively. Mean values of COFs are shown in Figure 4.33 (a). Coefficient of friction was observed to increase with the increase in the load, in all of the coatings.

The mean COFs for the TiC-C, Ti/TiN/TiCN/TiN/TiCN, AlCN/AlC and FeCrN coating are observed to be 0.21, 0.31 0.33 and 0.44. Figure 4.33 (b) shows that worn cap diameter

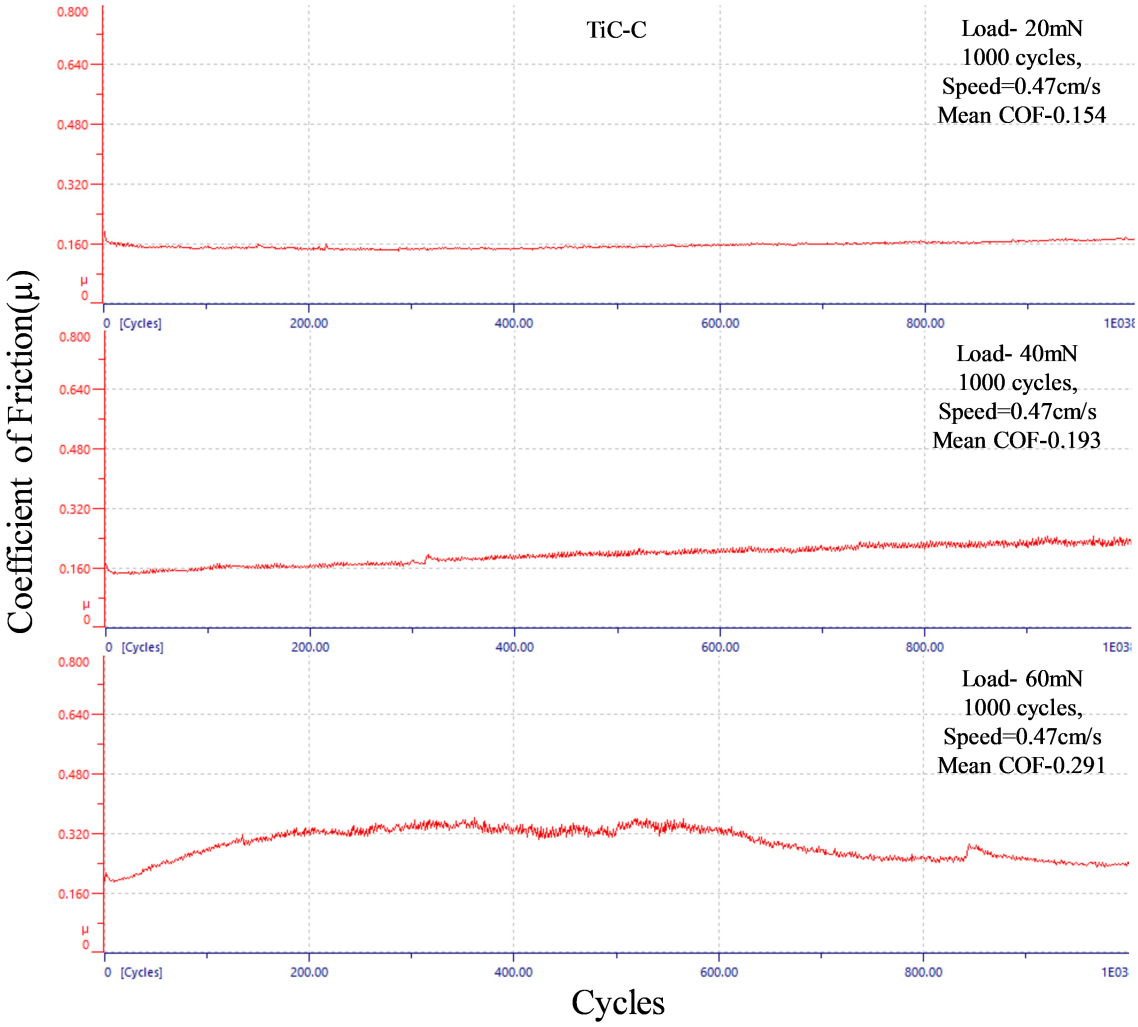

Figure 4.29: Friction traces during adhesive wear analysis of TiC-C coating

for all of the coatings has increased linearly with load. For the TiC-C coating worn cap diameter is less compared to the multilayer Ti/TiN/TiCN/TiN/TiCN coating due to higher hardness and absence of intermediate layers. Presence of TiC phase in TiC-C coatings are attributed to the reduced worn cap diameter. The highest COF and worn cap diameter are observed in Ti/TiN/TiCN/TiN/TiCN multilayer coating which is due to large surface roughness and low bonding in between the interlayers (critical load 47 mN).

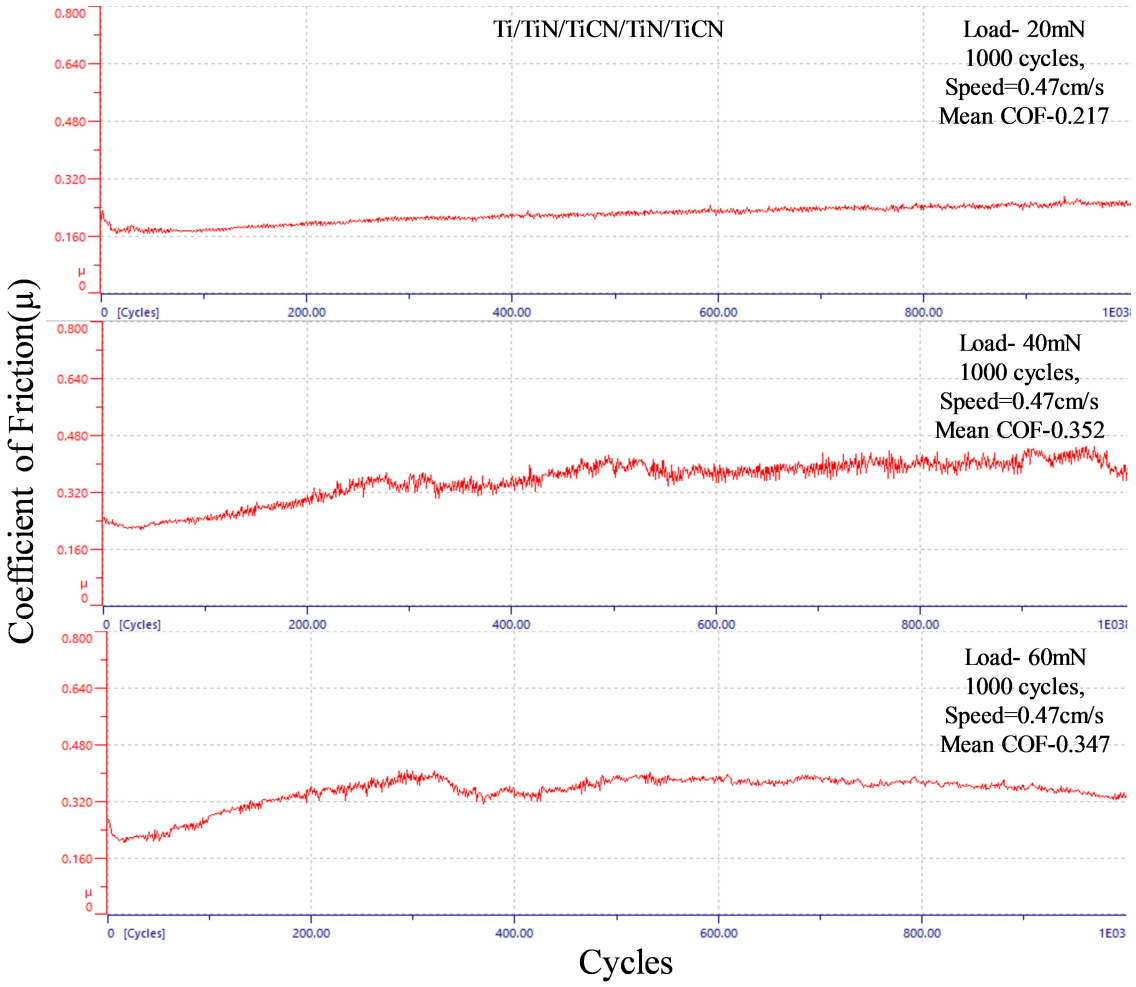

Figure 4.30: Friction traces during adhesive wear analysis of Ti/TiN/TiCN/TiN/TiCN coating

AlCN/AlC coating worn cap diameter (Figure 4.33 b) is low compared to FeCrN coating due to lower hardness and absence of hard phases. Presence of AlC phase in AlCN/AlC coatings attributed to the reduced worn cap diameter. The low COF and low wear rate are observed in FeCrN coating which is due to the presence of hard ferric and chromium nitride phases.

Volumetric wear loss is calculated by measuring the step height, wear scar length and width using optical profiler shown in Figure 4.34. Wear rate (W in $\mu m^3(mN\text{-}\mu m)^{-1}$) of the coating is calculated using the equation 4.2. (Budinski (2007), Kennedy and Hashmi (1998), Nohava et al. (2015) and Podgornik et al. (2000))

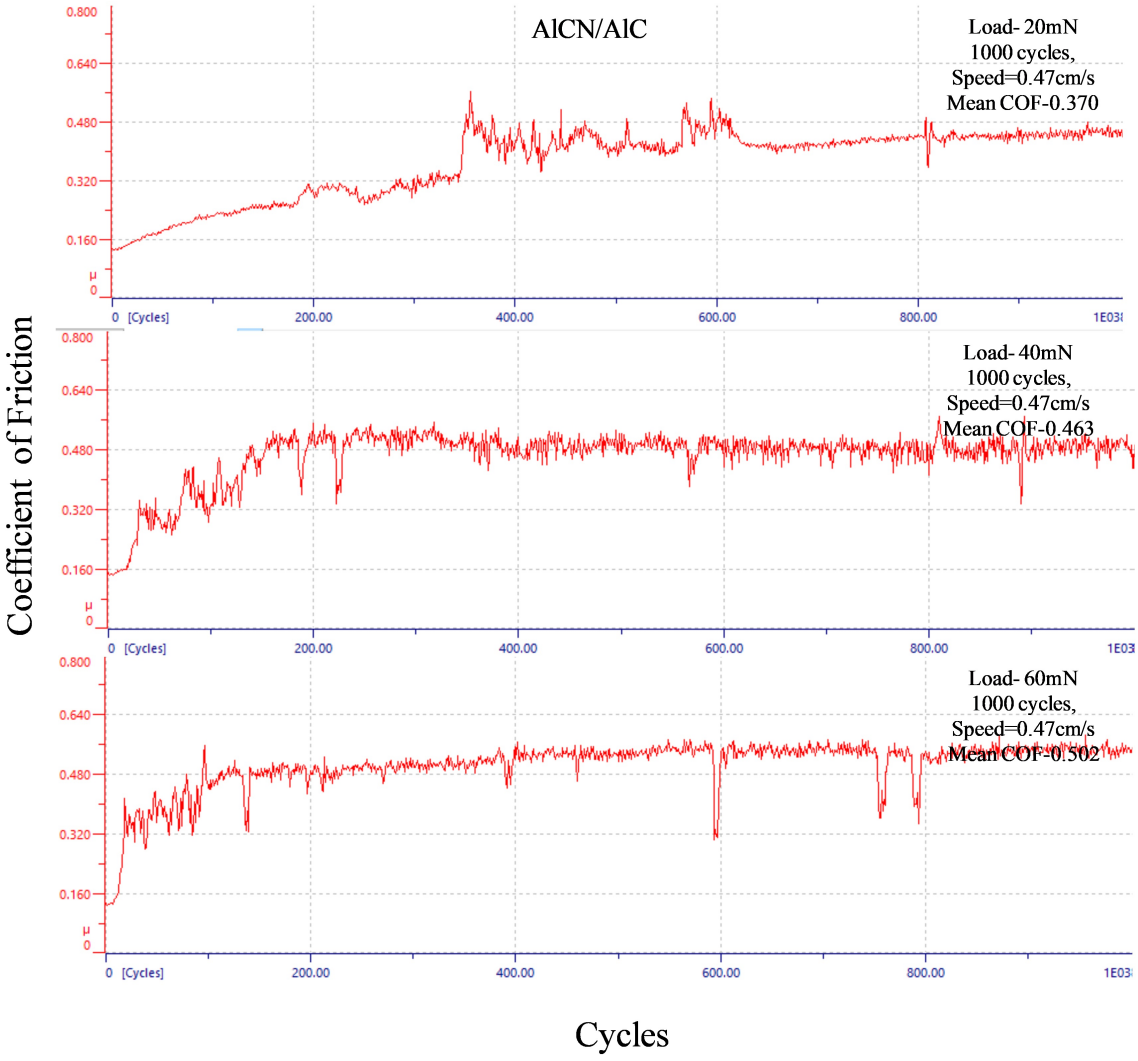

Figure 4.31: Friction traces during adhesive wear analysis of AlCN/AlC coating

$$W = \frac{V}{d \times P} \tag{4.2}$$

Here, W- wear rate, V is the volume of the removed material after the wear analysis, d is the total sliding distance and P is the normal load. Volumetric wear losses of the coated samples were calculated using the optical profiler wear track measurements.

Figure 4.33 (c) shows the results of wear rate for all the four coatings evaluated using the formula proposed by Holmberg and Matthews (1994); Kennedy and Hashmi (1998). With

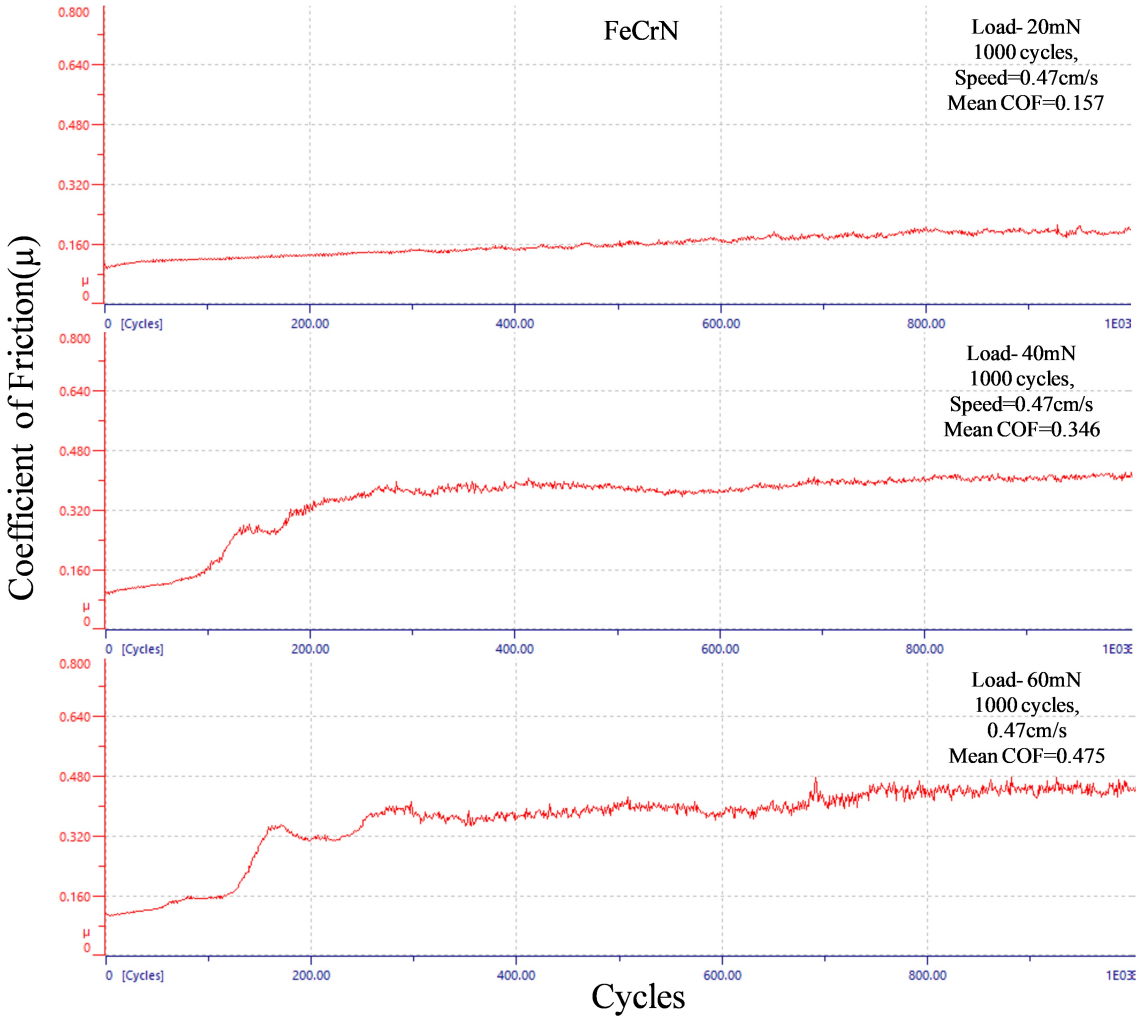

Figure 4.32: Friction traces during adhesive wear analysis of FeCrN coating

the increase in load, wear rate has increased in all the coatings. TiC-C coating exhibits the lowest wear rate and accordingly volumetric wear is lesser compared to the other coatings. Ti/TiN/TiCN/TiN/TiCN exhibited 1.12 times higher residual thickness compared to TiC-C coating which is due to the high hardness of the coating. In contrast, both the Ti-coatings perform better in wear-prone environments. In AlCN/AlC and FeCrN coatings, wear rate increased linearly with the load. AlCN/AlC coating exhibits a low wear rate compared to the FeCrN coating. FeCrN exhibits 1.11 times higher residual thickness compared to

AlCN/AlC coating which is due to the high hardness of the coating.

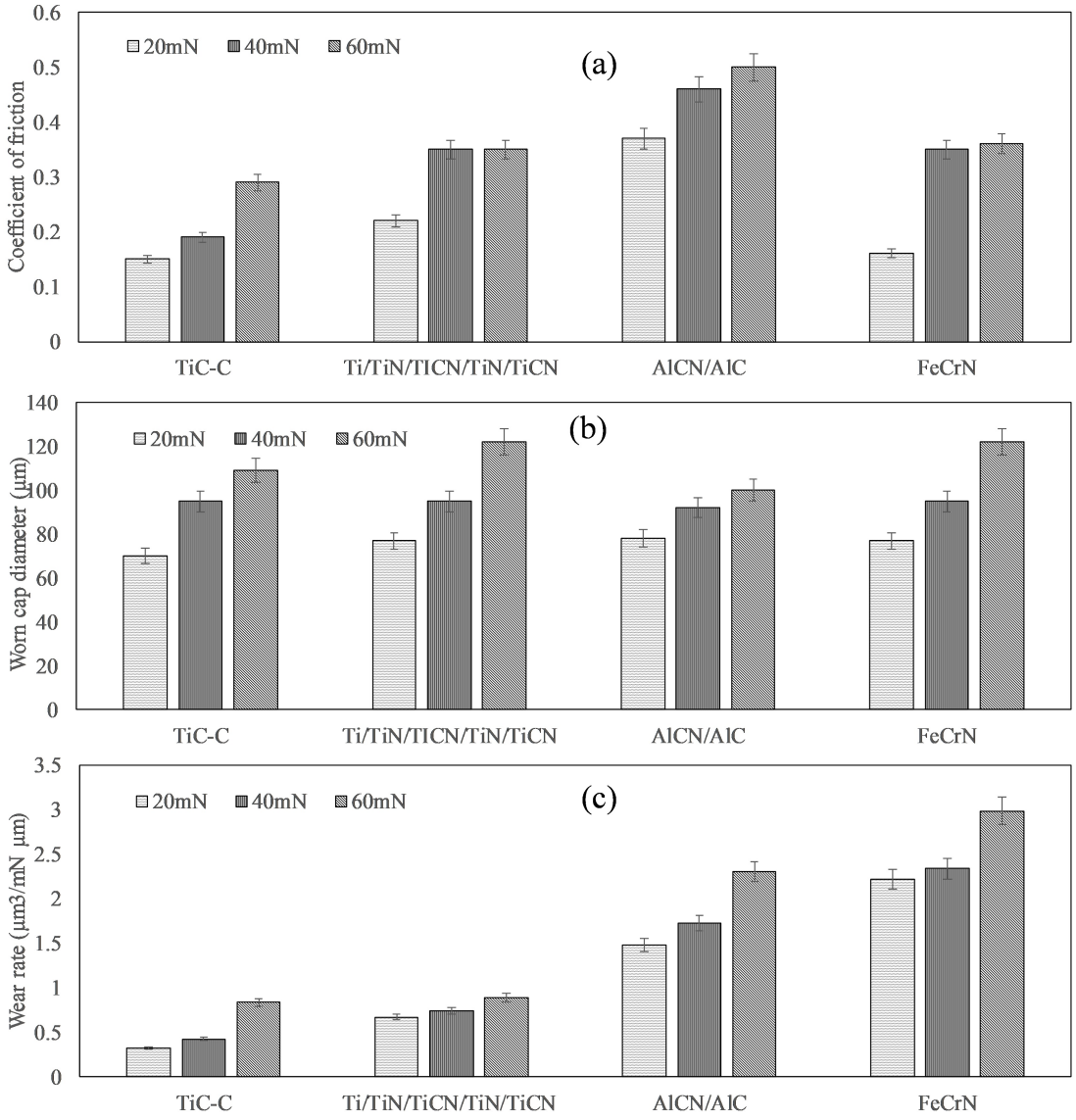

Figure 4.33: Plots of (a) COF, (b) Worn cap diameter and (c) wear rate during adhesive wear

4.4.2 Wear track analysis

Figure 4.35 - Figure 4.38 show the wear scar micrograph and worn cap diameter for TiC-C, Ti/TiN/TiCN/TiN/TiCN, AlCN/AlC and FeCrN thin solid films.

From the adhesive wear analysis TiC-C, Ti/TiN/TiCN/TiN/TiCN, AlCN/AlC and FeCrN have shown better performance with low wear rate and low COF measurements. Diffusion

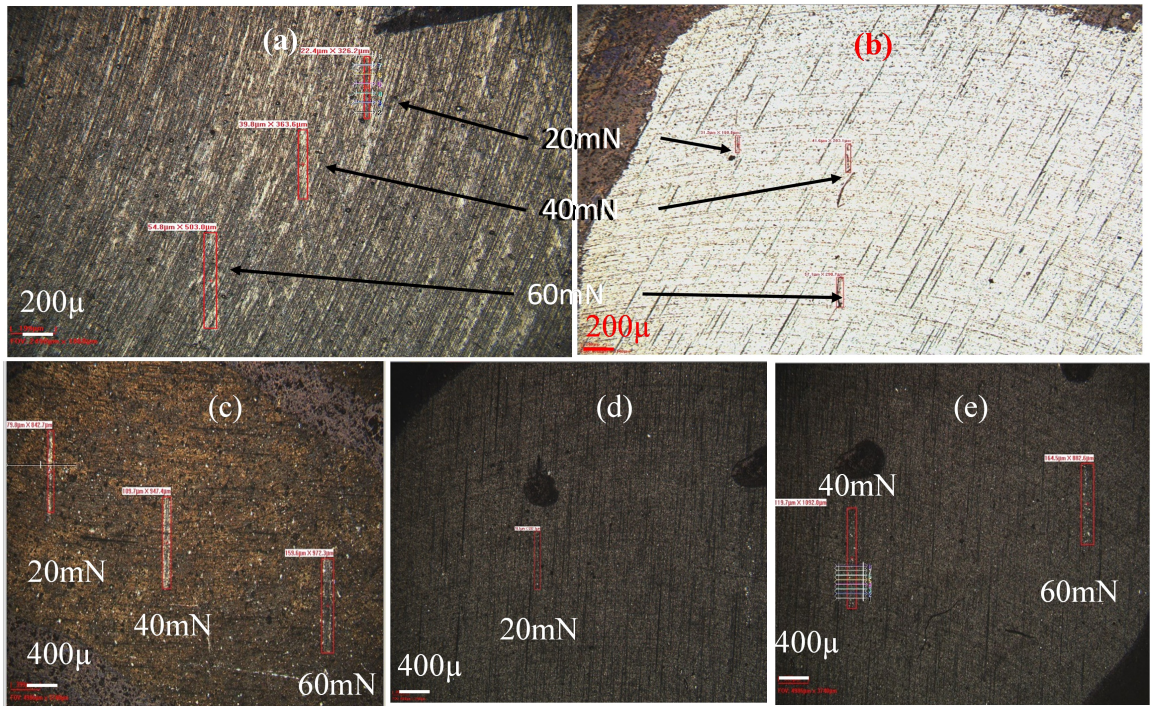

Figure 4.34: Optical profiler wear measurements of wear tracks on (a) TiC-C coating (b) Ti/TiN/TiCN/TiN/TiCN (c)AlCN/AlC and coating (d-e) wear tracks of FeCrN coating

and ploughing type of failure occurred on the coating due to the thickness and increased hardness of the coating. In the present work, both Ti (monolayer and multi-layer) coatings exhibited low friction and high wear resistance along with the presence of DLC. The low friction with high wear resistance characteristics in diamond-like and diamond coatings have been claimed by Holmberg and Matthews (1994). AlCN/AlC and FeCrN thin solid films also exhibit low friction and high wear resistance due to presence of hard Fe and Al nitrides. Wear track deformations were studied by using an optical profiler. Scratching and wear scars were observed on all the coatings and also on tribological counterpart (100Cr6 ball). Micromechanical scratching is observed on the 100Cr6 ball is due to surface roughness. Scuffing is observed in CrN coating, in developed Ti-coatings, there is no transfer of material from coating part to counterpart or vice-versa. From the micrograph of the wear scar, it has been observed that scratching, penetration and ploughing type of failure in Ti-coatings is due to thickness and increased hardness of the coating.

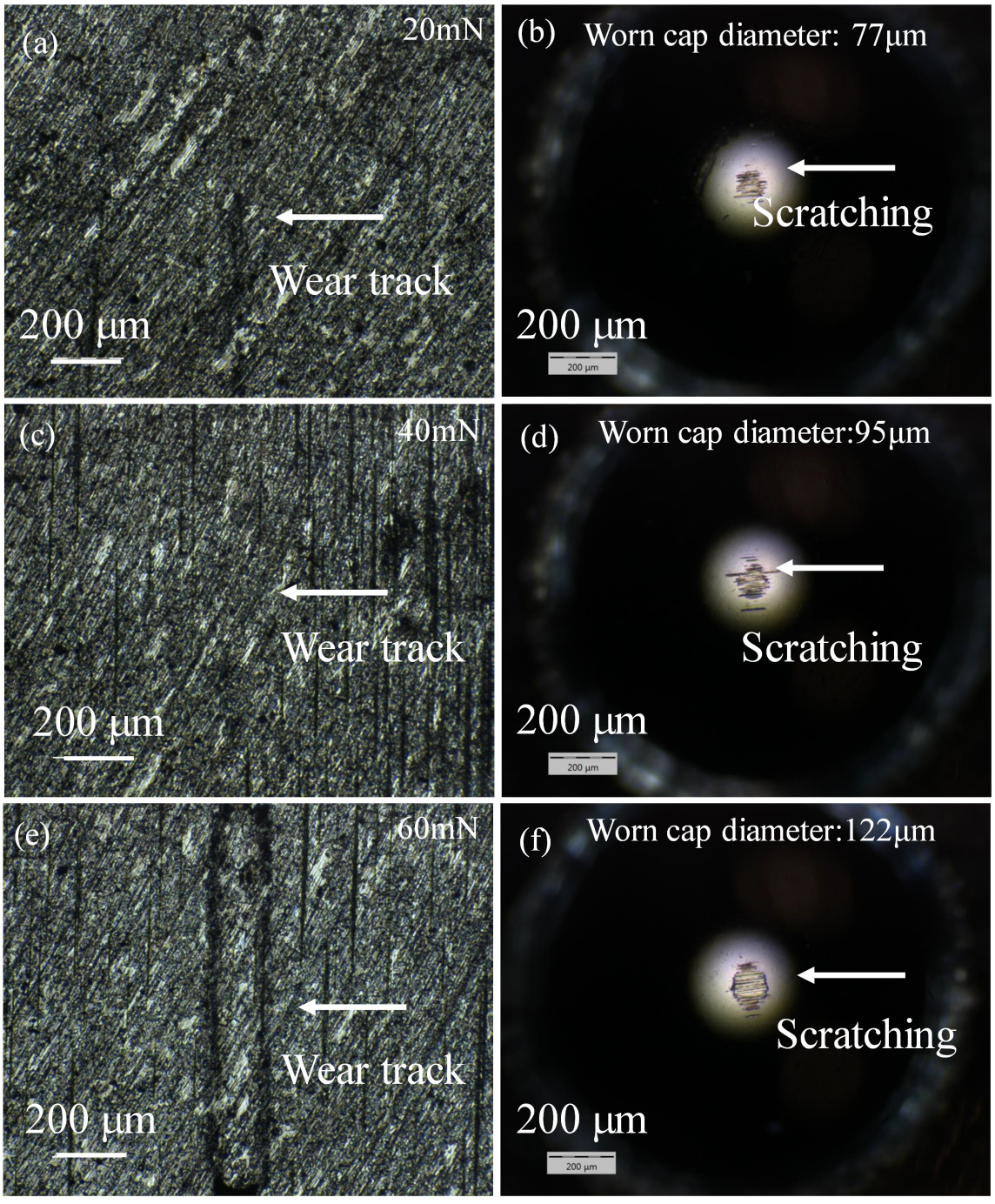

Figure 4.35: Wear tracks deformation measurements using microscopy (a-b) 20 mN (c-d) 40 mN and (e-f) 60 mN for TiC-C coating

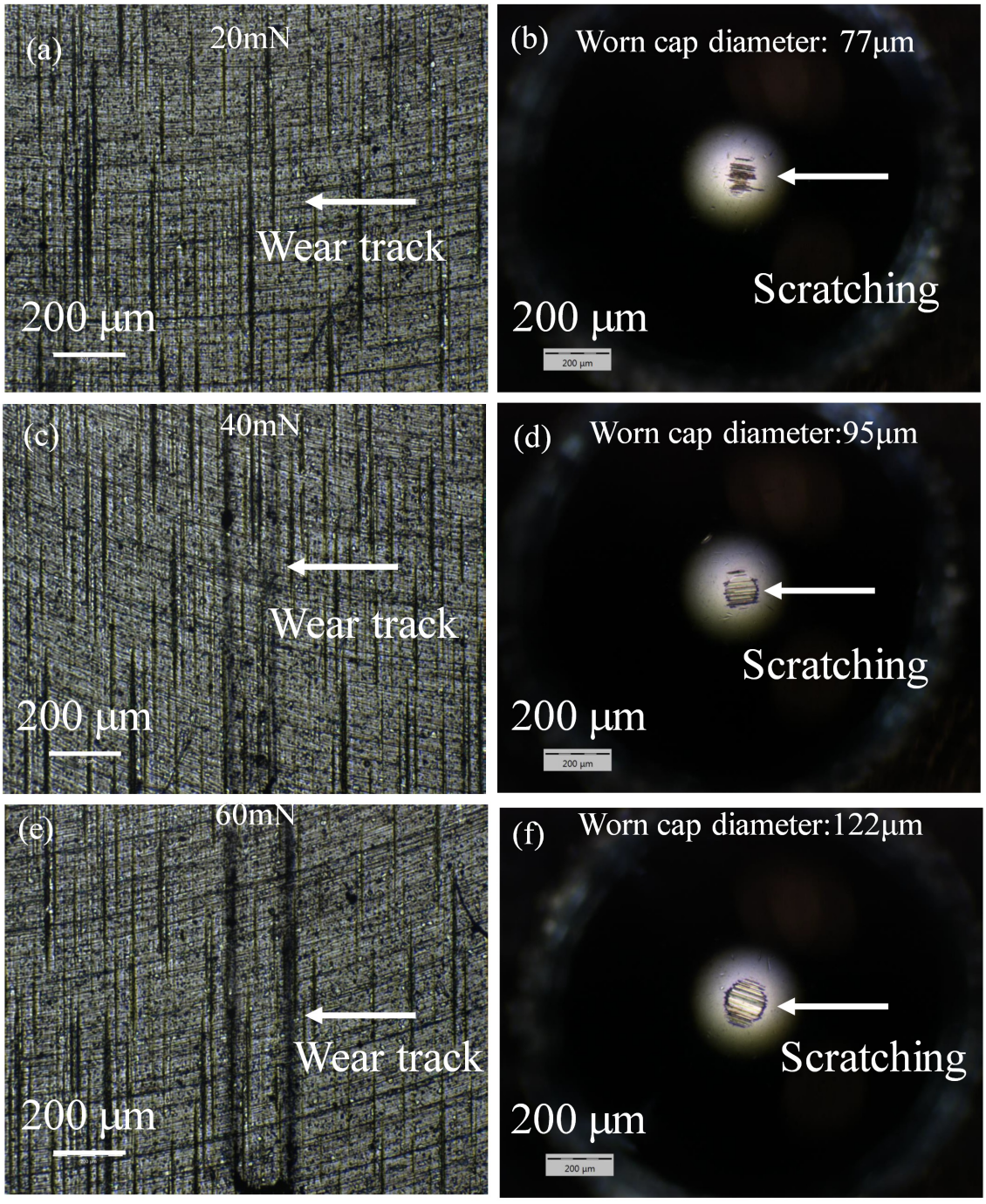

Figure 4.36: Wear tracks deformation measurements using microscopy (a-b) 20 mN (c-d) 40 mN and (e-f) 60 mN for Ti/TiN/TiCN/TiN/TiCN coating

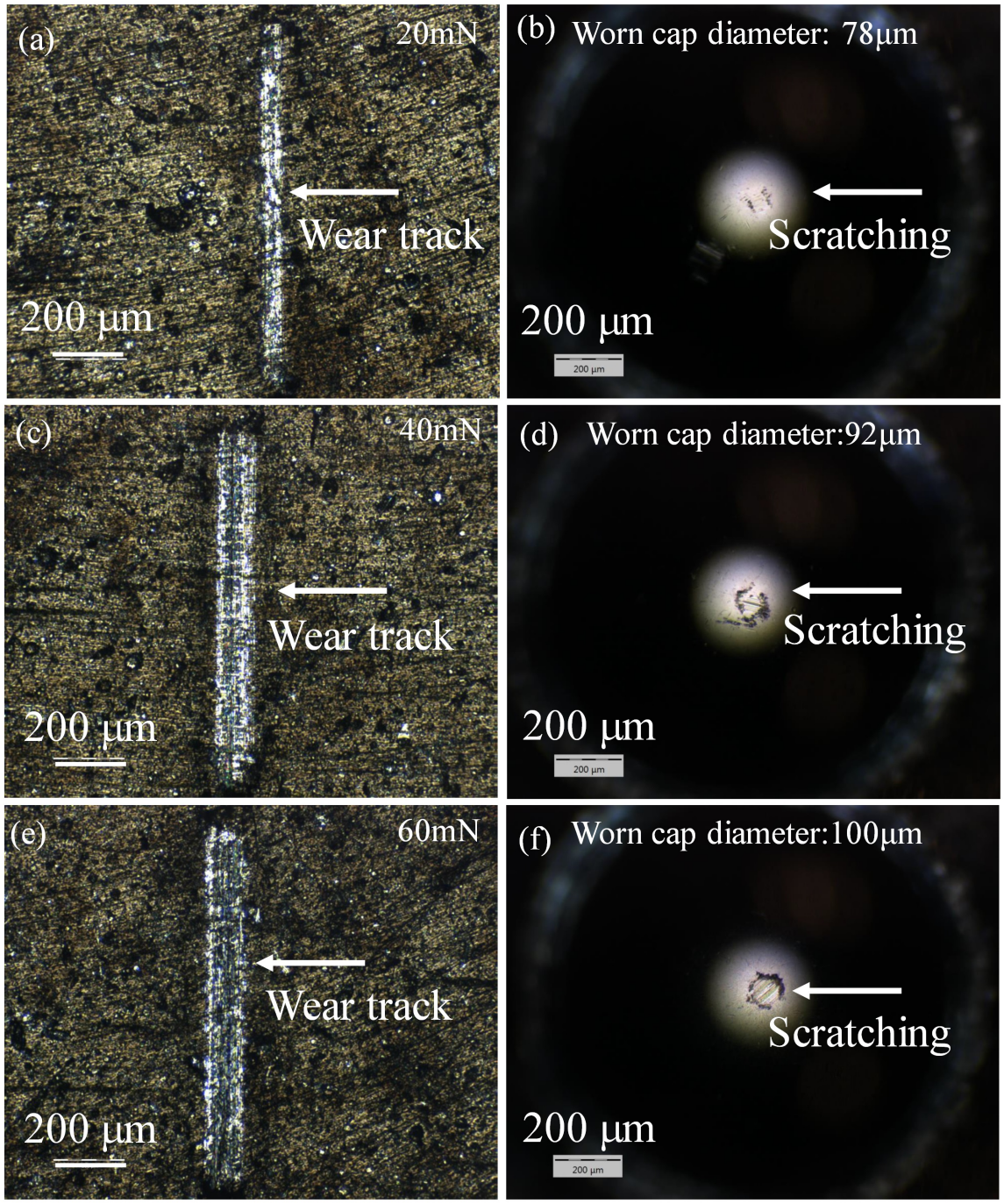

Figure 4.37: Wear tracks deformation measurements using microscopy (a-b) 20 mN (c-d) 40 mN and (e-f) 60 mN for AlCN/AlC coating

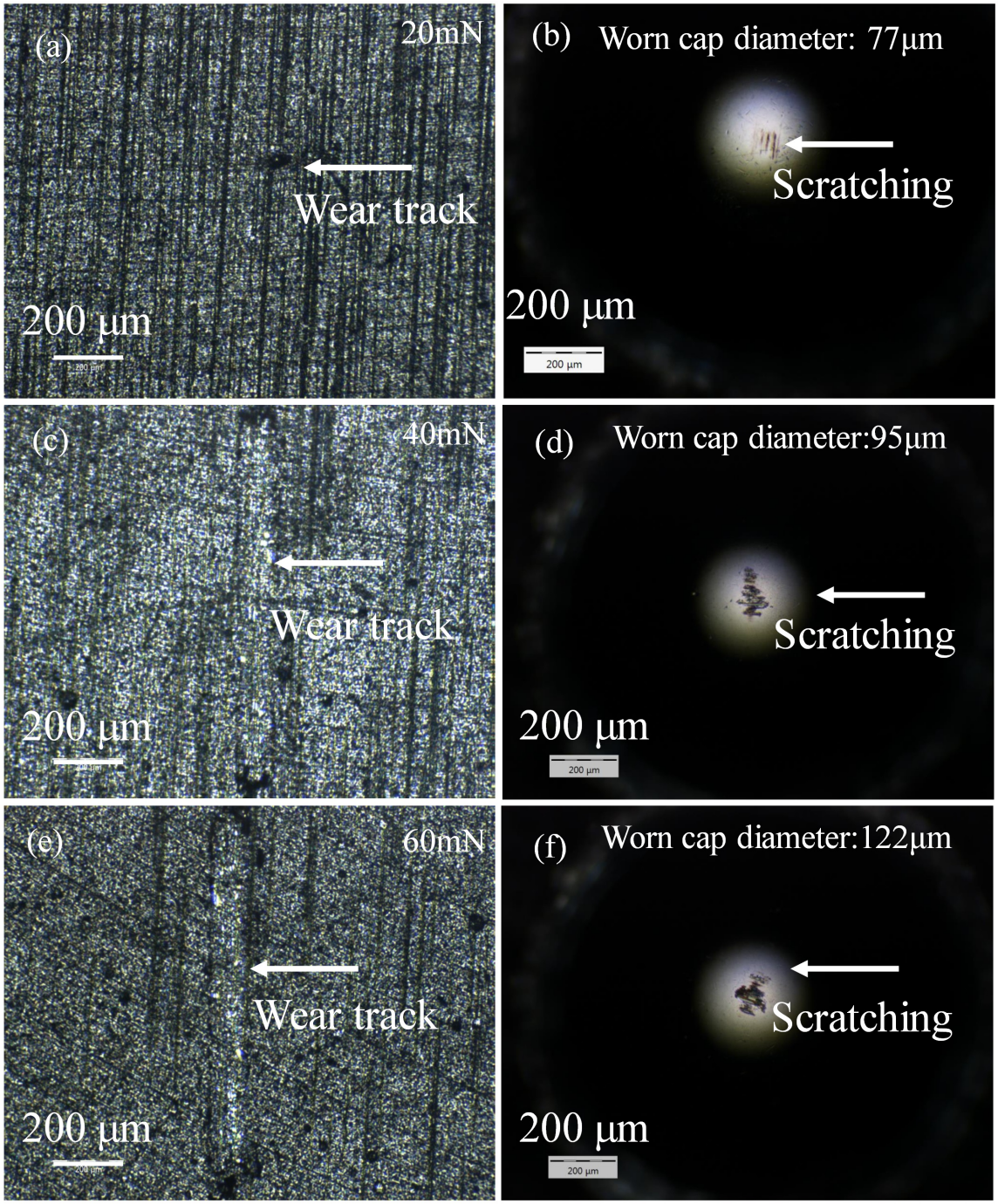

Figure 4.38: Wear tracks deformation measurements using microscopy (a-b) 20 mN (c-d) 40 mN and (e-f) 60 mN for FeCrN coating

4.5 Machinability studies

In the present work machinability studies are done for MDN431 using Ti-multilayer, TiC-C, AlCN/AlC and FeCrN coated tool insert. Experiments are designed based on FFD.

Experimental results for Ti-multilayer, TiC-C, AlCN/AlC and FeCrN coated inserts are presented in Table 4.2.

Inter-relation between cutting parameters (speed (V_c), feed rate (f) and depth of cut (a_p)) and responses (cutting force (F_x, F_y and F_z) and surface roughness (R_a) are determined for which, regressions models are established.

Quadratic regression models developed are represented in equations (4.3-4.18) and are used to validate for cutting force (F_x, F_y and F_z) and surface roughness (R_a).

Regression models represented in equation 4.3, 4.4 and 4.5are for cutting forces F_x, F_y and F_z and equation 4.6 for surface roughness (R_a) for the Ti-multilayer coated tool. Similarly 4.7-4.10 for TiC-C coated tool, 4.11-4.14 for AlCN/AlC coated tool and 4.15-4.18 for FeCrN coated tool. Anova results for cutting forces (F_x, F_y and F_z) and surface roughness(R_a) are represented in Table 4.3 and detailed Anova tables have been listed in Appendix. The probability value (P=0) for cutting forces and surface roughness in Anova table, which confirms the developed regression models are significant. Coefficient of determination (R^2) gives the capability of developed regression model. Coefficient of determination (R^2) for F_x, F_y, F_z and (R_a) are close to 1 which confirms developed models are adequate for the prediction of results.

Table 4.2: FFD experimental design with results

Process parameters			Ti-Multilayer coated tool				TiC-C coated tool				AlCN/AlC coated tool				FeCrN coated tool			
a_p	V_c	f	F_x	F_y	F_z	R_a	F_x	F_y	F_z	R_a	F_x	F_y	F_z	R_a	F_x	F_y	F_z	R_a
0.2	59	0.062	76.42	126.4	123.2	0.41	67.5	118.6	115.7	0.44	80.81	114.7	138.7	0.5	64.09	103.7	113.8	0.42
		0.093	76.72	124.5	154.7	0.6	65.5	127.4	134.6	0.6	80.2	117.2	144.5	0.63	104.2	123.8	156	0.64
		0.125	68.66	141.2	152.8	0.71	69.64	135.4	165.2	0.69	59.8	125	152.7	0.86	89.84	158.4	183.9	0.93
	75	0.062	68.88	109.8	111.3	0.45	60.79	111.4	115.1	0.54	91.55	115.7	102.8	0.48	71.29	109.4	143.6	0.47
		0.093	72.33	119.6	137.7	0.5	66.1	115.5	130.6	0.57	76.66	120.1	154.1	0.57	80.02	131.6	149.1	0.62
		0.125	74.65	140.4	178.1	0.64	59.81	126.1	137.7	0.73	93.02	133.9	190.3	0.89	85.94	139.4	183.8	0.96
	118	0.062	67.68	113.9	107.1	0.5	53.34	99.91	110.8	0.41	76.6	122.5	144.4	0.45	77.76	120.4	149.3	0.43
		0.093	71.41	132.6	144.4	0.54	128.1	147.8	162.4	0.52	127.4	137	169.1	0.5	88.81	140.6	184.7	0.6
		0.125	81.42	158.2	198.2	0.61	63.9	131.6	156.1	0.6	89.9	151.6	228	0.83	90.03	150.4	191.8	0.92
0.3	59	0.062	127.7	140.4	152.1	0.56	136.7	178.7	213.7	0.55	65.61	101.3	125.5	0.66	159.7	187.9	235.2	0.56
		0.093	95.7	138.9	181	0.67	140.3	186.9	282	0.79	84.35	123.4	149.8	0.76	80.81	121.9	145.7	0.67
		0.125	115.4	175.5	215.8	0.96	149.6	180.7	272.6	0.99	92.53	141.1	177.5	0.97	89.05	144.6	171.7	1.02
	75	0.062	90.94	123.7	163.9	0.85	163.5	205.7	294.4	0.61	62.99	95.52	127.4	0.46	76.72	117.6	130.8	0.64
		0.093	116.4	140.2	164.8	0.84	141.7	176.3	237.8	0.75	66.04	110.2	152.5	0.66	84.35	134.6	165.4	0.62
		0.125	109.8	162.7	226.1	0.98	163.5	205.7	294.4	1.09	137.7	148.4	169.8	1.05	98.33	143.9	190.5	0.93
	118	0.062	94.24	135.9	152.6	0.62	141.7	176.3	237.8	0.493	68.24	112.7	135.9	0.45	79.59	128.7	156	0.41
		0.093	101.8	150.1	207.5	0.8	214.7	188.5	276.6	0.66	109.6	120.6	143.1	0.59	137.9	148.9	170.6	0.58
		0.125	121.3	191	289.3	0.84	267.2	208.1	304.9	0.82	92.96	150.8	191.9	0.93	127.9	205.4	255.9	0.82

0.4	59	0.062	79.04	139.9	158.9	0.93	96.8	130.7	167	0.86	82.34	119.6	154.5	0.59	150.3	145.4	280.2	0.71
		0.093	113.8	169.6	216.2	0.7	111.3	150.8	215.3	0.9	111.6	140.6	209	0.87	162.8	172.1	242.9	0.86
		0.125	123.5	176.1	242.3	0.99	127.3	172.5	266.8	1.09	131.1	176.3	342.3	1.05	175.8	217	313.6	1.08
	75	0.062	95.52	143	172.1	0.76	115	143.6	193.7	0.61	92.22	122.7	161.9	0.57	140.4	172.5	229	0.62
		0.093	125.7	173.7	208.5	0.87	121.4	165.9	246.6	0.9	149.9	170.1	237.2	0.78	173.8	217.3	268.4	0.7
		0.125	136.2	195.7	243.2	0.99	239.2	192.3	287	1.11	143.2	160.3	243.8	1.06	182.6	227.1	326.1	1
	118	0.062	143	183.8	224.4	0.54	122.3	165.5	231.6	0.47	104.6	143.3	197	0.52	169.5	208.1	272.4	0.57
		0.093	127.9	185.5	230.6	0.93	126	41.69	70.43	0.67	158.9	191.8	228.8	0.68	222.4	217.8	326.1	0.64
		0.125	137.5	209.4	267.8	1.11	148.3	199.4	334.7	0.91	143.6	259.5	364.4	0.98	180.5	239.4	354.3	0.88

Table 4.3: ANOVA result summary

Ti-Multilayer coated tool									
Response	Sum of squares		Degrees of freedom		Mean square		F ratio	P*	CoD (R^2)
	Regression	Residual	Regression	Residual	Regression	Residual			
F_x	13004.6	2819.4	9	17	1444.95	165.85	8.71	0	0.8218
F_y	17797.6	1185.7	9	17	1977.51	69.74	28.35	0	0.9375
F_z	53595.3	4309.4	9	17	5955.04	253.49	23.49	0	0.9256
R_a	0.790151	0.17	9	17	0.087795	0.01115	7.97	0	0.8065
TiC-C coated tool									
F_x	59244.4	18838.9	9	17	6582.7	1108.2	5.93	0	0.7587
F_y	62069.9	4658.7	9	17	6896.7	274	25.17	0	0.6296
F_z	103595	35016	9	17	11510.5	2059.7	5.59	0	0.7474
R_a	1.05	0.06	9	17	0.12	0.004	30	0	0.9437
AlCN/AlC coated tool									
F_x	16857.1	5358.1	9	17	1873.01	315.19	5.94	0.001	0.7588
F_y	26001.5	3024.5	9	17	2889.05	177.91	16.23	0	0.8958
F_z	84434.1	12624.9	9	17	9381.6	742.6	12.63	0	0.8699
R_a	1.0482	0.0419	9	17	0.1165	0.0025	46.6	0	0.9616
FeCrN coated tool									
F_x	44059.3	8400	9	17	4895.8	494.12	9.90	0	0.8399

F_y	34367.6	7783.5	9	17	3818.62	457.85	8.34	0	0.8153
F_z	107451	12488	9	17	11939	734.6	16.25	0	0.8959
R_a	0.973737	0.033215	9	17	0.108193	0.001954	55.37	0	0.967
* significant at 95% confidence level									

(a) Regression models developed from full factorial design for Ti-multilayer coated tool

$$F_x = 24 + 549 \times a_p - 0.76 \times V_c - 386 \times f + 2.46 \times a_p \times V_c + 1794 \times a_p \times f + 0.03 \times V_c \times f - 1146 \times a_p^2 + 0.00086 \times V_c^2 + 355 \times f^2 \quad (4.3)$$

$$F_y = 222.6 - 94 \times a_p - 2.310 \times V_c - 813 \times f + 2.054 \times a_p \times V_c + 650 \times a_p \times f + 2.85 \times V_c \times f + 147 \times a_p^2 + 0.00943 \times V_c^2 + 5170 \times f^2 \quad (4.4)$$

$$F_z = 61 + 907 \times a_p - 2.64 \times V_c - 479 \times f + 2.55 \times a_p \times V_c + 275 \times a_p \times f + 8.58 \times V_c \times f - 1304 \times a_p^2 + 0.00844 \times V_c^2 + 4375 \times f^2 \quad (4.5)$$

$$R_a = -0.621 + 5.72 \times a_p + 0.0086 \times V_c - 4.87 \times f + 0.00029 \times a_p \times V_c + 6.91 \times a_p \times f - 0.0180 \times V_c \times f - 7.93 \times a_p^2 - 0.000058 \times V_c^2 + 27.9 \times f^2 \quad (4.6)$$

(b) Regression models developed from full factorial design for TiC-C coated tool

$$F_x = -540 + 3941 \times a_p + 2.34 \times V_c - 1651 \times f - 0.69 \times a_p \times V_c + 4509 \times a_p \times f + 9.2 \times V_c \times f + 6642 \times a_p^2 - 0.0137 \times V_c^2 + 595 \times f^2 \quad (4.7)$$

$$F_y = -281 + 3276 \times a_p + 2.13 \times V_c - 3314 \times f - 1.99 \times a_p \times V_c +$$
$$1668 \times a_p \times f + 3.59 \times V_c \times f - 5209 \times a_p^2 - 0.0108 \times V_c^2 + 15519 \times f^2 \quad (4.8)$$

$$F_z = -570 + 5420 \times a_p + 2.88 \times V_c - 4719 \times f - 1.68 \times a_p \times V_c +$$
$$4796 \times a_p \times f + 3.3 \times V_c \times f - 8817 \times a_p^2 - 0.0146 \times V_c^2 + 21168 \times f^2 \quad (4.9)$$

$$R_a = -0.713 + 4.27 \times a_p + 0.01289 \times V_c - 1.24 \times f - 0.01552 \times a_p \times V_c +$$
$$14.30 \times a_p \times f - 0.0029 \times V_c \times f - 4.92 \times a_p^2 - 0.000059 \times V_c^2 + 13.7 \times f^2 \quad (4.10)$$

(c) Regression models developed from full factorial design for AlCN/AlC coated tool

$$F_x = 47 - 1288 \times a_p + 2.44 \times V_c + 1644 \times f + 0.11 \times a_p \times V_c +$$
$$3826 \times a_p \times f + 0.21 \times V_c \times f + 1852 \times a_p^2 - 0.0121 \times V_c^2 - 12581 \times f^2 \quad (4.11)$$

$$F_y = 484 - 1827 \times a_p - 2.47 \times V_c - 1406 \times f + 3.13 \times a_p \times V_c +$$
$$4039 \times a_p \times f + 7.37 \times V_c \times f + 2299 \times a_p^2 + 0.00724 \times V_c^2 + 1489 \times f^2 \quad (4.12)$$

$$F_z = 719 - 2945 \times a_p - 3.36 \times V_c - 2848 \times f - 0.05 \times a_p \times V_c +$$
$$6679 \times a_p \times f + 6.29 \times V_c \times f + 4537 \times a_p^2 + 0.0179 \times V_c^2 + 8979 \times f^2 \quad (4.13)$$

$$R_a = -0.717 + 1.13 \times a_p - 0.00492 \times V_c - 7.80 \times f - 0.00284 \times a_p \times V_c +$$
$$6.89 \times a_p \times f + 0.0089 \times V_c \times f - 1.28 \times a_p^2 - 0.000018 \times V_c^2 + 63.7 \times f^2 \quad (4.14)$$

(d) Regression models developed from full factorial design for FeCrN coated tool

$$F_x = 334 - 1285 \times a_p - 4.23 \times V_c + 1212 \times f + 2.36 \times a_p \times V_c +$$
$$681 \times a_p \times f + 6.19 \times V_c \times f + 2452 \times a_p^2 + 0.0177 \times V_c^2 - 9124 \times f^2 \quad (4.15)$$

$$F_y = 332 - 1052 \times a_p - 1.73 \times V - 1153 \times f + 2.50 \times a_p \times V_c +$$
$$1133 \times a_p \times f + 4.58 \times V_c \times f + 1819 \times a_p^2 + 0.0051 \times V_c^2 + 5423 \times f^2 \quad (4.16)$$

$$F_z = 733 - 2394 \times a_p - 4.66 \times V_c - 3505 \times f + 1.63 \times a_p \times V_c +$$
$$1593 \times a_p \times f + 13.71 \times V_c \times f + 4586 \times a_p^2 + 0.0186 \times V_c^2 + 14380 \times f^2 \quad (4.17)$$

$$R_a = 0.320 + 0.90 \times a_p + 0.00142 \times V_c - 3.95 \times f - 0.01250 \times a_p \times V_c -$$
$$11.90 \times a_p \times f - 0.0081 \times V_c \times f + 3.09 \times a_p^2 + 0.000006 \times V_c^2 + 78.8 \times f^2 \quad (4.18)$$

4.5.1 Analysis of cutting force

Figure 4.39 and Figure 4.40 (a-c), (d-f) and (d-i) show the interaction effects of cutting force for the Ti-multilayer, TiC-C and Fig 4.40 AlCN/AlC and FeCrN coated tool.

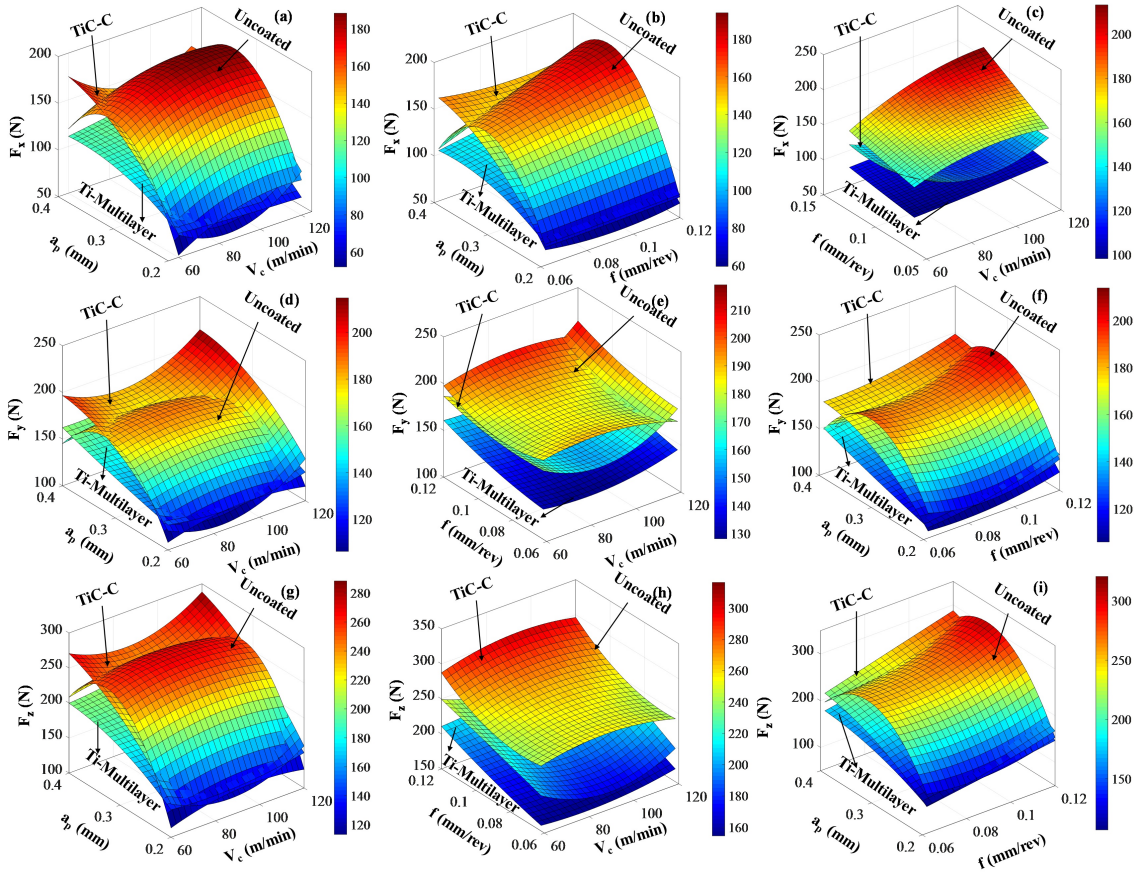

Figure 4.39: Interaction plots for cutting force during full factorial analysis for Ti-multilayer, TiC-C coated and uncoated WC tool

Figure 4.39 and Figure 4.40 (a), (d) and (g) present the effect of depth of cut and speed on cutting forces at a constant feed rate of 0.093 mm/rev.

From the interaction plots it has been observed that cutting forces are inversely proportional to feed rate. Figure 4.39 and 4.40 (b), (e) and (h) represent the effect of depth of cut and feed rate on cutting forces with a constant speed of 75 m/min. With the increase in feed rate, cutting forces are increased linearly. Figure 4.39 and 4.40 (c), (f) and (i) represent the effect of feed rate and speed on cutting forces with a constant depth of cut 0.4 mm. With the increase in feed rate cutting forces are increasing linearly and with an increase in speed, cutting forces are not affected much.

From the interaction plots, higher cutting forces are observed for uncoated tool. Ti

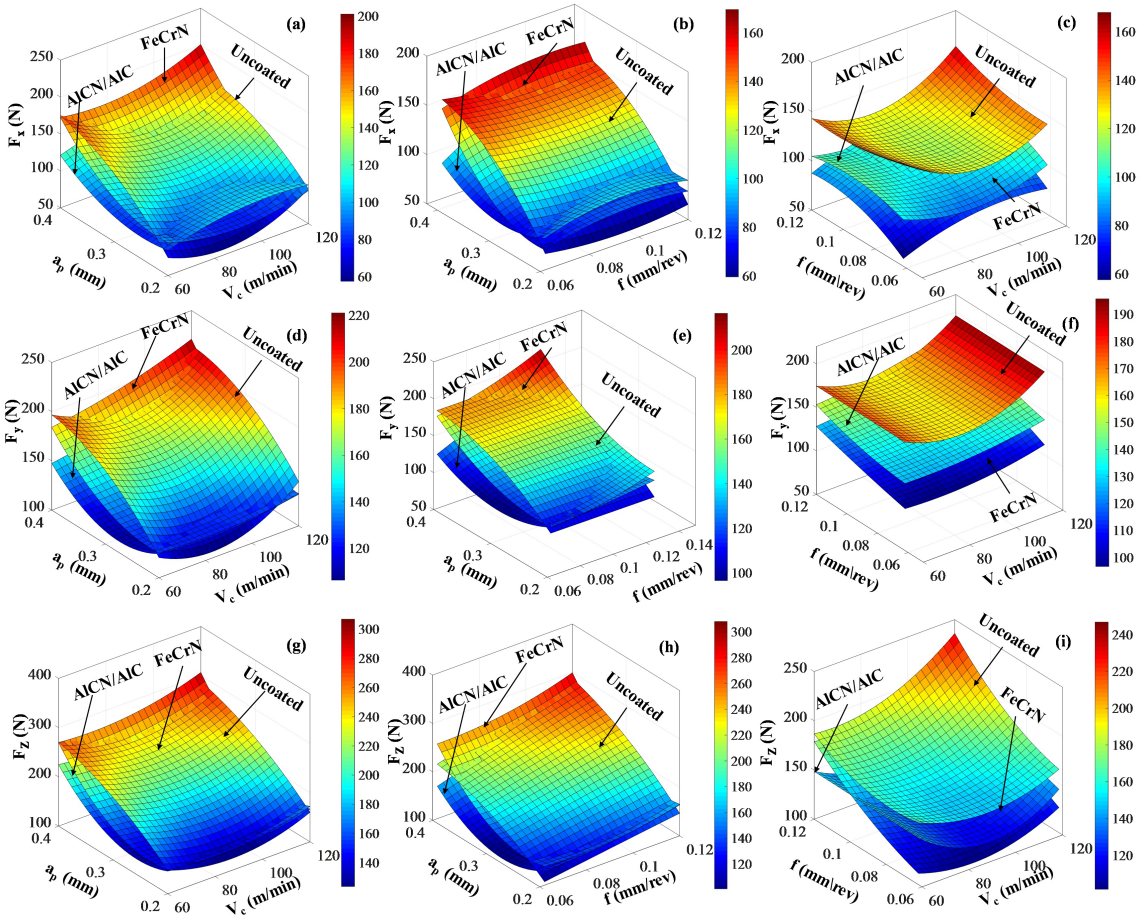

Figure 4.40: Interaction plots for cutting force during full factorial analysis for AlCN/AlC coated tool, FeCrN coated tool and WC uncoated tool

monolayer coating with less cutting force brings about better performance than Ti-multilayer coated tool. FeCrN coated tool show less cutting force compared to AlCN/AlC coated tool.

Feed rate and depth of cut are observed to be linearly affecting the cutting force. For lower feed rate and depth of cut, cutting forces have been reduced and with an increase in feed rate and speed steady rise in the cutting force are observed. Cutting speed does not influence cutting forces during machining so much as the feed rate and cut depth. Depth of cut and feed rate are contributing more to the cutting forces in the factorial analysis results compared to speed (Angadi *et al.*, 2015; Bouacha *et al.*, 2010).Summary of ANOVA

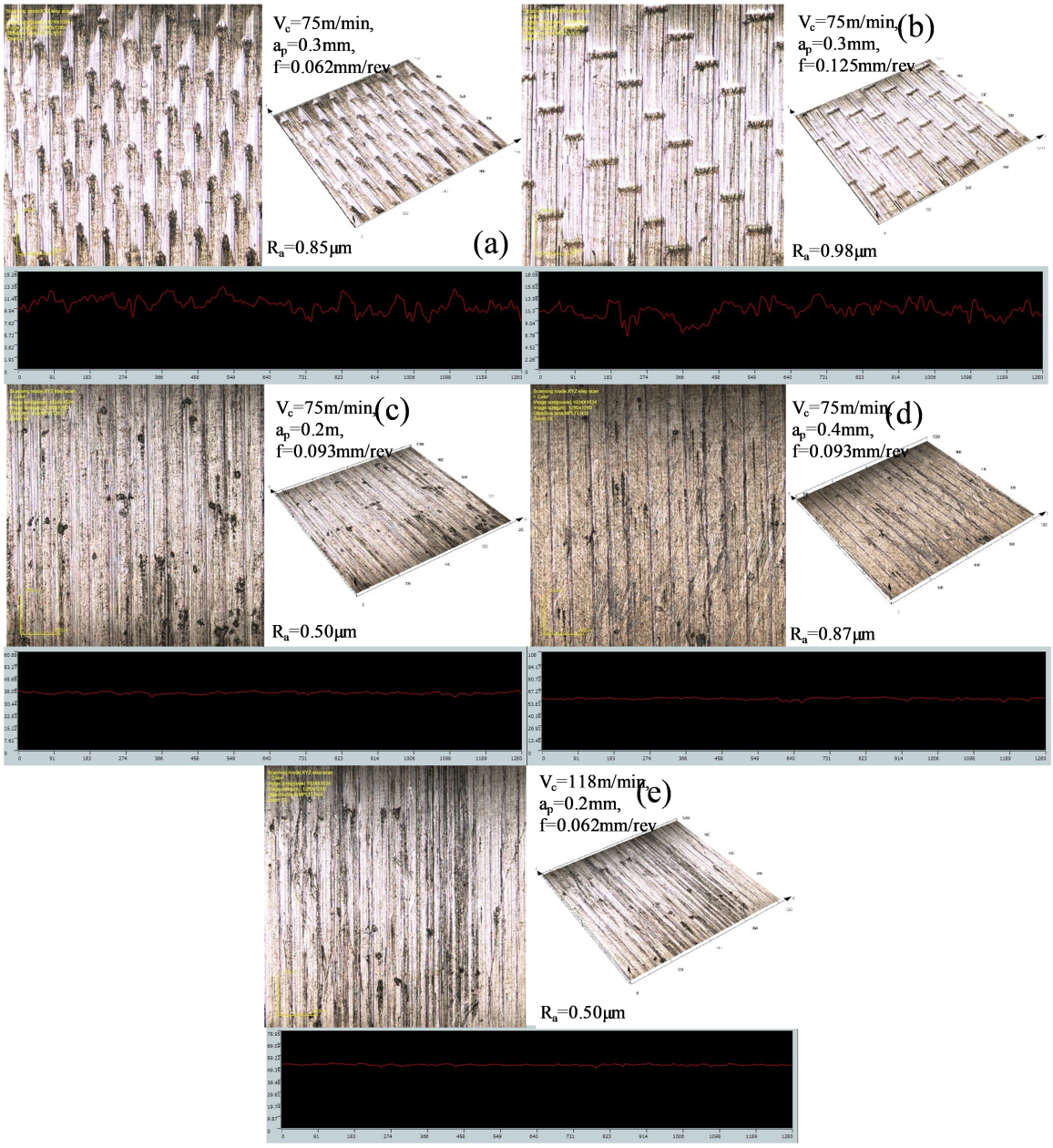

Figure 4.41: Machined surface topography for Ti-Multilayer coated tool

results in Table 4.3 indicates that both the regression models developed for cutting forces and surface roughness are significant ($P < 0.05$).

Figure 4.41 (c), Figure 4.42 (c) indicate the machined surface topography at the test condition of V_c=75 m/min, a_p=0.2 mm and f=0.093 mm/rev, cutting forces and surface of

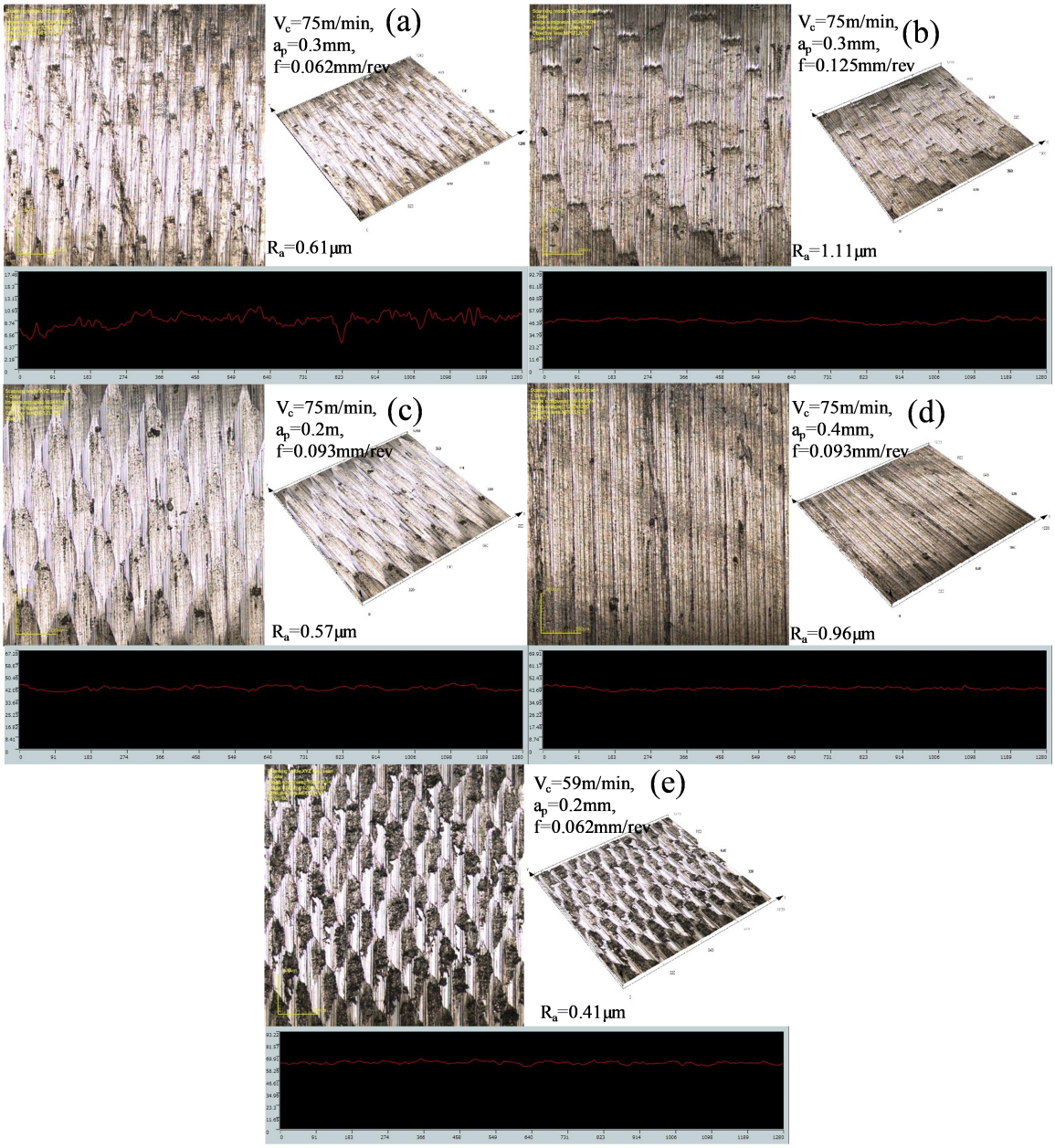

Figure 4.42: Machined surface topography for TiC-C Coated tool

F_x=72.33 N, F_y=119.6 N, F_z=137.7 N, R_a =0.50 μm and F_x=66.1 N, F_y=115.5 N, F_z=130.6 N, R_a=0.57 μm μm observed for Ti-multilayer and TiC-C coated tool respectively; lower the depth of cut lesser cutting force and surface roughness is observed. Similarly, a higher cut depth of a_p = 0.4 mm represented in Figure 4.41 (c) and Figure 4.42 (d) cutting forces

and surface roughness are increased to F_x=125.7 N, F_y=173.7 N, F_z=208.5 N, R_a=0.87 μm and F_x=121.4 N, F_y=165.9 N, F_z=246.6 N, R_a=0.9 μm for Ti-multilayer and TiC-C coated tool respectively.

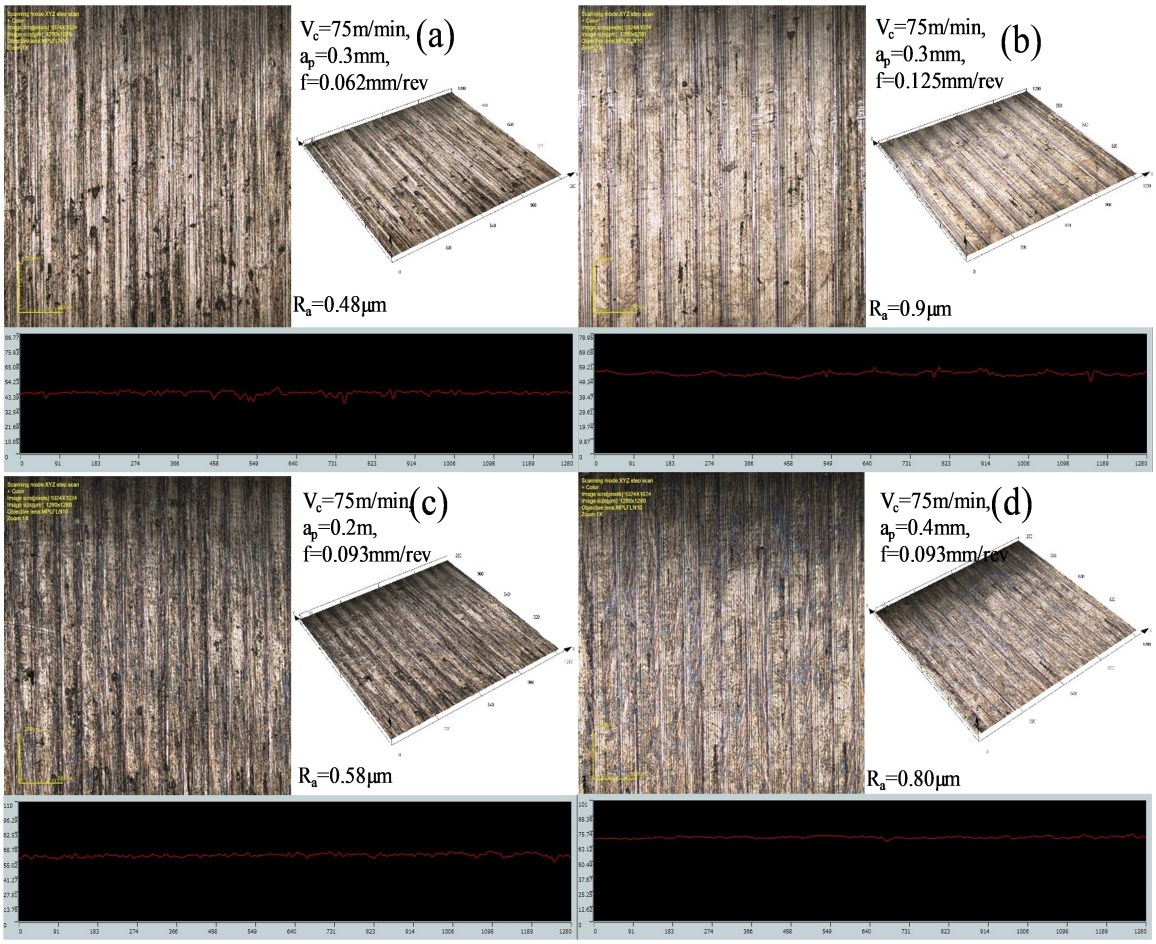

Figure 4.43: Machined surface topography for AlCN/AlC coated tool

Figure 4.43 (c) and Figure 4.44 (c) represent the machined surface topography at the test condition of V_c=75 m/min, a_p=0.2 mm and f=0.093 mm/rev, cutting forces and surface of F_x=76.66 N, F_y=120.1 N, F_z=154.1 N, R_a =0.57 μm and F_x 80.02 N, F_y=131.6 N, F_z=149.1 N, R_a=0.62 μm are observed for AlCN/AlC and FeCrN coated tool respectively; lower the depth of cut less cutting force and surface roughness is observed. Similarly, with a higher depth of cut of a_p=0.4 mm represented in Figure 4.43 (d) and Figure 4.44 (d) shows cutting forces and surface roughness increased to F_x=149.9 N, F_y=170.1 N, F_z=237.2 N, R_a=0.7

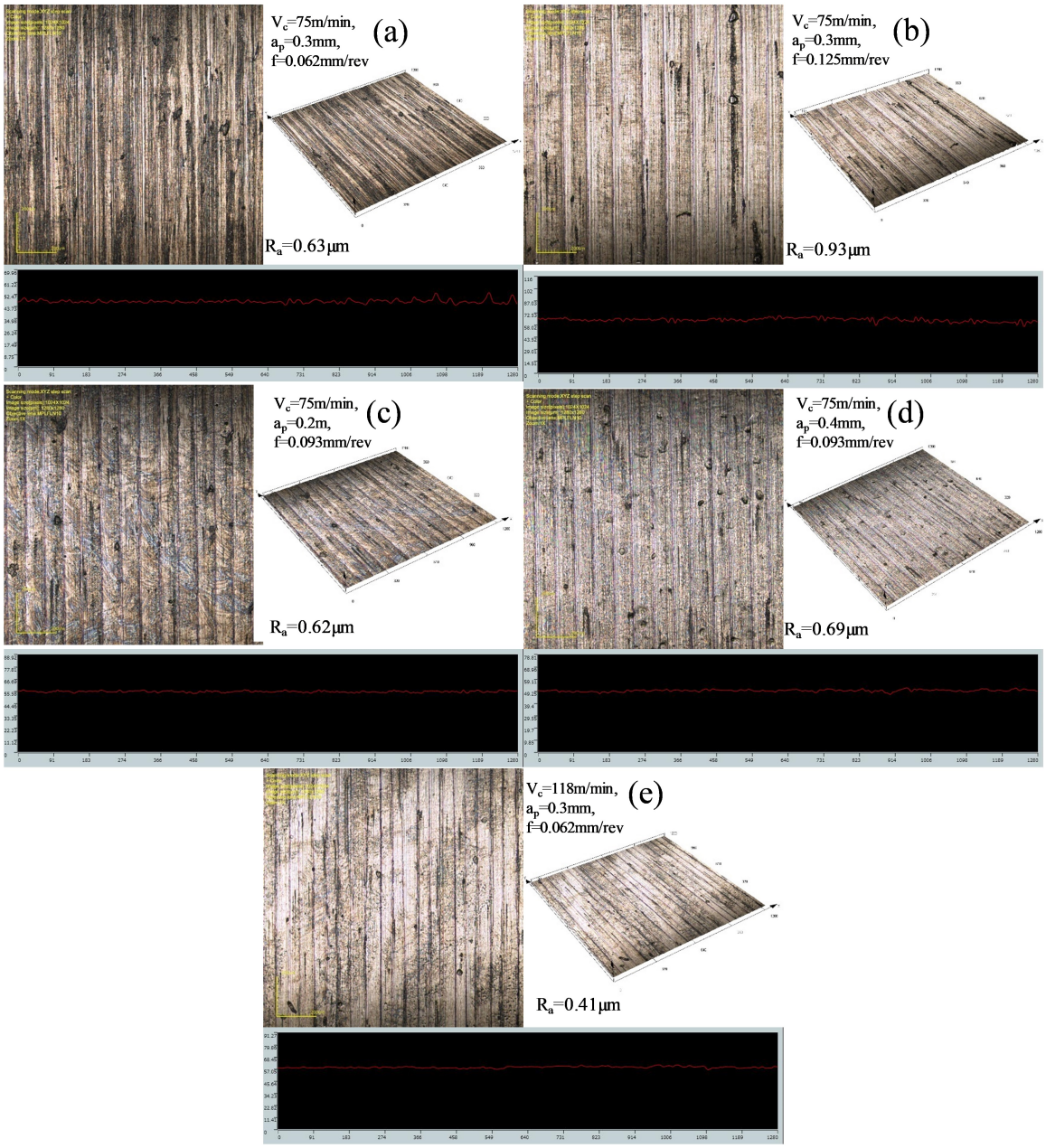

Figure 4.44: Machined surface topography for FeCrN coated tool

μm and F_x=173.8 N, F_y=217.3 N, F_z=268.4 N, R_a=0.70 μm for AlCN/AlC and FeCrN coated tool respectively. Amount of material removed increases with the depth of cut, the increased amount of material requires more force to deform the material plastically and hence the increase in cutting force is observed. Tool traverse speed against the work

material increases with the feed rate, this attributes to increase in the amount of material removed in less time resulted in a rise in cutting force. Cutting forces are reduced by 15 %, 5 %, 18 % and 4 % in Ti-multilayer, TiC-C, AlCN/AlC and FeCrN coated tool respectively compared to uncoated tool.

4.5.2 Analysis of surface roughness

Figure 4.45 and Figure 4.46 represent the interaction effects in case of surface roughness while using uncoated, Ti-multilayer, TiC-C, AlCN/AlC and FeCrN coated tool.

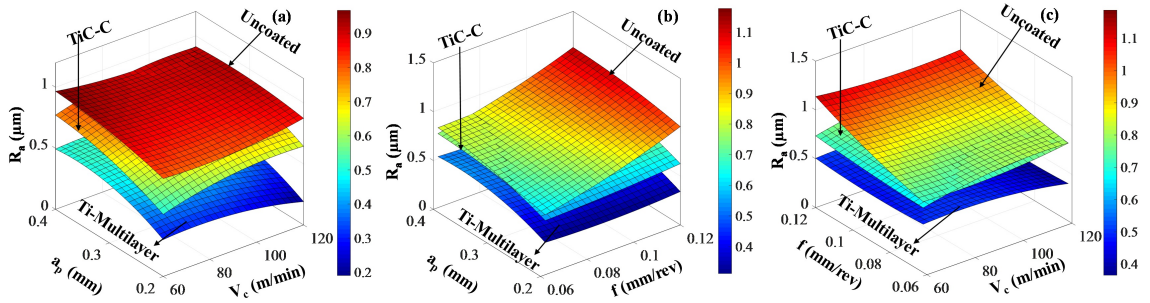

Figure 4.45: Interaction plots for surface roughness during full factorial analysis for Ti-multilayer, TiC-C coated and uncoated WC tool

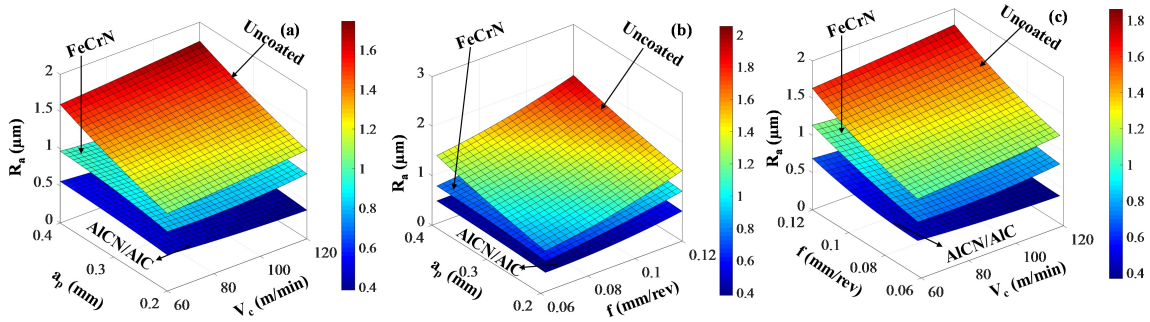

Figure 4.46: Interaction plots for surface roughness during full factorial analysis for AlCN/AlC coated tool, FeCrN coated tool and WC uncoated tool

Figure 4.45 (a) and Figure 4.46 (a) show the effect of depth of cut and speed on surface roughness at a constant feed rate of 0.093 mm/rev. Figure 4.45 (b) and Figure 4.46 (b) show the effect of depth of cut and feed rate on surface roughness at a constant speed of

75 m/min. Figure 4.45 (c) and Figure 4.46 (c) show the effect of feed rate and speed on surface roughness at a constant depth of cut of 0.3 mm. The effect of feed rate and speed is prodigious in the study of surface roughness. Increase in surface roughness is observed with increase in feed rate. Surface roughness has been less affected by the change in depth of cut during machining. Surface roughness tends to decrease with increase in speed. Slight change in feed rate and speed leads to variations in the surface roughness. Contact between tool and material reduces with increase in the speed, which leads to reducing in the surface roughness. Figure 4.45 (a) and Figure 4.46 (a) represent the machined surface topography at the test condition of V_c=75 m/min, a_p=0.3 mm and f=0.062 mm/rev, surface roughness of 0.85 μm and 0.61 μm observed for Ti-multilayer and TiC-C coated tool respectively; the lower is the feed rate, the less surface roughness is observed. Similarly, with a higher feed rate of f=0.125 mm/rev represented in Figure 4.45 (b) and Figure 4.46 (b) surface roughness increased to 0.98 μm and 1.11 μm for Ti-multilayer and TiC-C coated tool respectively. Figure 4.45 (a) and Figure 4.46 (a) represent the machined surface topography at the test condition of V_c=75 m/min, a_p=0.3 mm and f=0.062 mm/rev, surface roughness of 0.48 μm and 0.63 μm observed for AlCN/AlC and FeCrN coated tool respectively; the lower is the feed rate the less surface roughness observed. Similarly, with a higher feed rate of f=0.125 mm/rev represented in Figure 4.46 (b) and Figure 4.46 (b) surface roughness increases to 0.90 μm and 0.93 μm for AlCN/AlC and FeCrN coated tool respectively. With the increase in feed rate, tool traverse speed against the work material increases, surface roughness increases because of increased friction between tool and workpiece (Bouacha *et al.*, 2010). With the higher cutting speed, rotational torque of specimen is more in the material which reduces the surface roughness (Angadi *et al.*, 2015). AlCN/AlC coating performs better comparative to FeCrN coating with the lower magnitude of cutting force and surface roughness because of less surface roughness and presence of hard phases of AlC and AlN and AlCN.

4.5.3 Optimization of the results

Multi-objective optimization of cutting force and surface roughness was carried out using desirability and PSO optimization techniques. Desirability approach and PSO technique for the minimization of the cutting force and surface roughness adopted in the present work are indicated in Figure 4.47 and Figure 4.48 respectively.

Table 4.4: Optimal process parameters

Ti multilayer coated tool							
Parameters	V_c	f	a_p	F_x	F_y	F_z	R_a
Desirability	107.87	0.062	0.2	68.95	111.15	107.14	0.49
MOPSO	94.78	0.062	0.2	70.14	108.66	105.13	0.49
Experimental	118	0.062	0.2	67.68	113.9	107.1	0.5
TiC-C Coated tool							
Desirability	59	0.062	0.2	52.94	103.54	112.65	0.55
MOPSO	59	0.062	0.2	51.3	107.03	110.64	0.55
Experimental	59	0.062	0.2	67.5	118.6	115.7	0.44
AlCN/AlC coated tool							
Desirability	75	0.062	0.3	62.33	98.16	105.84	0.54
MOPSO	75	0.062	0.3	69.06	96.79	101.26	0.53
Experimental	75	0.062	0.3	62.99	95.52	127.4	0.46
FeCrN coated tool							
Desirability	118	0.062	0.2	62.11	114.46	129.49	0.44
MOPSO	118	0.062	0.2	63.3	114.38	127.44	0.44
Experimental	118	0.062	0.2	77.76	120.4	149.3	0.43

Combination of (V_c-118 m/min, f-0.062 mm/rev and a_p-0.2 mm) are the optimum conditions for the Ti-multilayer coated tool, similarly (V_c-59 m/min, f-0.062 mm/rev and a_p-0.2 mm) are the optimum conditions for TiC-C coated tool. Combination of (V_c-75 m/min, f-0.062 mm/rev and a_p-0.3 mm) are the optimum conditions for the AlCN/AlC

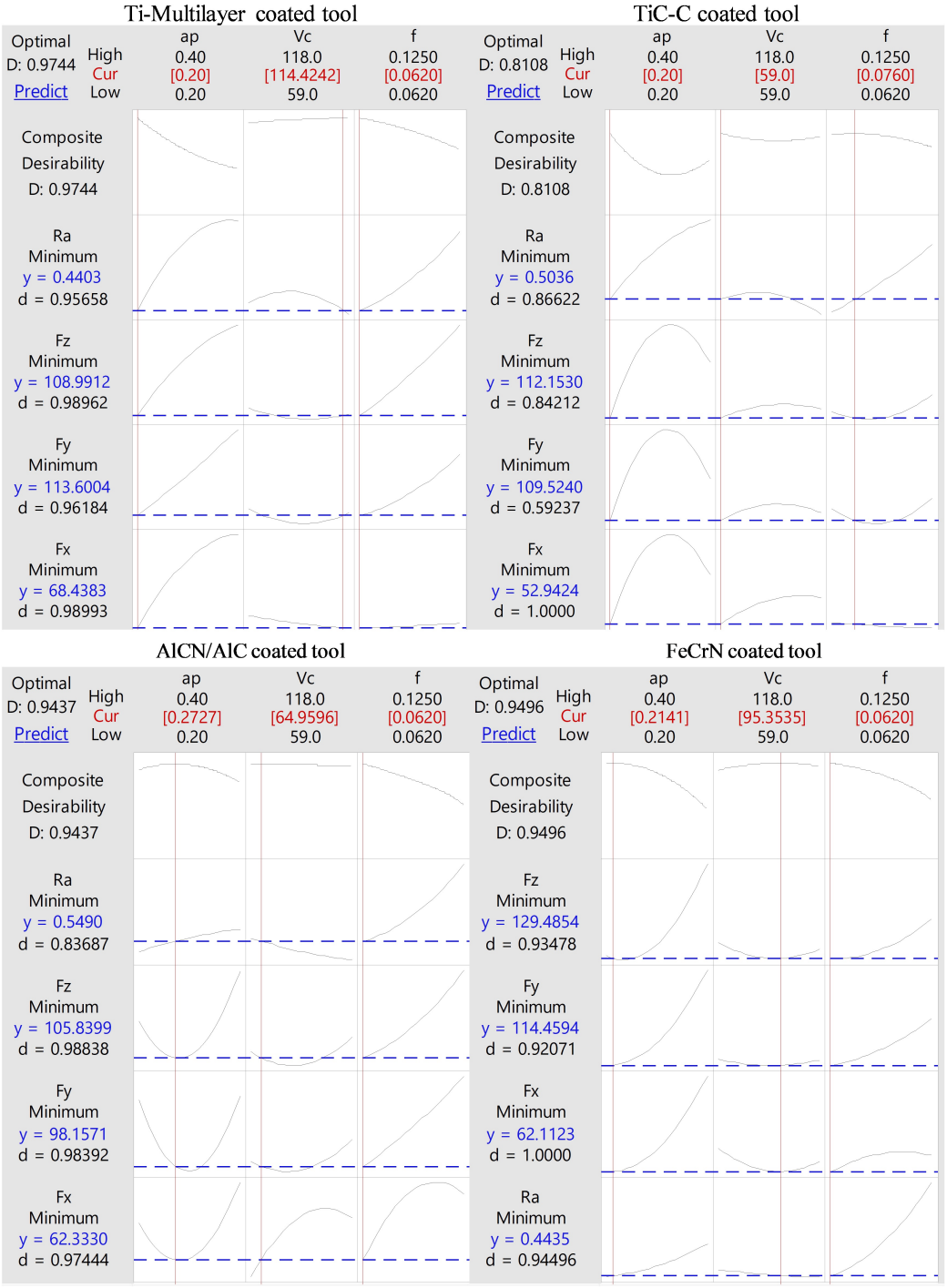

Figure 4.47: Optimisation plots using desiarability

coated tool. Likewise (V_c-118 m/min, f-0.062 mm/rev and a_c-0.2 mm) are the optimum conditions for FeCrN coated tool obtained from both of the desirability and PSO approach

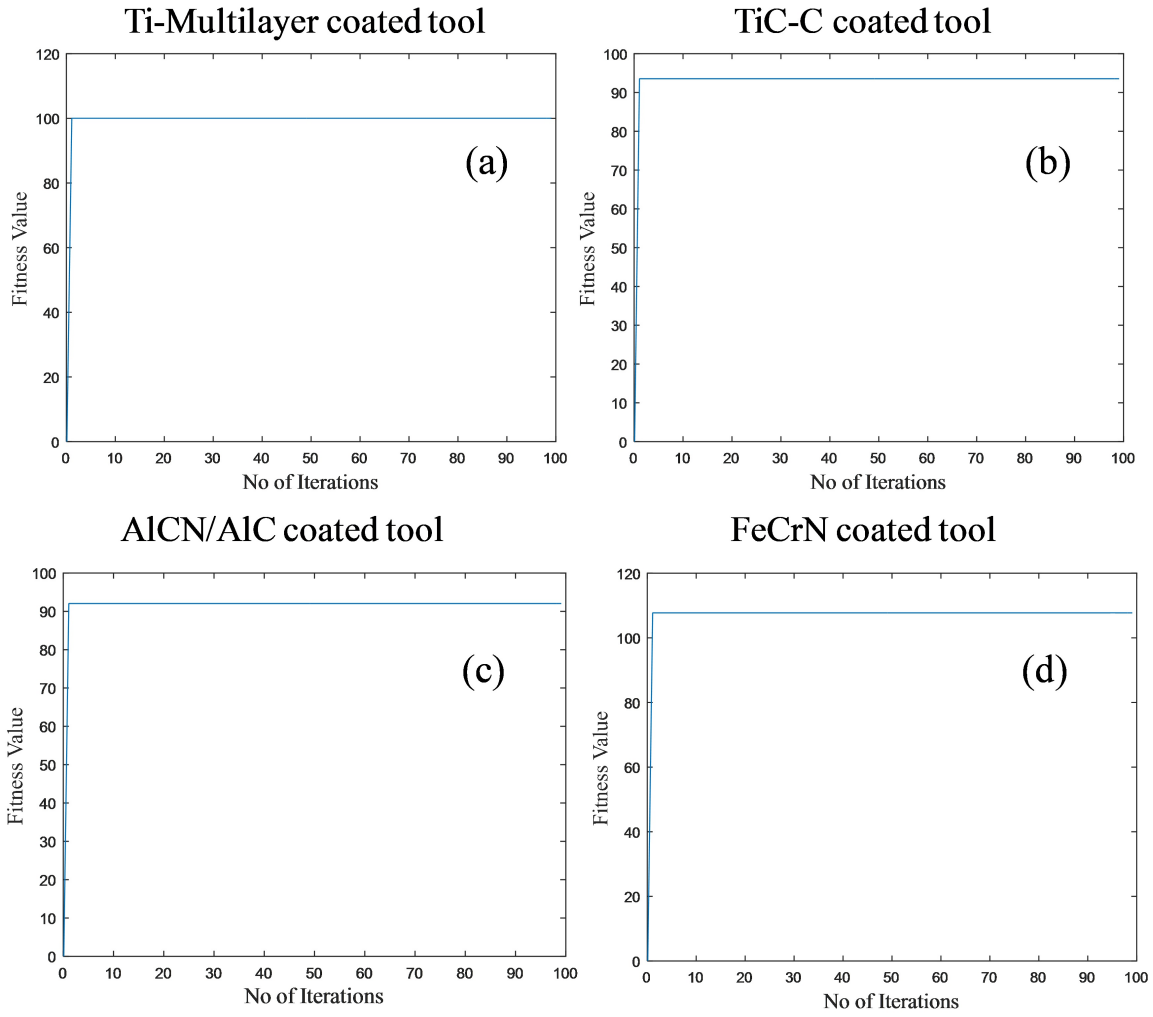

Figure 4.48: MOPSO convergernce graph (a)Ti-multilayer and (b)TiC-C coated tool (c) AlCN/AlC coated tool (d)FeCrN coated tool

as shown in Table 4.4. Figure 4.41 (e), 4.42 (e), 4.43 (a) and 4.44 (e) represent the optimum machined surface topographies for Ti-multilayer, TiC-C, AlCN/AlC and FeCrN coated tool respectively. With the depth of cut=0.2 mm the amount of material deformed is minimal, which in turn results in the better surface roughness (0.40-0.50 μm) and less cutting forces (95-130 N) during machining with Ti-multilayer, TiC-C and FeCrN coated tool. Feed rate of 0.062 mm/rev is ideal for achieving better roughness (¡0.50 [U+F06D]m), reduces cutting forces (¡130 N). Using Ti coated tool better surface and lesser cutting forces are observed which is due to reduced coefficient of friction with the Ti coatings (Badiger *et al.*,

2017). Optimum results are obtained at the speed of 118 m/min for Ti-multilayer whereas optimum results are obtained at 59 m/min for TiC-C coated tool. The surface roughness (0.50 μm) which is obtained at higher speed (118 m/min) for Ti-multilayer is achieved with lower speed (59 m/min) for TiC-C coated tool. Similarly, results obtained at higher speed (118 m/min) for FeCrN are achieved with lower speed (75 m/min) for AlCN/AlC coated tool. Mechanical properties of the coatings indicate that the TiC-C and FeCrN have better hardness and less coefficient of friction which make the coating perform better comparatively. Optimum results are obtained at the speed of 118 m/min for FeCrN whereas optimum results appear at for 75 m/min for AlCN/AlC coated tool.

4.5.4 Validation experiments

Trained ANN network and regression models were used to validate the results for all the experimental conditions. Figure 4.49, Figure 4.50, Figure 4.52 and Figure 4.51 show the comparison of experimental and predicted results obtained for Ti-multilayer, TiC-C, AlCN/AlC and FeCrN coated tools respectively.

Regression models are used to predict the results within the boundary limits, henceforth ANN models are developed to predict beyond the boundary limits. Coefficient of determination (R^2) represents the quality of the model. If it is closer to 1 the quality of the developed model is better. It is found that the predicted data by the regression model closely follows the experimental data. Mathematical models for the cutting forces and surface roughness are developed for Ti-multilayer, TiC-C, AlCN/AlC and FeCrN coated tool using ANN and mathematical regression models. Comparison of R^2 and error percentage values for all the coatings are reported in Table 4.5 and Table 4.8 respectively.

Plots of experimental and predicted results are found with least error and no significant deviation for the coated tools. COD (R^2) of both the predictive models are close to 1, confirming the developed models are adequate. Validation of the developed on models are represented in Table 4.5 and Table 4.8, and the results exhibit negligible flaw Angadi *et al.* (2015).

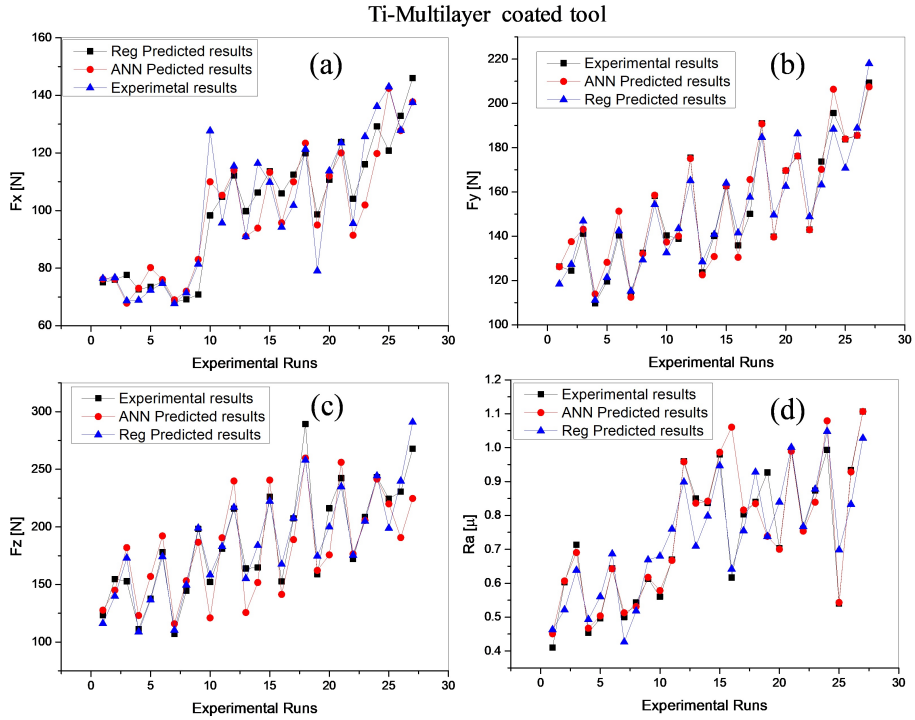

Figure 4.49: Plots of experimental and predicted results for Ti-multilayer coated tool

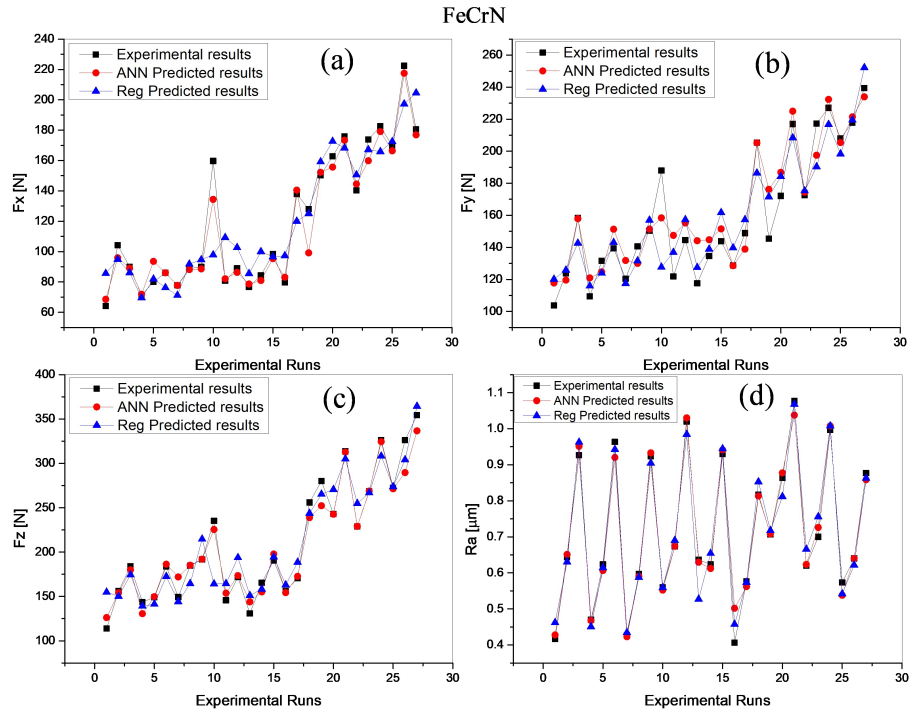

Figure 4.51: Plots of experimental and predicted results for FeCrN coated tool

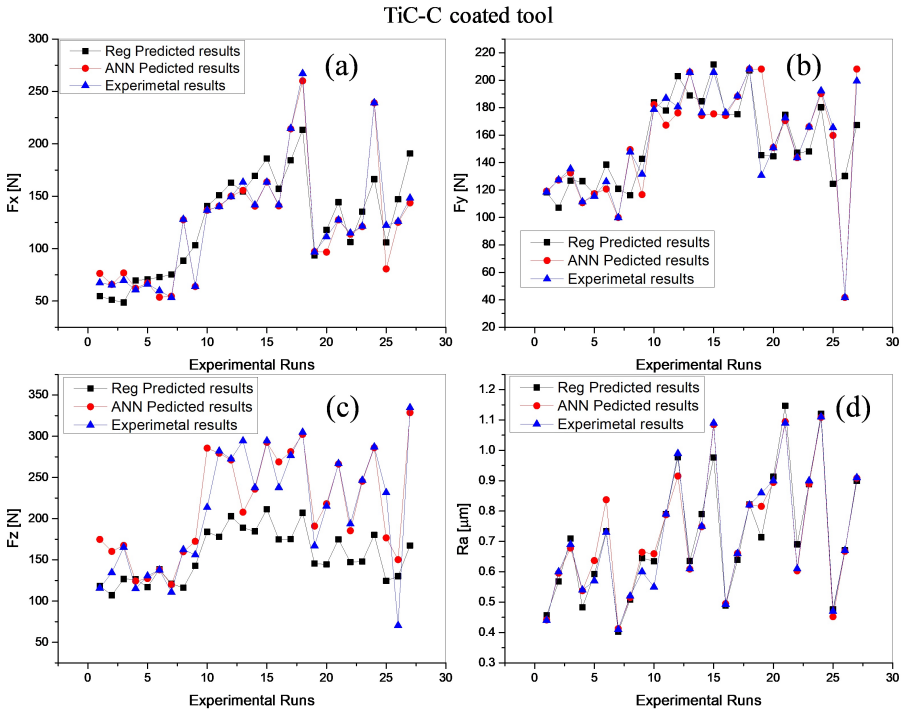

Figure 4.50: Plots of experimental and predicted results for TiC-C coated tool

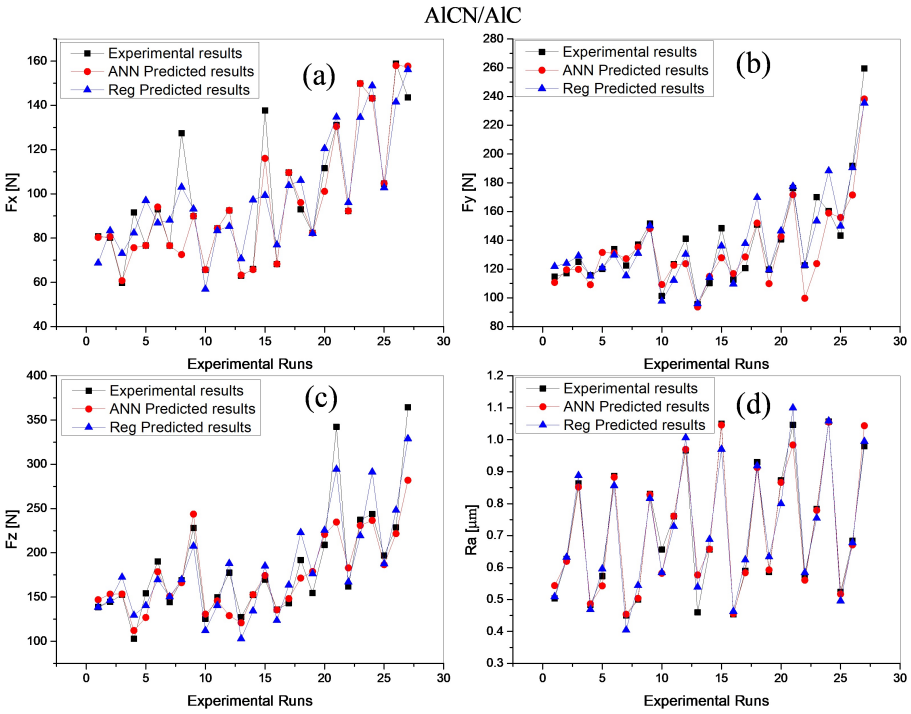

Figure 4.52: Plots of experimental and predicted results for AlCN/AlC coated tool

Table 4.5: Validation results for Ti multilayer coated tool

Input			F_x			F_y			F_z			R_a		
a_p	**V_c**	**f**	**Exp**	**Reg***	**ANN***	**Exp**	**Reg***	**ANN***	**Exp**	**Reg***	**ANN***	**Exp**	**Reg***	**ANN***
0.2	59	0.062	72.66	75.07	71.74	116.56	118.45	112.18	118.64	116.22	123.33	0.45	0.46	0.42
0.25	75	0.07	88.65	89.96	72.72	125.88	121.41	113.44	138.69	141.73	136.15	0.66	0.64	0.69
0.35	118	0.078	126.6	120.96	139.37	167.5	163.36	142.13	215.69	206.38	202.81	0.8	0.75	0.86
0.2	59	0.087	78.54	75.74	91.31	123.45	124.84	119.12	129.79	134.58	144.54	0.49	0.51	0.43
0.25	118	0.093	93.66	93.67	102.87	144.12	143.13	142.94	198.65	181.93	207.68	0.66	0.66	0.59
0.35	75	0.1	118.56	116.22	119.48	155.31	156.04	161.93	206.45	205.42	205.37	0.88	0.89	0.86
0.2	59	0.117	76.15	77.14	68.44	145.84	141.03	154.01	178.65	163.84	222.13	0.61	0.6	0.62
0.25	118	0.125	99.56	98.24	70.45	178.69	169.14	189.24	248.65	231.74	269.82	0.86	0.82	0.65
0.35	75	0.078	113.6	109.48	121.34	147.98	143.98	144.08	177.69	182.54	170.96	0.81	0.8	0.83
*Predicted results														

Table 4.6: Validation results for TiC-C coated tool

Input			**F_x**			**F_y**			**F_z**			**R_a**		
a_p	**V_c**	**f**	**Exp**	**Reg***	**ANN***	**Exp**	**Reg***	**ANN***	**Exp**	**Reg***	**ANN***	**Exp**	**Reg***	**ANN***
0.2	59	0.062	55.64	54.71	50.01	72.01	118.3	123.07	124.11	121.21	117.9	0.45	0.46	0.48
0.25	75	0.07	138.68	130.62	103.92	125.5	166.07	149.75	220.64	211.19	236.37	0.58	0.6	0.59
0.35	118	0.078	164.56	165.59	168.67	227.8	160.53	108.57	238.64	236.27	186.38	0.66	0.58	0.64
0.2	59	0.087	53.65	51.72	50.49	72.01	106.9	125.75	108.65	110.86	116.08	0.54	0.54	0.56
0.25	118	0.093	151.96	152.94	159.04	125.5	158.76	181.28	220.65	213.01	257.62	0.56	0.59	0.47
0.35	75	0.1	178.65	174.04	172.02	227.8	183.12	201.12	264.53	269.19	284.45	0.88	0.89	0.91
0.2	59	0.117	50.06	49.12	51.08	72.01	118.83	121.67	135.6	133.38	168.12	0.69	0.67	0.68
0.25	118	0.125	175.16	174.97	173.07	125.5	187.89	198.18	264.55	260.33	196.19	0.77	0.75	0.61
0.35	75	0.078	159.65	158.18	158.36	227.8	176.48	197.68	235.65	247.82	134.64	0.76	0.76	0.76
*Predicted results														

Table 4.7: Validation results for AlCN/AlC coated tool

Input			F_x			F_y			F_z			R_a		
a_p	**V_c**	**f**	**Exp**	**Reg***	**ANN***	**Exp**	**Reg***	**ANN***	**Exp**	**Reg***	**ANN***	**Exp**	**Reg***	**ANN***
0.2	59	0.062	72.55	68.76	80.55	120.55	121.92	120.83	136.88	138.61	102.8	0.5	0.51	0.49
0.25	75	0.07	78.66	79.55	66.01	101.59	102.66	116.64	107.99	108.66	102.8	0.48	0.53	0.46
0.35	118	0.078	100.56	105.2	102.95	135.55	141.44	128.09	170.66	168.07	161.94	0.55	0.56	0.46
0.2	59	0.087	72.35	82.43	71.34	118.64	123.39	117.41	140.56	143.52	102.8	0.6	0.6	0.62
0.25	118	0.093	100.86	98.81	115.92	118.64	128.66	117.58	154.66	155.27	135.44	0.55	0.59	0.5
0.35	75	0.1	120.56	115.29	134.73	127.8	134.08	159.15	180.55	177.42	102.8	1	0.78	1.02
0.2	59	0.117	60.55	78.08	64.18	172.01	127.61	154	162.68	164.23	152.8	0.8	0.81	0.78
0.25	118	0.125	90.89	95.04	92.58	150.88	154.2	154.53	145.3	203.93	206.78	0.88	0.87	0.92
0.35	75	0.078	99.86	98.59	87.47	120.66	115.91	125.2	143.66	143.12	142.8	0.62	0.63	0.55
* Predicted Results														

Table 4.8: Validation results for FeCrN coated tool

Input			F_x			F_y			F_z			R_a		
a_p	**V_c**	**f**	**Exp**	**Reg***	**ANN***	**Exp**	**Reg***	**ANN***	**Exp**	**Reg***	**ANN***	**Exp**	**Reg***	**ANN***
0.2	59	0.062	83.25	85.65	78.17	105.7	120.15	103.7	130.65	154.85	124.66	0.44	0.46	0.45
0.25	75	0.07	75.66	76.55	70.23	116.24	118.64	103.7	133.56	132.19	124.84	0.45	0.5	0.43
0.35	118	0.078	148.35	143.23	155.24	200.53	173.19	180.65	222.56	217.91	244	0.5	0.52	0.44
0.2	59	0.087	95.3	94.5	93.96	131.58	123.93	105.58	156.86	148.98	134.4	0.56	0.59	0.51
0.25	118	0.093	86.33	99.77	88.07	144.5	139.91	124.58	156.2	165.09	148.96	0.62	0.57	0.63
0.35	75	0.1	130.52	128.54	125.33	160.89	164.51	176.61	200.68	207.05	190.46	0.79	0.74	0.71
0.2	59	0.117	88.65	90.08	99.78	156.55	137.42	158.97	170.83	165.66	189.71	0.8	0.86	0.78
0.25	118	0.125	102.58	103.74	100.66	200.28	167.19	199.97	200.87	217.76	222.09	0.88	0.87	0.94
0.35	75	0.078	112.55	122.14	101.65	150.23	152.37	151.12	193.56	192.96	180.12	0.7	0.63	0.89
*Predicted results														

Table 4.9: Comparision on R^2 values for Regression models and ANN

R^2	Ti-multilayer		TiC-C		AlCN/AlC		FeCrN	
	Reg	ANN	Reg	ANN	Reg	ANN	Reg	ANN
F_x	0.8218	0.9480	0.7587	0.9375	0.7588	0.9146	0.8399	0.9823
F_y	0.9256	0.9781	0.6292	0.8385	0.8958	0.9037	0.8153	0.9433
F_z	0.9356	0.9737	0.7474	0.8963	0.8699	0.8970	0.8959	0.9141
R_a	0.8065	0.8817	0.9437	0.9822	0.9616	0.9855	0.9670	0.9919

Table 4.10: Comparision on error percentage for Regression models and ANN

Error %	Ti-multilayer		TiC-C		AlCN/AlC		FeCrN	
	Reg	ANN	Reg	ANN	Reg	ANN	Reg	ANN
F_x	0.95	4.12	3.30	0.80	2.11	2.59	2.30	1.56
F_y	0.19	1.07	6.50	0.50	0.33	1.95	1.16	3.56
F_z	1.39	0.50	5.94	7.70	0.80	2.28	1.29	2.33
R_a	1.38	2.61	0.40	1.30	0.36	0.36	0.34	0.43

4.6 Tool wear measurements

Tool wear during machining of the uncoated and coated tools at respective optimal process parameters are studied with increments of time. Similar results are obtained from studies conducted by Musfirah *et al.* (2017) during machining of Inconel 718 using dry and cryogenic environments.

Figure 4.53 - Figure 4.55 represents the tool wear analysis measured by confocal microscope for uncoated and coated tool. According to the test results, the progression of tool wear under the uncoated tool is higher compared to the coated tool. Tool wear in TiC-C coated tools are less compared to Ti-multilayer coated tool. Similarly, tool wear in AlCN/AlC coated tools are less compared to FeCrN coated tool. Formation of built-up-edge (BUE) is observed in uncoated tool (Figure 4.54(d-e)) and BUE is reduced in coated tools. The abrasion wear mechanism observed in Figure 4.54 and Figure 4.55 for both the

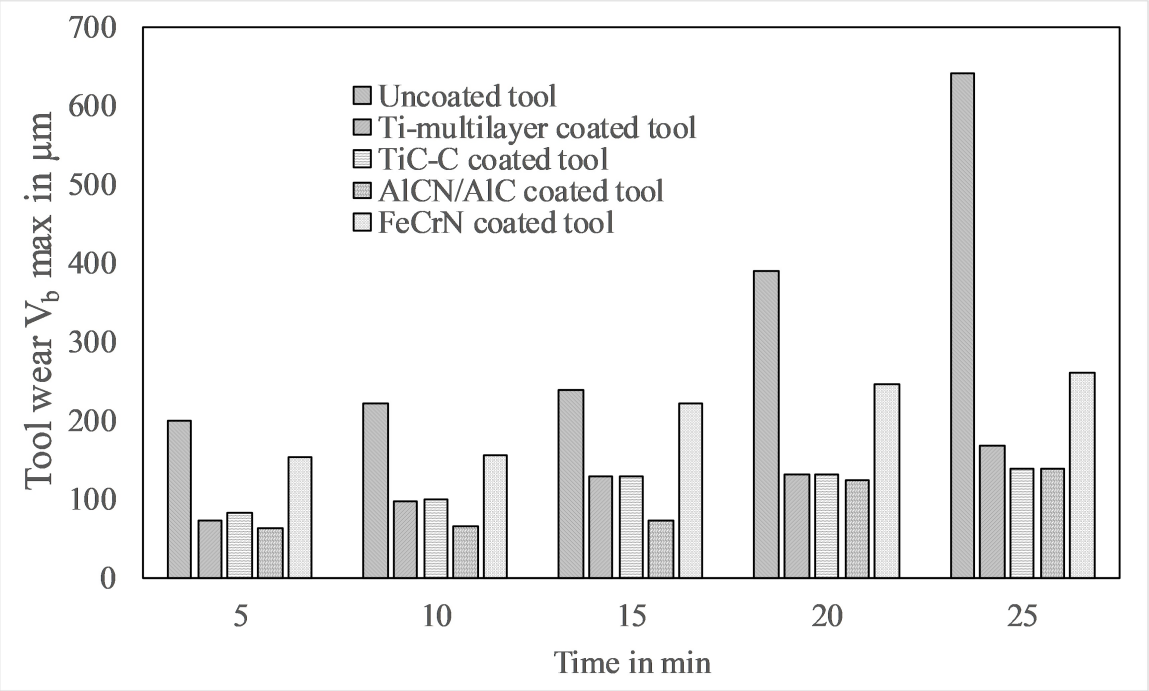

Figure 4.53: Tool wear analysis for uncoated and coated tools

coated and uncoated cutting tool inserts. Which is attributed due to the presence of Cr and Ni phases in the MDN431 material (Coelho *et al.*, 2007). Flank wear is observed in both the coated and uncoated tools. Tool wear is reduced by 65 %, 66 %, 72.7 % and 32.6 % in Ti-multilayer, TiC-C, AlCN/AlC and FeCrN coated tool respectively when compared to uncoated tool.

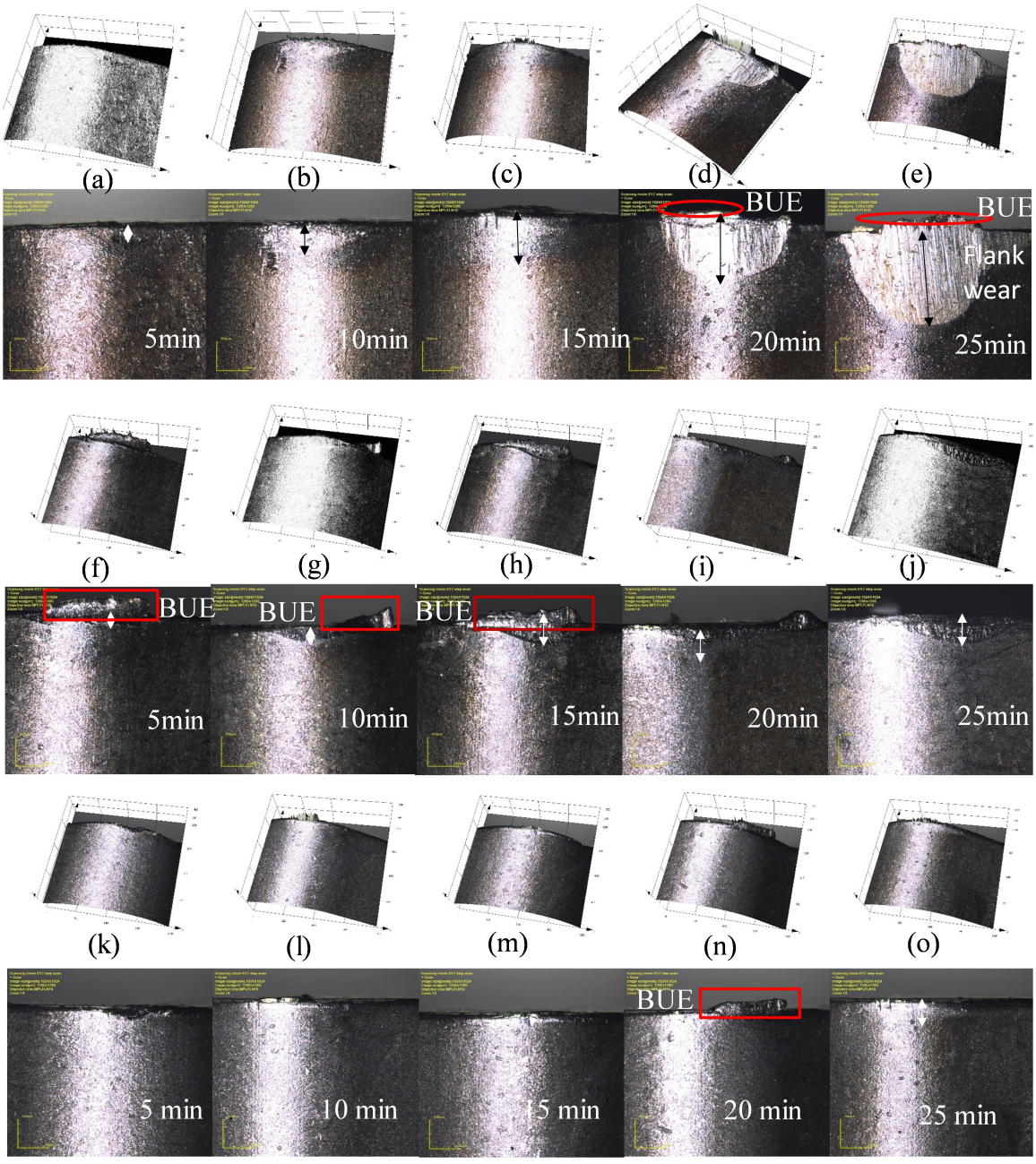

Figure 4.54: Tool wear measurements for (a-e)uncaoted tool, (f-j) Ti-multilayer coated tool and (k-o) TiC-C coated tool

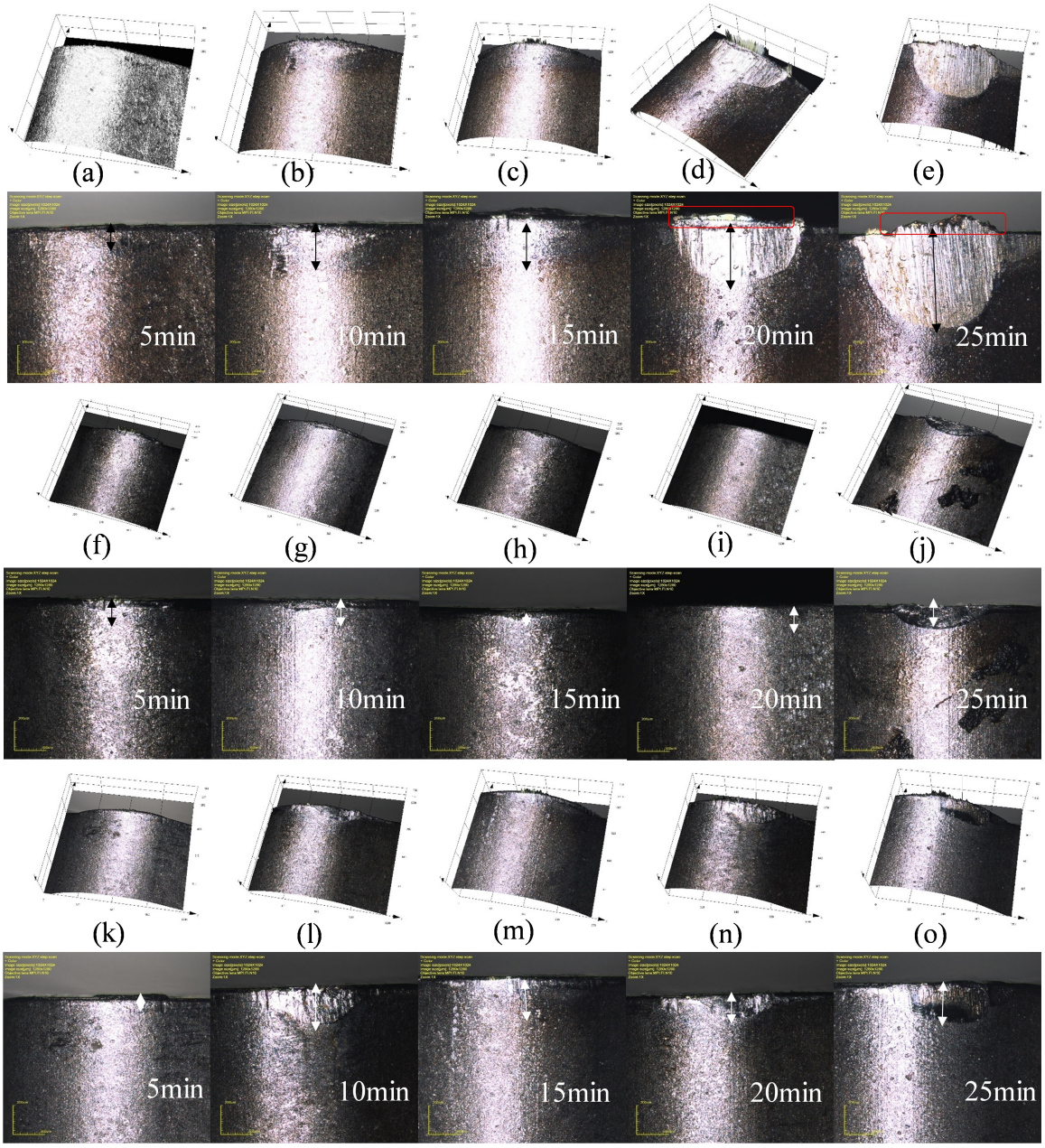

Figure 4.55: Tool wear measurements for (a-e) uncoated tool, (f-j) AlCN/AlC coated tool and (k-o) FeCrN coated tool

Chapter 5

CONCLUSIONS

Ti-based monolayer, Ti-multilayer, monolayer Al and Fe coatings were successfully developed on the MDN121 and WC-Co SNMG120408 substrate using plasma assisted cathodic arc evaporation. TiC-C, Ti/TiN/TiCN/TiN/TiCN, AlCN/AlC and FeCrN coating compositions are confirmed by GAXRD, Raman spectral analysis and mapping studies.

Developed coatings exhibited better mechanical properties. The hardness improved by 24.5% in TiC-C and 29.4 % in Ti/TiN/TiCN/TiN/TiCN, 8.70 % in AlCN/AlC and 50.79 % in FeCrN coatings compared to the uncoated SNMG120408 WC substrate. Raman spectral analysis confirmed the presence of DLC, TiC and TiN compounds in both TiC-C and Ti/TiN/TiCN/TiN/TiCN coatings and the presence of Fe and Al compounds in AlCN/AlC and FeCrN.

In case of fretting wear least COF (0.21-0.27) was observed in TiC-C and FeCrN compared to AlCN/AlC and Ti-multilayer coatings. Based on the experimental results relative volumetric wear loss of the various coatings under the study can be arranged in the following sequence:

$$FeCrN < TiC-C < AlCN/AlC < Ti/TiN/TiCN/TiN/TiCN$$

In case of adhesive wear least COF (0.21-0.31) is observed in TiC-C and FeCrN compared to AlCN/AlC and Ti- multilayer coatings. Based on the experimental results, relative wear rate of the various coating under the study can be arranged in the following sequence:

$$TiC-C < Ti/TiN/TiCN/TiN/TiCN < AlCN/AlC < FeCrN$$

In case of machinability studies, full factorial design is used for the experimental planning, analysis and validation. Mathematical regression models for cutting forces and surface roughness are developed.

Optimum machining parameters for least cutting force and surface roughness with Ti-multilayer, TiC-C, AlCN/AlC and FeCrN coated tool are (V_c=118 m/min; f=0.062 mm/rev; a_p=0.2 mm) (V_c=59 m/min; f=0.062 mm/rev; a_p=0.2 mm), (V_c=75 m/min; f=0.062 mm/rev; a_p=0.3 mm) and (V_c=118 m/min; f=0.062 mm/rev; a_p=0.2 mm) respectively.

Coefficient of determination (R(R^2) in case of both regression and ANN model is close to 1, which confirms the developed model is adequate. Experimental validation show that the developed models can be used for the optimization of machine tool parameters and cutting tools in the process planning.

Cutting forces are reduced by 15 %, 5 %, 18 % and 4 % in Ti-multilayer, TiC-C, AlCN/AlC and FeCrN coated tool respectively compared to uncoated tool. Whereas, surface roughness is reduced by 19 %, 15 %, 22 % and 22 % in Ti-multilayer, TiC-C, AlCN/AlC and FeCrN coated tool respectively compared to uncoated tool.

Tool wear is reduced by 65 %, 66 %, 73 % and 33 % in Ti-multilayer, TiC-C, AlCN/AlC and FeCrN coated tool respectively when compared to uncoated tool.

Relative tool wear of the various coatings measured with increments of time can be arranged in the following sequence:

$$FeCrN > Ti/TiN/TiCN/TiN/TiCN > TiC-C > AlCN/AlC$$

Closing remarks:

1. Ti-Multilayer and AlCN/AlN coatings are highly recommended for the machining of super alloys.

2. All the four coatings are recommended for the machining of steels with the hardness of 35-47 HRC.

3. All the Four coatings are recommended for the applications which require low COF.

Future scope of work:

1. Erosion and corrosion studies of the coating developed.
2. Machining using coated inserts in different environments such as wet, MQL and cryogenic machining.

Reference

Abusuilik, S. B. (2015). Pre-, intermediate, and post-treatment of hard coatings to improve their performance for forming and cutting tools. *Surface and Coatings Technology*, **284**, 384–395.

Amanov, A., **T. Watabe**, **R. Tsuboi**, and **S. Sasaki** (2013). Fretting wear and fracture behaviors of cr-doped and non-doped dlc films deposited on ti–6al–4v alloy by unbalanced magnetron sputtering. *Tribology International*, **62**, 49–57.

Ananthakumar, R., **B. Subramanian**, **A. Kobayashi**, and **M. Jayachandran** (2012). Electrochemical corrosion and materials properties of reactively sputtered tin/tialn multilayer coatings. *Ceramics International*, **38**(1), 477–485.

Anderson, M. J. and **P. J. Whitcomb**, *RSM simplified: optimizing processes using response surface methods for design of experiments*. Productivity press, 2016.

Angadi, S., **R. Melinamani**, **V. Gaitonde**, **M. Doddamani**, and **S. Karnik**, Experimental investigations on drilling characteristics of cenosphere reinforced epoxy composites. *In Applied Mechanics and Materials*, volume 766. Trans Tech Publ, 2015.

Anuwar, M., **R. Jayaganthan**, **V. Tewari**, and **N. Arivazhagan** (2007). A study on the hot corrosion behavior of ti–6al–4v alloy. *Materials Letters*, **61**(7), 1483–1488.

Aouici, H., **M. A. Yallese**, **K. Chaoui**, **T. Mabrouki**, and **J.-F. Rigal** (2012). Analysis of surface roughness and cutting force components in hard turning with cbn tool: Prediction model and cutting conditions optimization. *Measurement*, **45**(3), 344–353.

Arulkirubakaran, D. and **V. Senthilkumar** (2017). Performance of tin and tialn coated micro-grooved tools during machining of ti-6al-4v alloy. *International Journal of Refractory Metals and Hard Materials*, **62**, 47–57.

Ashrafizadeh, F. (2000). Adhesion evaluation of pvd coatings to aluminium substrate. *Surface and Coatings Technology*, **130**(2-3), 186–194.

Aslantas, K., **I. Ucun**, and **A. Cicek** (2012). Tool life and wear mechanism of coated and uncoated al2o3/ticn mixed ceramic tools in turning hardened alloy steel. *Wear*, **274**, 442–451.

Badiger, P. V., **V. Desai**, and **M. Ramesh** (2017). Development and characterization of ti/tic/tin coatings by cathodic arc evaporation technique. *Transactions of the Indian Institute of Metals*, **70**(9), 2459–2464.

Benea, L., **S.-B. Başa**, **E. Dănăilă**, **N. Caron**, **O. Raquet**, **P. Ponthiaux**, and **J.-P. Celis** (2015). Fretting and wear behaviors of ni/nano-wc composite coatings in dry and wet conditions. *Materials & Design (1980-2015)*, **65**, 550–558.

Bernstein, H. L., **T. S. Grant**, **R. C. McClung**, and **J. M. Allen**, Prediction of thermal-mechanical fatigue life for gas turbine blades in electric power generation. *In Thermomechanical Fatigue Behavior of Materials*. ASTM International, 1993.

Bernstein, H. L. *et al.*, Materials issues for users of gas turbines. *In Proceedings of the 35th Turbomachinery Symposium*. Texas A&M University. Turbomachinery Laboratories, 2006.

Bhat, D. D. G. (1999). A review of:handbook of physical vapor deposition (pvd) processing flim formation, adhesion, surface preparation and contamination control. *Materials and Manufacturing Processes*, **14**(5), 783–787. URL `https://doi.org/10.1080/10426919908907566`.

Bouacha, K., **M. A. Yallese**, **T. Mabrouki**, and **J.-F. Rigal** (2010). Statistical analysis of surface roughness and cutting forces using response surface methodology in hard turning of aisi 52100 bearing steel with cbn tool. *International Journal of Refractory Metals and Hard Materials*, **28**(3), 349–361.

Bromark, M., **M. Larsson**, **P. Hedenqvist**, and **S. Hogmark** (1997). Wear of pvd ti/tin multilayer coatings. *Surface and Coatings Technology*, **90**(3), 217–223.

Brookes, K. J. (2018). Introduction to surface engineering peter a. dearnley. *Metal Powder Report*, **73**(3), 126–127.

Budinski, K. G., *Guide to friction, wear and erosion testing*. ASTM International West Conshohocken, PA, 2007.

Bunshah, R. F. and **C. Weissmantel** (2001). Handbook of hard coatings.

Bushlya, V., **D. Johansson**, **F. Lenrick**, **J.-E. Ståhl**, and **F. Schultheiss** (2017). Wear mechanisms of uncoated and coated cemented carbide tools in machining lead-free silicon brass. *Wear*, **376**, 143–151.

Cadena, N. L., **R. Cue-Sampedro**, **H. R. Siller**, **A. M. Arizmendi-Morquecho**, **C. I. Rivera-Solorio**, and **S. Di-Nardo** (2013). Study of pvd alcrn coating for reducing carbide cutting tool deterioration in the machining of titanium alloys. *Materials*, **6**(6), 2143–2154.

Castelli, M. G., Characterization of damage progression in scs-6/timetal 21s [0] 4 under thermomechanical fatigue loading. *In Life prediction methodology for titanium matrix composites*. ASTM International, 1996.

Chabbi, A., **M. A. Yallese**, **I. Meddour**, **M. Nouioua**, **T. Mabrouki**, and **F. Girardin** (2017). Predictive modeling and multi-response optimization of technological parameters in turning of polyoxymethylene polymer (pom c) using rsm and desirability function. *Measurement*, **95**, 99–115.

Cheng, Y. and **Y. Zheng** (2007). Characterization of tin, tic and ticn coatings on ti–50.6 at.% ni alloy deposited by piii and deposition technique. *Surface and Coatings Technology*, **201**(9-11), 4909–4912.

Ciurana, J., **G. Arias**, and **T. Ozel** (2009). Neural network modeling and particle swarm optimization (pso) of process parameters in pulsed laser micromachining of hardened aisi h13 steel. *Materials and Manufacturing Processes*, **24**(3), 358–368.

Coelho, R. T., **E.-G. Ng**, and **M. Elbestawi** (2007). Tool wear when turning hardened aisi 4340 with coated pcbn tools using finishing cutting conditions. *International Journal of Machine Tools and Manufacture*, **47**(2), 263–272.

Creus, J., **A. Billard**, and **F. Sanchette** (2004). Corrosion behaviour of amorphous al–cr and al–cr–(n) coatings deposited by dc magnetron sputtering on mild steel substrate. *Thin Solid Films*, **466**(1-2), 1–9.

Das, D., **R. K. Thakur**, **A. K. Chaubey**, and **A. K. Sahoo** (2018). Optimization of machining parameters and development of surface roughness models during turning al-based metal matrix composite. *Materials Today: Proceedings*, **5**(2), 4431–4437.

Das, S. R., **D. Dhupal**, and **A. Kumar** (2015). Experimental investigation into machinability of hardened aisi 4140 steel using tin coated ceramic tool. *Measurement*, **62**, 108–126.

Dearnley, P. A. (2007). Engineering titanium surfaces. *Surface Engineering*, **23**(6), 399–400.

Downey, J., **R. Raghavendra**, *et al.* (2014). Comparison and analysis of audible sound energy emissions during single point machining of hsts with pvd ticn cutter insert across full tool life. *Wear*, **313**(1-2), 53–62.

Durst, O., **J. Ellermeier**, and **C. Berger** (2008). Influence of plasma-nitriding and surface roughness on the wear and corrosion resistance of thin films (pvd/pecvd). *Surface and Coatings Technology*, **203**(5-7), 848–854.

Efeoglu, I. and **F. Bulbul** (2005). Effect of crystallographic orientation on the friction and wear properties of moxsy–ti coatings by pulsed-dc in nitrogen and humid air. *Wear*, **258**(5-6), 852–860.

Eriksson, A. (2013). *Cathodic Arc Synthesis of Ti-Si-CN Thin Films: Plasma Analysis and Microstructure Formation*. Ph.D. thesis, Linköping University Electronic Press.

Eriksson, J. and **M. Olsson** (2011). Tribological testing of commercial crn,(ti, al) n and crc/c pvd coatings—evaluation of galling and wear characteristics against different high strength steels. *Surface and Coatings Technology*, **205**(16), 4045–4051.

FUKUI, H. (2016). Evolutional history of coating technologies for cemented carbide inserts—chemical vapor deposition and physical vapor deposition. *SEI TECHNICAL REVIEW*, (82), 39.

Gaitonde, V. and **S. Karnik** (2012). Minimizing burr size in drilling using artificial neural network (ann)-particle swarm optimization (pso) approach. *Journal of Intelligent Manufacturing*, **23**(5), 1783–1793.

Grzesik, W., **P. Niesłony**, **W. Habrat**, **J. Sieniawski**, and **P. Laskowski** (2018). Investigation of tool wear in the turning of inconel 718 superalloy in terms of process performance and productivity enhancement. *Tribology International*, **118**, 337–346.

Halling, J., *Introduction to tribology*. 5. Taylor & Francis Group, 1976.

Hanief, M., **M. Wani**, and **M. Charoo** (2017). Modeling and prediction of cutting forces during the turning of red brass (c23000) using ann and regression analysis. *Engineering science and technology, an international journal*, **20**(3), 1220–1226.

Harlin, P., **P. Carlsson**, **U. Bexell**, and **M. Olsson** (2006). Influence of surface roughness of pvd coatings on tribological performance in sliding contacts. *Surface and coatings Technology*, **201**(7), 4253–4259.

Hashemi, R. and **G. Hussain** (2015). Wear performance of al/tin dispersion strengthened surface composite produced through friction stir process: A comparison of tool geometries and number of passes. *Wear*, **324**, 45–54.

Hirano, H. and **T. Yoshikawa**, A study on two-step search using global-best in pso for multi-objective optimization problems. *In Soft Computing and Intelligent Systems (SCIS) and 13th International Symposium on Advanced Intelligent Systems (ISIS), 2012 Joint 6th International Conference on*. IEEE, 2012.

Holmberg, K. and **A. Matthews** (1994). Coatings tribology: Properties, mechanisms, techniques and applications in surface engineering tribology series: 56.

Hsu, C.-H., **K.-H. Huang**, and **Y.-H. Lin** (2013). Microstructure and wear performance of arc-deposited ti–n–o coatings on aisi 304 stainless steel. *Wear*, **306**(1-2), 97–102.

Ibrahim, R., **M. Rahmat**, **R. Oskouei**, and **R. S. Raman** (2015). Monolayer tialn and multilayer tialn/crn pvd coatings as surface modifiers to mitigate fretting fatigue of aisi p20 steel. *Engineering Fracture Mechanics*, **137**, 64–78.

Jao, J.-Y., **S. Han**, **L.-S. Chang**, **C.-L. Chang**, **Y.-C. Liu**, and **H. C. Shih** (2010). Bias voltage effect on the structure and property of chromium copper–diamond-like carbon multilayer films fabricated by cathodic arc plasma. *Applied Surface Science*, **256**(24), 7490–7495.

Jegadeeswaran, N., **M. Ramesh**, and **K. U. Bhat** (2014). Oxidation resistance hvof sprayed coating 25%(cr3c2-25 (ni20cr))+ 75% nicraly on titanium alloy. *Procedia materials science*, **5**, 11–20.

Kale, A., **R. Brusa**, and **A. Miotello** (2012). Structural and electrical properties of aln films deposited using reactive rf magnetron sputtering for solar concentrator application. *Applied Surface Science*, **258**(8), 3450–3454.

Kang, S., **H.-P. Lim**, and **K. Lee** (2015). Effects of ticn interlayer on bonding characteristics and mechanical properties of dlc-coated ti-6al-4v eli alloy. *International Journal of Refractory Metals and Hard Materials*, **53**, 13–16.

Kennedy, D. and **M. Hashmi** (1998). Methods of wear testing for advanced surface coatings and bulk materials. *Journal of Materials Processing Technology*, **77**(1-3), 246–253.

Kim, T. S., **J. S. Park**, **K. S. Son**, **J. S. Jung**, **K.-H. Lee**, **W. J. Maeng**, **H.-S. Kim**, **J.-Y. Kwon**, **B. Koo**, and **S. Lee** (2011). Transparent amoled display driven by hafnium-indium-zinc oxide thin film transistor array. *Current Applied Physics*, **11**(5), 1253–1256.

Kıvak, T. (2014). Optimization of surface roughness and flank wear using the taguchi method in milling of hadfield steel with pvd and cvd coated inserts. *Measurement*, **50**, 19–28.

Kong, X., **L. Yang**, **H. Zhang**, **K. Zhou**, and **Y. Wang** (2015). Cutting performance and coated tool wear mechanisms in laser-assisted milling k24 nickel-based superalloy. *The International Journal of Advanced Manufacturing Technology*, **77**(9-12), 2151–2163.

Kong, Y., **X. Tian**, **C. Gong**, and **P. K. Chu** (2018). Enhancement of toughness and wear resistance by crn/crcn multilayered coatings for wood processing. *Surface and Coatings Technology*, **344**, 204–213.

Kreines, L., **G. Halperin**, **I. Etsion**, **M. Varenberg**, **A. Hoffman**, and **R. Akhvlediani** (2004). Fretting wear of thin diamond films deposited on steel substrates. *Diamond and related materials*, **13**(9), 1731–1739.

Kumar, B. R., **H. Vardhan**, **M. Govindaraj**, and **G. Vijay** (2013). Regression analysis and ann models to predict rock properties from sound levels produced during drilling. *International Journal of Rock Mechanics and Mining Sciences*, **58**, 61–72.

Kumar, R. and **S. Chauhan** (2015). Study on surface roughness measurement for turning of al 7075/10/sicp and al 7075 hybrid composites by using response surface methodology (rsm) and artificial neural networking (ann). *Measurement*, **65**, 166–180.

Kumar, R., **R. Das**, **A. Sahoo**, **P. Mishra**, and **M. Ukamanal**, Comparative assessment on cutting performances of multi coated carbide insert in dry and spray impingement cooling environments. *In IOP Conference Series: Materials Science and Engineering*, volume 377. IOP Publishing, 2018.

Li, Q., **F.-q. Jiang**, **Y.-x. Leng**, **R.-h. Wei**, and **N. Huang** (2013). Microstructure and tribological properties of ti (cr) sicn coating deposited by plasma enhanced magnetron sputtering. *Vacuum*, **89**, 168–173.

Ma, L. W., **J. M. Cairney**, **M. J. Hoffman**, and **P. Munroe** (2006). Deformation and fracture of tin and tialn coatings on a steel substrate during nanoindentation. *Surface and Coatings Technology*, **200**(11), 3518–3526.

Malghan, R. L., **K. M. Rao**, **A. K. Shettigar**, **S. S. Rao**, and **R. D'Souza** (2017). Application of particle swarm optimization and response surface methodology for machining parameters optimization of aluminium matrix composites in milling operation. *Journal of the Brazilian Society of Mechanical Sciences and Engineering*, **39**(9), 3541–3553.

Manjaiah, M., **R. F. Laubscher**, **A. Kumar**, and **S. Basavarajappa** (2016). Parametric optimization of mrr and surface roughness in wire electro discharge machining (wedm) of d2 steel using taguchi-based utility approach. *International Journal of Mechanical and Materials Engineering*, **11**(1), 7.

Marin, E., **R. Offoiach**, **M. Regis**, **S. Fusi**, **A. Lanzutti**, and **L. Fedrizzi** (2016). Diffusive thermal treatments combined with pvd coatings for tribological protection of titanium alloys. *Materials & Design*, **89**, 314–322.

Mattox, D. M., *Handbook of physical vapor deposition (PVD) processing*. William Andrew, 2010.

Mattox, D. M. and **V. Mattox**, *Vacuum coating technology*. Springer, 2003.

Mia, M. and **N. R. Dhar** (2016). Response surface and neural network based predictive models of cutting temperature in hard turning. *Journal of advanced research*, **7**(6), 1035–1044.

Milošev, I., **H.-H. Strehblow**, and **B. Navinšek** (1997). Comparison of tin, zrn and crn hard nitride coatings: Electrochemical and thermal oxidation. *Thin solid films*, **303**(1-2), 246–254.

Miyoshi, K. (1996). Friction and wear properties of as-deposited and carbon ion-implanted diamond films. *Materials Science and Engineering: A*, **209**(1-2), 38–53.

Musfirah, A., **J. Ghani**, and **C. C. Haron** (2017). Tool wear and surface integrity of inconel 718 in dry and cryogenic coolant at high cutting speed. *Wear*, **376**, 125–133.

Navinšek, B., **P. Panjan**, and **I. Milošev** (1997). Industrial applications of crn (pvd) coatings, deposited at high and low temperatures. *Surface and Coatings Technology*, **97**(1-3), 182–191.

Nohava, J., **P. Dessarzin**, **P. Karvankova**, and **M. Morstein** (2015). Characterization of tribological behavior and wear mechanisms of novel oxynitride pvd coatings designed for applications at high temperatures. *Tribology International*, **81**, 231–239.

Nordin, M., **M. Larsson**, and **S. Hogmark** (1999*a*). Mechanical and tribological properties of multilayered pvd tin/crn. *Wear*, **232**(2), 221–225.

Nordin, M., **M. Larsson**, and **S. Hogmark** (1999*b*). Wear resistance of multilayered pvd tin/tan on hss. *Surface and Coatings Technology*, **120**, 528–534.

Nouioua, M., **M. A. Yallese**, **R. Khettabi**, **S. Belhadi**, **M. L. Bouhalais**, and **F. Girardin** (2017). Investigation of the performance of the mql, dry, and wet turning by response surface methodology (rsm) and artificial neural network (ann). *The International Journal of Advanced Manufacturing Technology*, **93**(5-8), 2485–2504.

Ono, T., **T. Kenmotsu**, and **T. Muramoto**, Simulation of the sputtering process. *In Reactive Sputter Deposition*. Springer, 2008, 1–42.

PalDey, S. and **S. Deevi** (2003). Single layer and multilayer wear resistant coatings of (ti, al) n: a review. *Materials Science and Engineering: A*, **342**(1-2), 58–79.

Pazhanivel, B., **T. P. Kumar**, and **G. Sozhan** (2015). Machinability and scratch wear resistance of carbon-coated wc inserts. *Materials Science and Engineering: B*, **193**, 146–152.

Pech, D., **N. Schupp**, **P. Steyer**, **T. Hack**, **Y. Gachon**, **C. Héau**, **A.-S. Loir**, and **J. C. Sánchez-López** (2009). Duplex sicn/dlc coating as a solution to improve fretting—corrosion resistance of steel. *Wear*, **266**(7-8), 832–838.

Podgornik, B., **J. Vižintin**, **H. Ronkainen**, and **K. Holmberg**, Tribological characteristics of duplex treated aisi 4140 steel. *In Tribology Series*, volume 38. Elsevier, 2000, 525–532.

Pomeroy, M. (2005). Coatings for gas turbine materials and long term stability issues. *Materials & design*, **26**(3), 223–231.

Prabhakara, H. (). Plasma assisted physical vapour deposition. *Dostupné na:¡ http://www. bangaloreplasmatek. com/plasma. html*.

Rahmati, B., **E. Zalnezhad**, **A. A. Sarhan**, **Z. Kamiab**, **B. N. Tabrizi**, and **W. Abas** (2015). Enhancing the adhesion strength of tantalum oxide ceramic thin film coating

on biomedical ti–6al–4v alloy by thermal surface treatment. *Ceramics International*, **41**(10), 13055–13063.

Rajendran, R. (2012). Gas turbine coatings–an overview. *Engineering Failure Analysis*, **26**, 355–369.

Ramamoorthy, B. and **B. C. Yeldose** (2009). An investigation into the adhesion strength of diamond like carbon multilayer coating (dlc/tin/ti/cu/ni). *Intelligent Information Management*, **1**(03), 179.

Roy, P., **S. Sarangi**, **A. Ghosh**, and **A. Chattopadhyay** (2009). Machinability study of pure aluminium and al–12% si alloys against uncoated and coated carbide inserts. *International Journal of Refractory Metals and Hard Materials*, **27**(3), 535–544.

Sahoo, A. K. and **B. Sahoo** (2012). Experimental investigations on machinability aspects in finish hard turning of aisi 4340 steel using uncoated and multilayer coated carbide inserts. *Measurement*, **45**(8), 2153–2165.

Sahoo, A. K. and **B. Sahoo** (2013*a*). A comparative study on performance of multilayer coated and uncoated carbide inserts when turning aisi d2 steel under dry environment. *Measurement*, **46**(8), 2695–2704.

Sahoo, A. K. and **B. Sahoo** (2013*b*). Performance studies of multilayer hard surface coatings (tin/ticn/al2o3/tin) of indexable carbide inserts in hard machining: Part-ii (rsm, grey relational and techno economical approach). *Measurement*, **46**(8), 2868–2884.

Sanchette, F., **T. H. Loi**, **A. Billard**, and **C. Frantz** (1995). Structure—properties relationship of metastable al-cr and al-ti alloys deposited by rf magnetron sputtering: role of nitrogen. *Surface and Coatings Technology*, **74**, 903–909.

Saravanan, R., **R. S. Sankar**, **P. Asokan**, **K. Vijayakumar**, and **G. Prabhaharan** (2005). Optimization of cutting conditions during continuous finished profile machining

using non-traditional techniques. *The International Journal of Advanced Manufacturing Technology*, **26**(1-2), 30–40.

Scheerer, H., **H. Hoche**, **E. Broszeit**, **B. Schramm**, **E. Abele**, and **C. Berger** (2005). Effects of the chromium to aluminum content on the tribology in dry machining using (cr, al) n coated tools. *Surface and Coatings Technology*, **200**(1-4), 203–207.

Seibert, F., **M. Döbeli**, **D. M. Fopp-Spori**, **K. Glaentz**, **H. Rudigier**, **N. Schwarzer**, **B. Widrig**, and **J. Ramm** (2013). Comparison of arc evaporated mo-based coatings versus cr1n1 and ta–c coatings by reciprocating wear test. *Wear*, **298**, 14–22.

Sidhu, T., **R. Agrawal**, and **S. Prakash** (2005). Hot corrosion of some superalloys and role of high-velocity oxy-fuel spray coatings—a review. *Surface and coatings technology*, **198**(1-3), 441–446.

Singh, J., **F. Quli**, **D. E. Wolfe**, **J. Schriempf**, and **J. Singh** (1999). An overview: Electron beam-physical vapor deposition technology-present and future applications. *Applied Research Laboratory, Pennsylvania State University, USA*.

Siow, P. C., **J. A. Ghani**, **M. J. Ghazali**, **T. R. Jaafar**, **M. A. Selamat**, and **C. H. C. Haron** (2013). Characterization of ticn and ticn/zrn coatings for cutting tool application. *Ceramics International*, **39**(2), 1293–1298.

Suresh, R., **S. Basavarajappa**, and **V. Gaitonde** (2015). Experimental studies on the performance of multilayer coated carbide tool in hard turning of high strength low alloy steel. *Journal of Materials Research*, **30**(20), 3056–3064.

Suresh, R., **S. Basavarajappa**, **V. Gaitonde**, and **G. Samuel** (2012). Machinability investigations on hardened aisi 4340 steel using coated carbide insert. *International Journal of Refractory Metals and Hard Materials*, **33**, 75–86.

Tkadletz, M., **N. Schalk**, **R. Daniel**, **J. Keckes**, **C. Czettl**, and **C. Mitterer** (2016). Advanced characterization methods for wear resistant hard coatings: a review on recent progress. *Surface and Coatings Technology*, **285**, 31–46.

Valli, J. (1986). A review of adhesion test methods for thin hard coatings. *Journal of Vacuum Science & Technology A: Vacuum, Surfaces, and Films*, **4**(6), 3007–3014.

Wang, J., **W. Lauwerens**, **E. Wieers**, **L. Stals**, **J. He**, and **J.-P. Celis** (2001). Structure and tribological properties of mosx coatings prepared by bipolar dc magnetron sputtering. *Surface and Coatings Technology*, **139**(2-3), 143–152.

Whitehouse, D. J., *Handbook of surface and nanometrology*. CRC press, 2010.

Wilson, J. A.-B., **S. Banfield**, **J. Eichler**, **A. Leyland**, **A. Matthews**, and **J. Housden** (2012). An investigation into the tribological performance of physical vapour deposition (pvd) coatings on high thermal conductivity cu-alloy substrates and the effect of an intermediate electroless ni–p layer prior to pvd treatment. *Thin Solid Films*, **520**(7), 2922–2931.

Yasuoka, M., **P. Wang**, and **R.-i. Murakami** (2012). Comparison of the mechanical performance of cutting tools coated by either a ticxn1- x single-layer or a tic/tic0. 5n0. 5/tin multilayer using the hollow cathode discharge ion plating method. *Surface and Coatings Technology*, **206**(8-9), 2168–2172.

Zhang, L., **G. Ma**, **H. Ma**, and **G. Lin** (2014). Effect of pulsed bias voltage on the structure and mechanical properties of ti–c–n composite films by pulsed bias arc ion plating. *Nuclear Instruments and Methods in Physics Research Section B: Beam Interactions with Materials and Atoms*, **333**, 1–5.

Zhang, S., **W. Wu**, **W. Chen**, and **S. Yang** (2015). Structural optimisation and synthesis of multilayers and nanocomposite alcrtisin coatings for excellent machinability. *Surface and Coatings Technology*, **277**, 23–29.

APPENDIX

Appendix for TiCC

Analysis of variance F_x							
Source	DF	Seq SS	Contribution	Adj SS	Adj MS	F-Value	P-Value
Regression	9	59244.4	75.87%	59244.4	6582.7	5.94	0.001
a_p	1	18235.4	23.35%	20934.8	20934.8	18.89	0
V_c	1	4551.4	5.83%	394.5	394.5	0.36	0.559
f	1	6082.7	7.79%	369.3	369.3	0.33	0.571
$a_p * a_p$	1	26467.9	33.90%	26467.9	26467.9	23.88	0
$V_c * V_c$	1	497.4	0.64%	497.4	497.4	0.45	0.512
f*f	1	2.1	0.00%	2.1	2.1	0	0.966
$a_p * V_c$	1	53.9	0.07%	53.9	53.9	0.05	0.828
$a_p * f$	1	2420.6	3.10%	2420.6	2420.6	2.18	0.158
$V_c * f$	1	933	1.19%	933	933	0.84	0.372
Error	17	18838.9	24.13%	18838.9	1108.2		
Total	26	78083.4	100.00%				
Model Summary							
S	R-sq	R-sq(adj)	PRESS	R-sq(pred)			
33.2892	75.87%	63.10%	55473.3	28.96%			

Analysis of variance F_y							
Source	DF	Seq SS	Contribution	Adj SS	Adj MS	F-Value	P-Value
Regression	9	25233.9	62.92%	25233.9	2803.8	3.2	0.019
a_p	1	3435.7	8.57%	14462.9	14462.9	16.53	0.001
V_c	1	104.9	0.26%	327.9	327.9	0.37	0.548
f	1	2759.4	6.88%	1487.6	1487.6	1.7	0.21
$a_p * a_p$	1	16283	40.60%	16283	16283	18.61	0
$V_c * V_c$	1	310.9	0.78%	310.9	310.9	0.36	0.559
f*f	1	1422	3.55%	1422	1422	1.63	0.219
$a_p * V_c$	1	443.8	1.11%	443.8	443.8	0.51	0.486
$a_p * f$	1	331.1	0.83%	331.1	331.1	0.38	0.547
$V_c * f$	1	143.1	0.36%	143.1	143.1	0.16	0.691
Error	17	14872.8	37.08%	14872.8	874.9		
Total	26	40106.7	100.00%				
Model Summary							
S	R-sq	R-sq(adj)	PRESS	R-sq(pred)			
29.5782	62.92%	43.28%	43985.4	0.00%			

Analysis of variance F_z							
Source	DF	Seq SS	Contribution	Adj SS	Adj MS	F-Value	P-Value
Regression	9	103595	74.74%	103595	11510.5	5.59	0.001
a_p	1	34229	24.69%	39602	39601.6	19.23	0
V_c	1	42	0.03%	596	595.9	0.29	0.598
f	1	16297	11.76%	3017	3017	1.46	0.243
$a_p * a_p$	1	46644	33.65%	46644	46644.3	22.65	0
$V_c * V_c$	1	563	0.41%	563	563.1	0.27	0.608
f*f	1	2645	1.91%	2645	2645.4	1.28	0.273
$a_p * V_c$	1	317	0.23%	317	317.2	0.15	0.7
$a_p * f$	1	2739	1.98%	2739	2738.6	1.33	0.265
$V_c * f$	1	118	0.08%	118	117.8	0.06	0.814
Error	17	35016	25.26%	35016	2059.7		
Total	26	138611	100.00%				

Model Summary				
S	R-sq	R-sq(adj)	PRESS	R-sq(pred)
45.3844	74.74%	61.36%	101060	27.09%

Analysis of variance R_a

Source	DF	Seq SS	Contribution	Adj SS	Adj MS	F-Value	P-Value
Regression	9	1.04502	94.37%	1.04502	0.116113	31.66	0
a_p	1	0.32536	29.38%	0.02455	0.024546	6.69	0.019
V_c	1	0.12703	11.47%	0.01195	0.011949	3.26	0.089
f	1	0.51627	46.62%	0.00021	0.000207	0.06	0.815
$a_p * a_p$	1	0.01454	1.31%	0.01454	0.014537	3.96	0.063
$V_c * V_c$	1	0.00938	0.85%	0.00938	0.009377	2.56	0.128
f*f	1	0.00111	0.10%	0.00111	0.001108	0.3	0.59
$a_p * V_c$	1	0.02691	2.43%	0.02691	0.026913	7.34	0.015
$a_p * f$	1	0.02434	2.20%	0.02434	0.024336	6.64	0.02
$V_c * f$	1	0.00009	0.01%	0.00009	0.000091	0.02	0.877
Error	17	0.06235	5.63%	0.06235	0.003667		
Total	26	1.10736	100.00%				

Model Summary

S	R-sq	R-sq(adj)	PRESS	R-sq(pred)
0.0605596	94.37%	91.39%	0.168344	84.80%

Appendix for Ti multilayer coated tool

Analysis of variance for F_x

Source	DF	Seq SS	Contribution	Adj SS	Adj MS	F-Value	P-Value
Regression	9	13004.6	82.18%	13004.6	1444.95	8.71	0
a_p	1	9987.1	63.11%	405.9	405.93	2.45	0.136
V_c	1	298.1	1.88%	41.9	41.86	0.25	0.622
f	1	868.7	5.49%	20.2	20.23	0.12	0.731
$a_p * a_p$	1	787.6	4.98%	787.6	787.61	4.75	0.044
$V_c * V_c$	1	2	0.01%	2 les	1.96	0.01	0.915
f*f	1	0.7	0.00%	0.7	0.75	0	0.947
$a_p * V_c$	1	677.3	4.28%	677.3	677.27	4.08	0.059
$a_p * f$	1	383	2.42%	383	383.05	2.31	0.147
$V_c * f$	1	0	0.00%	0	0.01	0	0.994
Error	17	2819.4	17.82%	2819.4	165.85		
Total	26	15824	100.00%				

Model Summary

S	R-sq	R-sq(adj)	PRESS	R-sq(pred)
12.8782	82.18%	72.75%	8407.1	46.87%

Analysis of variance F_y							
Source	DF	Seq SS	Contribution	Adj SS	Adj MS	F-Value	P-Value
Regression	9	17797.6	93.75%	17797.6	1977.51	28.35	0
a_p	1	9343.4	49.22%	11.8	11.83	0.17	0.686
V_c	1	1241.9	6.54%	383.9	383.93	5.5	0.031
f	1	6193.9	32.63%	89.5	89.48	1.28	0.273
$a_p * a_p$	1	13	0.07%	13	13	0.19	0.671
$V_c * V_c$	1	236	1.24%	236	236.03	3.38	0.083
f*f	1	157.8	0.83%	157.8	157.78	2.26	0.151
$a_p * V_c$	1	471.5	2.48%	471.5	471.49	6.76	0.019
$a_p * f$	1	50.2	0.26%	50.2	50.24	0.72	0.408
$V_c * f$	1	89.9	0.47%	89.9	89.86	1.29	0.272
Error	17	1185.7	6.25%	1185.7	69.74		
Total	26	18983.3	100.00%				

Model Summary				
S	R-sq	R-sq(adj)	PRESS	R-sq(pred)
8.35133	93.75%	90.45%	3613.48	80.96%

Analysis of variance F_z							
Source	DF	Seq SS	Contribution	Adj SS	Adj MS	F-Value	P-Value
Regression	9	53595.3	92.56%	53595.3	5955.04	23.49	0
a_p	1	23944	41.35%	1109.5	1109.53	4.38	0.052
V_c	1	3418	5.90%	500.2	500.18	1.97	0.178
f	1	23359.7	40.34%	31	31.03	0.12	0.731
$a_p * a_p$	1	1020.1	1.76%	1020.1	1020.08	4.02	0.061
$V_c * V_c$	1	189.3	0.33%	189.3	189.32	0.75	0.4
f*f	1	113	0.20%	113	112.99	0.45	0.513
$a_p * V_c$	1	725.8	1.25%	725.8	725.82	2.86	0.109
$a_p * f$	1	9	0.02%	9	9.02	0.04	0.853
$V_c * f$	1	816.3	1.41%	816.3	816.34	3.22	0.091
Error	17	4309.4	7.44%	4309.4	253.49		
Total	26	57904.7	100.00%				
Model Summary							
S	R-sq	R-sq(adj)	PRESS	R-sq(pred)			
15.9215	92.56%	88.62%	13783.7	76.20%			

Analysis of variance R_a

Source	DF	Seq SS	Contribution	Adj SS	Adj MS	F-Value	P-Value
Regression	9	0.790151	80.65%	0.790151	0.087795	7.87	0
a_p	1	0.452306	46.17%	0.0441	0.0441	3.95	0.063
V_c	1	0.001259	0.13%	0.005287	0.005287	0.47	0.5
f	1	0.276122	28.18%	0.003216	0.003216	0.29	0.598
$a_p * a_p$	1	0.037692	3.85%	0.037692	0.037692	3.38	0.084
$V_c * V_c$	1	0.008895	0.91%	0.008895	0.008895	0.8	0.384
f*f	1	0.004592	0.47%	0.004592	0.004592	0.41	0.53
$a_p * V_c$	1	0.000009	0.00%	0.000009	0.000009	0	0.977
$a_p * f$	1	0.005691	0.58%	0.005691	0.005691	0.51	0.485
$V_c * f$	1	0.003584	0.37%	0.003584	0.003584	0.32	0.578
Error	17	0.189585	19.35%	0.189585	0.011152		
Total	26	0.979737	100.00%				

Model Summary

S	R-sq	R-sq(adj)	PRESS	R-sq(pred)
0.105603	80.65%	70.40%	0.565652	42.26%

Appendix for AlCN/AlC

Analysis of variance F_x							
Source	DF	Seq SS	Contribution	Adj SS	Adj MS	F-Value	P-Value
Regression	9	16857.1	75.88%	16857.1	1873.01	5.94	0.001
a_p	1	6479.8	29.17%	2236.3	2236.28	7.1	0.016
V_c	1	1560.1	7.02%	428.9	428.92	1.36	0.259
f	1	3688.6	16.60%	366.2	366.18	1.16	0.296
$a_p * a_p$	1	2057.9	9.26%	2057.9	2057.94	6.53	0.02
$V_c * V_c$	1	391.4	1.76%	391.4	391.43	1.24	0.281
f*f	1	934.4	4.21%	934.4	934.41	2.96	0.103
$a_p * V_c$	1	1.4	0.01%	1.4	1.43	0	0.947
$a_p * f$	1	1742.9	7.85%	1742.9	1742.91	5.53	0.031
$V_c * f$	1	0.5	0.00%	0.5	0.47	0	0.97
Error	17	5358.1	24.12%	5358.1	315.19		
Total	26	22215.3	100.00%				
Model Summary							
S	R-sq	R-sq(adj)	PRESS	R-sq(pred)			
17.7535	75.88%	63.11%	12204	45.06%			

Analysis of variance F_y							
Source	DF	Seq SS	Contribution	Adj SS	Adj MS	F-Value	P-Value
Regression	9	26001.5	89.58%	26001.5	2889.05	16.24	0
a_p	1	6670.1	22.98%	4499.7	4499.72	25.29	0
V_c	1	3520.5	12.13%	440.4	440.39	2.48	0.134
f	1	8846.2	30.48%	267.8	267.75	1.5	0.237
$a_p * a_p$	1	3171.9	10.93%	3171.9	3171.85	17.83	0.001
$V_c * V_c$	1	139.1	0.48%	139.1	139.07	0.78	0.389
f*f	1	13.1	0.05%	13.1	13.09	0.07	0.789
$a_p * V_c$	1	1095.5	3.77%	1095.5	1095.49	6.16	0.024
$a_p * f$	1	1942.9	6.69%	1942.9	1942.9	10.92	0.004
$V_c * f$	1	602.3	2.07%	602.3	602.27	3.39	0.083
Error	17	3024.5	10.42%	3024.5	177.91		
Total	26	29025.9	100.00%				

Model Summary				
S	R-sq	R-sq(adj)	PRESS	R-sq(pred)
13.3383	89.58%	84.06%	8561.08	70.51%

Analysis of variance F_z							
Source	DF	Seq SS	Contribution	Adj SS	Adj MS	F-Value	P-Value
Regression	9	84434.1	86.99%	84434.1	9381.6	12.63	0
a_p	1	28345.8	29.20%	11690	11690	15.74	0.001
V_c	1	3417.5	3.52%	810.9	810.9	1.09	0.311
f	1	33237.4	34.24%	1099	1099	1.48	0.24
$a_p * a_p$	1	12351.8	12.73%	12351.8	12351.8	16.63	0.001
$V_c * V_c$	1	855.2	0.88%	855.2	855.2	1.15	0.298
f*f	1	476	0.49%	476	476	0.64	0.434
$a_p * V_c$	1	0.3	0.00%	0.3	0.3	0	0.986
$a_p * f$	1	5312.1	5.47%	5312.1	5312.1	7.15	0.016
$V_c * f$	1	438	0.45%	438	438	0.59	0.453
Error	17	12624.9	13.01%	12624.9	742.6		
Total	26	97059	100.00%				
Model Summary							
S	R-sq	R-sq(adj)	PRESS	R-sq(pred)			
27.2514	86.99%	80.11%	36804.9	62.08%			

Analysis of variance R_a							
Source	DF	Seq SS	Contribution	Adj SS	Adj MS	F-Value	P-Value
Regression	9	1.04824	96.16%	1.04824	0.116471	47.31	0
a_p	1	0.10631	9.75%	0.00172	0.001724	0.7	0.414
V_c	1	0.0494	4.53%	0.00174	0.001743	0.71	0.412
f	1	0.8593	78.83%	0.00825	0.008248	3.35	0.085
$a_p * a_p$	1	0.00098	0.09%	0.00098	0.00098	0.4	0.537
$V_c * V_c$	1	0.00085	0.08%	0.00085	0.000851	0.35	0.564
f*f	1	0.02397	2.20%	0.02397	0.023966	9.73	0.006
$a_p * V_c$	1	0.0009	0.08%	0.0009	0.000903	0.37	0.553
$a_p * f$	1	0.00565	0.52%	0.00565	0.005654	2.3	0.148
$V_c * f$	1	0.00088	0.08%	0.00088	0.000876	0.36	0.559
Error	17	0.04186	3.84%	0.04186	0.002462		
Total	26	1.0901	100.00%				

Model Summary				
S	R-sq	R-sq(adj)	PRESS	R-sq(pred)
0.0496193	96.16%	94.13%	0.101438	90.69%

Appendix for FeCrN

Analysis of variance F_x							
Source	DF	Seq SS	Contribution	Adj SS	Adj MS	F-Value	P-Value
Regression	9	44059.3	83.99%	44059.3	4895.48	9.91	0
a_p	1	36101.6	68.82%	2225.4	2225.45	4.5	0.049
V_c	1	990.2	1.89%	1290.3	1290.27	2.61	0.125
f	1	935.8	1.78%	199.1	199.09	0.4	0.534
$a_p * a_p$	1	3607.7	6.88%	3607.7	3607.71	7.3	0.015
$V_c * V_c$	1	832.7	1.59%	832.7	832.67	1.69	0.212
f*f	1	491.5	0.94%	491.5	491.46	0.99	0.333
$a_p * V_c$	1	620.1	1.18%	620.1	620.07	1.25	0.278
$a_p * f$	1	55.3	0.11%	55.3	55.28	0.11	0.742
$V_c * f$	1	424.6	0.81%	424.6	424.6	0.86	0.367
Error	17	8400	16.01%	8400	494.12		
Total	26	52459.3	100.00%				
Model Summary							
S	R-sq	R-sq(adj)	PRESS	R-sq(pred)			
22.2288	83.99%	75.51%	20484.9	60.95%			

Analysis of variance F_y

Source	DF	Seq SS	Contribution	Adj SS	Adj MS	F-Value	P-Value
Regression	9	34367.6	81.53%	34367.6	3818.62	8.34	0
a_p	1	22684.5	53.82%	1491.2	1491.16	3.26	0.089
V_c	1	2234.4	5.30%	215.3	215.31	0.47	0.502
f	1	6139.3	14.56%	180.2	180.23	0.39	0.539
$a_p * a_p$	1	1985	4.71%	1985	1985.01	4.34	0.053
$V_c * V_c$	1	68.9	0.16%	68.9	68.89	0.15	0.703
f*f	1	173.6	0.41%	173.6	173.62	0.38	0.546
$a_p * V_c$	1	696.3	1.65%	696.3	696.3	1.52	0.234
$a_p * f$	1	152.8	0.36%	152.8	152.84	0.33	0.571
$V_c * f$	1	232.7	0.55%	232.7	232.68	0.51	0.486
Error	17	7783.5	18.47%	7783.5	457.85		
Total	26	42151	100.00%				

Model Summary

S	R-sq	R-sq(adj)	PRESS	R-sq(pred)
21.3975	81.53%	71.76%	18828.2	55.33%

Analysis of variance F_z							
Source	DF	Seq SS	Contribution	Adj SS	Adj MS	F-Value	P-Value
Regression	9	107451	89.59%	107451	11939	16.25	0
a_p	1	74369	62.01%	7726	7725.7	10.52	0.005
V_c	1	3745	3.12%	1561	1561	2.13	0.163
f	1	11893	9.92%	1665	1664.6	2.27	0.151
$a_p * a_p$	1	12616	10.52%	12616	12616.4	17.17	0.001
$V_c * V_c$	1	923	0.77%	923	922.8	1.26	0.278
f*f	1	1221	1.02%	1221	1220.9	1.66	0.215
$a_p * V_c$	1	296	0.25%	296	296.5	0.4	0.534
$a_p * f$	1	302	0.25%	302	302	0.41	0.53
$V_c * f$	1	2085	1.74%	2085	2085.2	2.84	0.11
Error	17	12488	10.41%	12488	734.6		
Total	26	119939	100.00%				
Model Summary							
S	R-sq	R-sq(adj)	PRESS	R-sq(pred)			
27.1031	89.59%	84.08%	31307.7	73.90%			

Analysis of variance R_a							
Source	DF	Seq SS	Contribution	Adj SS	Adj MS	F-Value	P-Value
Regression	9	0.97374	96.70%	0.973737	0.108193	55.38	0
a_p	1	0.06282	6.24%	0.001082	0.001082	0.55	0.467
V_c	1	0.06416	6.37%	0.000146	0.000146	0.07	0.788
f	1	0.76919	76.39%	0.00211	0.00211	1.08	0.313
$a_p * a_p$	1	0.00574	0.57%	0.005738	0.005738	2.94	0.105
$V_c * V_c$	1	0.0001	0.01%	0.000103	0.000103	0.05	0.821
f*f	1	0.03669	3.64%	0.036695	0.036695	18.78	0
$a_p * V_c$	1	0.01746	1.73%	0.01746	0.01746	8.94	0.008
$a_p * f$	1	0.01686	1.67%	0.016856	0.016856	8.63	0.009
$V_c * f$	1	0.00072	0.07%	0.000721	0.000721	0.37	0.551
Error	17	0.03321	3.30%	0.033215	0.001954		
Total	26	119939	100.00%				

Model Summary				
S	R-sq	R-sq(adj)	PRESS	R-sq(pred)
0.0442018	96.70%	94.96%	0.0772769	92.33%

PUBLICATIONS BASED ON THE THESIS

The thesis outlines Investigations On Characteristics And Performance Of Hard Thin Films Developed By Cathodic Arc Evaporation and is a result of the research carried at the Department of Mechanical Engineering, National Institute of Technology Karnataka between July 2015 and December 2018. The research during this period has resulted in the following publications:

Sl. No.	**Title of the paper**	**Authors (in the same order as in the paper. Underline the Research Scholar's name)**	**Name of the Journal / Conference, Vol., No., Pages**	**Month, Year of Publication**	**Category***
1	Development and Characterization of Ti/TiC/TiN Coatings by Cathodic Arc Evaporation Technique	**Pradeep V. Badiger**, Vijay Desai, M. R. Ramesh.	Transactions of Indian Institute of Metals. (SCIE), Vol 70, Issue 9, 2459-2464.	Mar-17	1

2	Effect of cutting parameters on tool wear, cutting force and surface roughness in machining of MDN431 alloy using Al and Fe coated tools	**Pradeep V. Badiger**, Vijay Desai, M. R. Ramesh, Prajwala B K, K Raveendra	Material Research Express (SCIE), Vol 6, (2019) 016401	Oct-18	1
3	Tribological behavior of monolayer and multilayer Ti-based thin solid films developed on alloy steel	**Pradeep V. Badiger**, Vijay Desai, M. R Ramesh, Sharanappa Joladarashi, Hemanth Gourkar.	Material Research Express (SCIE), Vol 6 (2019) 026419	Nov-18	1
4	Optimization of machining parameters in turning process of MDN431 using Ti-multilayer coated tool	**Pradeep V. Badiger**, Vijay Desai, M. R. Ramesh, K Raveendra.	International Journal of Modern Manufacturing Technology (Scopus) Vol 10, Issue 1, 7-12.	Jun-18	1
5	Performance of Ti-multilayer coated tool during machining of MDN431 alloyed steel	**Pradeep V. Badiger**, Vijay Desai., M. R. Ramesh.	AIP conference series Proceedings (Scopus), Vol 1943, Issue 1, 020064.	Apr-18	1

6	Performance of DLC coated tool during machining of MDN431 alloyed steel	**Pradeep V. Badiger**, Vijay Desai, M. R. Ramesh.	Materials Today Proceedings (Scopus), Vol 5, Issue 9, 17360-17370.	Jun-18	1
7	Fretting and Adhesive wear behavior of monolayer and multilayer Al and Fe-based coatings developed on alloy steel	**Pradeep V. Badiger**, Vijay Desai, M. R. Ramesh, Hemanth Gourkar.	Journal of Material Engineering and Performance (SCIE)	Revision submitted	1
8	Performance of Ti monolayer and multilayer-coated tools during machining of MDN431 alloyed steel	**Pradeep V. Badiger**, Vijay Desai, M. R. Ramesh, Prajwala B K, K Raveendra	Silicon (SCIE)	Under review	1
9	Cutting forces and surface roughness quality assessment using ANN and PSO approach during machining of MDN431 using TiN/AlN coated cutting tool	**Pradeep V. Badiger**, Vijay Desai, M. R. Ramesh, Prajwala B. K., K. Raveendra	The Arabian Journal of Science and Engineering (SCIE)	Under review	1

10	Microstructure and mechanical properties of Ti-TiC-TiN-TiC-TiN coatings produced by cathodic arc evaporation technique	**Pradeep V. Badiger**, Vijay Desai, M. R. Ramesh.	International Conference on Emerging Trends in Materials and Manufacturing Engineering, NIT Trichy, TN, India.	Mar-17	3
11	Fretting wear behavior of monolayer and multilayer Ti-based coatings developed on alloy steel	**Pradeep V. Badiger**, Vijay Desai, M. R. Ramesh, Sharanappa Joladarashi	TACT 2017 International Thin Film Conference, National Dong Hwa University in Hualien, Taiwan.	Oct-17	3
12	Performance of DLC coated tool during machining of MDN431 alloyed steel	**Pradeep V. Badiger**, Vijay Desai, M. R. Ramesh.	International Conference on Advances in Materials & Processing: Challenges & Opportunities IIT Roorkee.	Dec-17	3

13	Performance of Ti-multilayer coated tool during machining of MDN431 alloyed steel	**Pradeep V. Badiger**, Vijay Desai, M. R. Ramesh.	Advances in International Conference on Design, Materials & Manufacture, NITK Surathkal.	Jan-18	3
14	Influence of Ti-multilayer coated tools on surface roughness and cutting forces in turning process of MDN431	**Pradeep V. Badiger**, Vijay Desai, M. R. Ramesh.	7th International Engineering Symposium, Kumamoto University, Japan.	Mar-18	3
15	Influence of Ti-coated tools on surface roughness and cutting forces in turning process of MDN431	**Pradeep V. Badiger**, Vijay Desai., M. R. Ramesh., Prajwala B. K., K. Raveendra	ICAMMS, TIIM Trivandrum chapter Trivandrum	Oct 2018	3

*Category: 1: Journal paper, full paper reviewed. 2: Journal paper, Abstract reviews. 3: Conference/Symposium paper, full paper reviewed.

4: Conference/Symposium paper, abstract reviewed. 5: others (including papers in Workshops, NITK Research Bulletins, Short notes etc.)

Pradeep V. Badiger	**Prof. Vijay Desai**	**Dr. M. R. Ramesh**
Research Scholar	Research Guide	Research Guide
Name & Signature, with Date	Name & Signature, with Date	Name & Signature, with Date

Bio-Data

NAME	: Pradeep V. badiger
DATE OF BIRTH	: 22-June-1992

EDUCATIONAL QUALIFICATIONS

2013	**Bachelor of Engineering (B.E.)**
Institute	:Sapthagiri College of Engineering, Bengaluru.
University	:VTU, Belgaum
Specialization	: Mechanical Engineering
2015	**Master of Technology (M.Tech)**
Institute	:Siddaganga Institute of Technology, Tumakuru
University	:VTU, Belgaum
Specialization	: Manufacturing Science and Engineering
2019	**Doctor of Philosophy (Ph.D)**
Institute	: National Institute of Technology Karnataka, Surathkal
Registration Date	: 09-July-2015
Registration Number	:155130ME15F10

PERMANENT ADDRESS :

S/o V. K. Badiger, Assistant Director (TSWO-Hosadura)

C/o Sunil Seth, Vidyanagar 7th cross,

Hosadurga-Tq,Chitradurga-Dist-577527.

CONTACT Number :+91-9980556720

Email ID :*pvb.badiger@gmail.com*

PRESENT ADDRESS :

Assistant Professor, Department of Mechanical Engineering

Nitte Meenakshi Institute of Technology

P.B.No.6429, Govindapura, Gollahalli

Yelahanka Bangalore-560064, Karnataka.

Contact Number :+91-7676419815

Email ID :*pradeep.v.badiger@nmit.ac.in*

Papers Published: **08**

Papes under review: **01**

Conference attended: **07**

Awards and Recognitions

- *MHRD Scholarship for perusing Ph.D.*
- *Best oral presentation award at NIT Trichy.*
- *JASSO Scholarship at Kumamoto University, Japan.*

I declare that the above information is true and correct to the best of my knowledge.

PRADEEP V. BADIGER